Spring 2019

A novel approach to spatial assessments of surface water nitrate trends in selected Iowa rivers and lakes

Matthew James Meulemans
University of Iowa

A NOVEL APPROACH TO SPATIAL ASSESSMENTS OF SURFACE WATER NITRATE TRENDS IN SELECTED IOWA RIVERS AND LAKES

by

Matthew James Meulemans

A thesis submitted in partial fulfillment
of the requirements for the Master of Science
degree in Civil and Environmental Engineering in the
Graduate College of
The University of Iowa

May 2019

Thesis Supervisors: Professor Larry Weber
Adjunct Associate Professor Nathan Young

Graduate College
The University of Iowa
Iowa City, Iowa

CERTIFICATE OF APPROVAL

_____

MASTER'S THESIS

_____

This is to certify that the Master's thesis of

Matthew James Meulemans

has been approved by the Examining Committee for
the thesis requirement for the Master of Science degree
in Civil and Environmental Engineering at the May 2019 graduation.

Thesis Committee: _____
Larry Weber, Thesis Supervisor

_____
Nathan Young, Thesis Supervisor

_____
Craig Just

_____
Christopher Jones

_____
James Niemeier

ABSTRACT

Overabundant nitrate in Iowa's surface water threatens stream health, drinking water safety, and significantly contributes to hypoxic zones in the Gulf of Mexico. Researchers have quantified surface water nitrate loads historically with grab samples and, more recently, *in-situ* sensors. *In-situ* sensor networks capture changes in nitrate concentration over small time scales, providing high temporal resolution data to accurately calculate nitrate loading. However, because advanced sensors are expensive, spatial resolution is often compromised when sensors are deployed on large rivers. To collect high spatial resolution nitrate samples that complement the high temporal resolution data from *in-situ* sensors, we first used traditional grab samples on small, non-navigable streams in the Clear Creek and the English River watersheds. Dense grab samples across watersheds provide higher resolution data, but not at the spatial resolution achievable on navigable streams with newly developed, boat-deployed sensor technology.

We constructed a boat-deployed sensor system that automatically measured nitrate concentrations, temperature, dissolved oxygen, conductivity, and pH as we navigated a boat on a given waterbody. We used the system on the Iowa and Cedar Rivers to capture spatial and temporal changes never previously observed in Iowa. Our data suggest nitrate concentrations and yields were highest in low-relief landforms dominated by row crop agriculture. Nitrate concentrations were lower in higher-relief landforms with less row crop production.

We also measured water in Storm Lake, IA with the boat-deployed system. We measured little heterogeneity of nitrate concentrations in the lake, but observed significant nitrate reduction in a large wetland just upstream. The system captured fine

scale spatial dynamics of nitrate reduction in the wetland and low nitrate concentrations throughout Storm Lake.

Our newly developed sensor platform captured high resolution water quality data, complementing the high temporal resolution data collected with *in-situ* sensors. High spatial resolution data in this and similar studies provide powerful insights for decision makers to target problematic areas, reduce nitrate, and improve water quality.

PUBLIC ABSTRACT

High nitrate in Iowa streams threatens local stream health, drinking water safety, and damages ecosystem health in the Gulf of Mexico. Recent studies have focused on how much nitrate is delivered from Iowa streams, but have lacked spatial resolution necessary to decide where to build small scale nitrate removal practices. To collect high spatial resolution nitrate data and better inform the placement of nitrate removal practices, we used traditional and novel water quality sampling methods.

Specifically, we collected traditional water samples in containers for later lab analysis along Clear Creek and the English River and tributaries. Our dense sampling protocol allowed us to identify areas of each river that contributed high nitrate and phosphorus concentrations. Highest contributions were often related to the amount of corn and soybean production upstream of each sample. We challenged this old, grab sample method with the use of advanced sensors to collect high resolution water quality data on navigable waterways.

We developed a boat-deployed sensor system that automatically measured nitrate concentration, temperature, dissolved oxygen, conductivity, and pH every five seconds as we navigated a waterbody. We measured water in the Iowa and Cedar Rivers and identified areas with highest nitrate inputs. Often, highest nitrate inputs occurred where land was flat and intense corn and soybean production existed. We observed nitrate reduction in specific river reaches and in a wetland draining agricultural land. This and similar studies provide powerful insights for decision makers who wish to reduce nitrate and improve water quality.

TABLE OF CONTENTS

LIST OF TABLES

LIST OF FIGURES

CHAPTER 1: INTRODUCTION

1.1 Background and Motivation

Extensive row crop agriculture in the U.S. Midwestern state of Iowa contributes to elevated surface water nitrate concentrations and loads, which adversely affects Iowans and those downstream (Schilling and Libra, 2000; Carpenter et al, 1998; Jones et al, 2018a). At the local scale, high nitrate concentrations in drinking water may disrupt the ability for blood to carry oxygen, a condition known as methemoglobinemia (Fewtrell, 2004). Methoemoglobinemia can be fatal to young humans and livestock (Fewtrell, 2004). Correlations between high nitrate concentrations, bladder, and ovarian cancers also exist (Weyer et al, 2001). To ensure human safety, processes designed to reduce nitrate levels below the maximum allowable level of 10 mg L^{-1} in drinking water increase water treatment costs in Iowa and elsewhere (Vedachalam et al. 2018).

Stream nitrate loads also pose a national problem. Increased nitrate loading to the Gulf of Mexico is the primary driver for algal blooms, leading to large hypoxic zones (Turner et al, 2006; Howarth et al, 2006; Zhao and Quigg, 2014). In response to nutrient load increases, the U.S. Environmental Protection Agency (USEPA) developed the National Nutrient Strategy in 2007 and subsequently called for a 45% nitrate load reduction to the Mississippi River Basin (USEPA 2008). If nitrate loads are reduced by 45%, we will begin to reduce the size of the annual hypoxia area in the Gulf of Mexico (USEPA 2008). In the last decade, efforts have been made to better model, sample, and reduce total NO_3^-N loads flowing to the Gulf of Mexico. Activities within Iowa have been central to nitrate reduction efforts, because the state contributes 29% of the nitrate

flowing to the Mississippi Basin while occupying only 4.5% of the total land area (Fig. 1.1) (Jones et al. 2018a).

Figure 1.1: The state of Iowa (outlined in red) occupies 4.5% of the land comprising the Mississippi River Watershed (outlined in yellow). However, the state contributes 29% of the NO_3^- on average.

The Iowa Nutrient Reduction Strategy, created in 2012, identifies several practices that reduce nitrate from point and nonpoint sources. The strategy intends to reduce nutrient loading 45% from baseline levels (Iowa nutrient reduction strategy 2017). The voluntary nonpoint source strategy aims to guide land owners and farm operators wanting to reduce nitrogen and phosphorus delivery from farm fields to the stream network with management (fertilizer rate reduction, nitrification inhibitor, side dressing N, cover crops, and reduced tillage), land use (extended crop rotations, energy crops, and land retirement), and edge-of-field practices (wetlands, bioreactors, buffer strips, grassed

waterways, saturated buffers, and blind inlets) (Iowa nutrient reduction strategy, 2017). Despite these efforts, nitrate loads from Iowa continue to increase (Jones et al. 2018b).

Increasing nitrate concentrations and loads in Iowa are alarming, considering significant ongoing statewide funding and efforts to decrease surface water nitrate. Previous studies have quantified nitrate trends at high temporal resolution over extended periods of time, giving consideration to varying seasonal and yearly precipitation (Jones et al. 2018a.; Jones et al. 2018b.; Jones et al. 2018c.; Jones et al. 2018d.). While studies that accurately quantify nitrate loads are necessary, they often lack the spatial resolution needed to identify the best locations to focus efforts to implement nutrient removal practices. The motivation of our research is to better understand spatial dynamics of surface water nitrate transport in the Iowa River Basin and Storm Lake. We hope that future precision nutrient management based on this and similar studies can help reverse increasing nitrate loading trends in Iowa and elsewhere.

1.2 Objectives

To identify subwatersheds that contributed high proportions of nitrate (NO_3^-) and provide decision makers with data necessary for precision nutrient management practices, we collected water quality data at high spatial resolutions using traditional and novel sampling methods. We intended to provide spatial water quality data for the Iowa Watershed Approach (IWA) project prior to management practice implementation. Specifically, this work focused on the Iowa/Cedar River Basin and Storm Lake, IA. Several IWA watersheds, including the Middle Cedar River, Clear Creek, English River, and North Raccoon River were assessed. We sought to compare spatial differences in

water quality and nutrient transport within these watersheds and explored potential causes of any spatial heterogeneity. We also aimed to challenge traditional grab sample methods by assessing the error associated with NO_3^- load estimates when samples are collected at varying time scales.

1.3 Overview

Field measurements were conducted and instrumentation was developed between the summers of 2017 and 2018. We explored spatial and temporal nitrate and phosphate concentrations in the Clear Creek and English River watersheds using traditional grab samples in the summer of 2017. Then we designed a boat-deployed water quality sensor system in the winter of 2017-2018 and measured water in the Iowa/Cedar River watershed and Storm Lake, IA with the system during the summer of 2018. Chapter 2 outlines spatial patterns of nitrate and phosphorus concentrations in Clear Creek and the English River. A study relating temporal resolution of samples to the accuracy of nitrate load estimates in Iowa streams is outlined in Chapter 3. The production of a boat-deployed continuous water quality measurement system is outlined in Chapter 4, and the data collected with the system on the Iowa River, Cedar River, and Storm Lake is described in Chapters 5 and 6. The thesis is summarized in Chapter 7.

CHAPTER 2: EVALUATION OF WATER QUALITY IN THE ENGLISH RIVER AND CLEAR CREEK USING GRAB SAMPLES

2.1 Motivation

The Iowa Watershed Approach (IWA) is a project funded by the United States Department of Housing and Urban development in 2016. The primary objective of the IWA is flood risk reduction, but a secondary goal of the project is water quality improvement. The English River and Clear Creek are two watersheds involved with the IWA and are located in the Iowa River Watershed (Fig. 2.1). To provide IWA watershed coordinators high spatial resolution water quality data before IWA practices were implemented, we collected dense grab samples along the English River and Clear Creek. Our water quality samples also provided a baseline from which water quality improvements could be evaluated after implementing IWA practices.

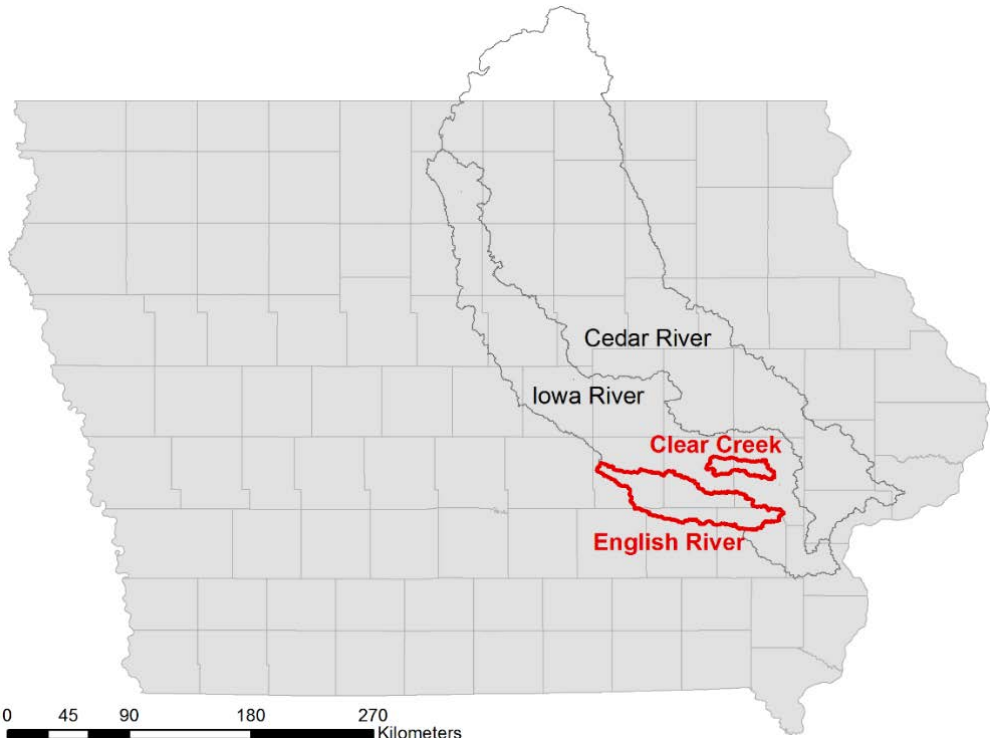

Figure 2.1: Clear Creek and the English River (highlighted in red) are located in the Iowa River Basin and contribute flow to the lower Iowa River, upstream of the Cedar River confluence.

2.2 Methodology

We chose sampling locations on the English River and Clear Creek watersheds based on accessibility, drainage area, and potential point source pollution from urban areas. We sampled 35 locations in the English River watershed (Fig. 2.2) and the 40 locations in the Clear Creek watershed (Fig. 2.3). Sampled subwatersheds on the English River averaged 47 km^2 across the 1656 km^2 watershed. The Clear Creek watershed is 266 km^2, so we were able to sample subwatersheds of only 6.7 km^2 on average.

Our sampling protocol took into account the potential changes in nutrient concentrations, temperature, and salts at temporal scales less than one day (Brauer et al. 2009). To minimize impacts of temporal water quality dynamics in the stream, we sampled each watershed in less than five hours. To collect samples as efficiently as possible, we sampled under bridges. We parked safely near the bridge and lowered a bucket from the bridge into each stream to collect water. Temperature, specific conductivity, and pH were immediately measured at the stream with a YSI Professional Plus sensor. Additionally, subsamples were stored in 250 mL HDPE bottles and cooled to test nitrate and orthophosphate concentration in a lab within 24 hours.

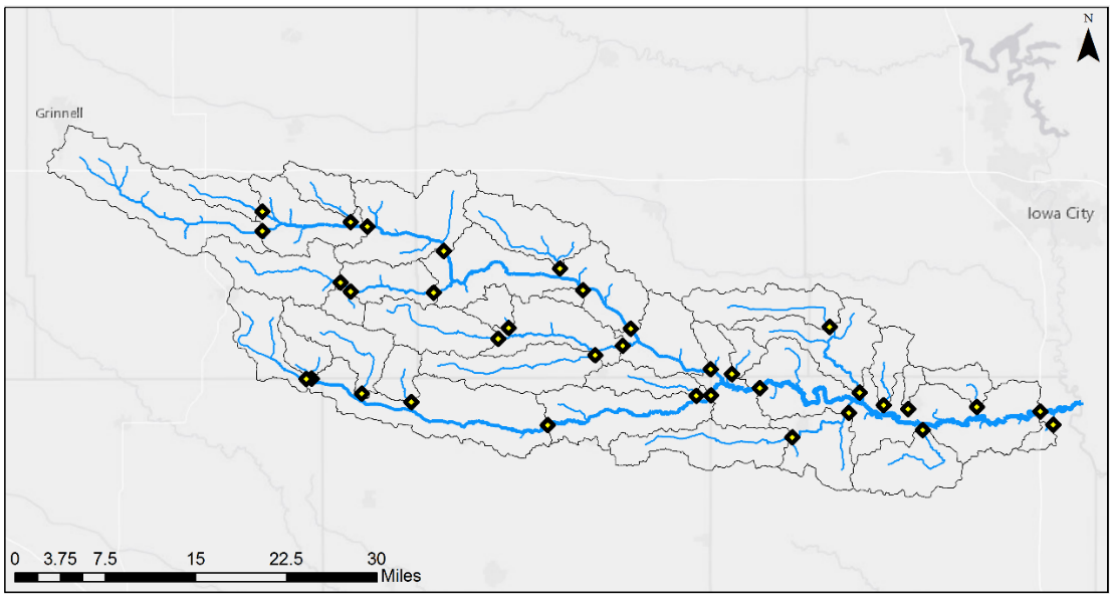

Figure 2.2: Sampling Locations in the English River Watershed and the watershed that drains into each point. Subwatersheds averaged 47 km^2.

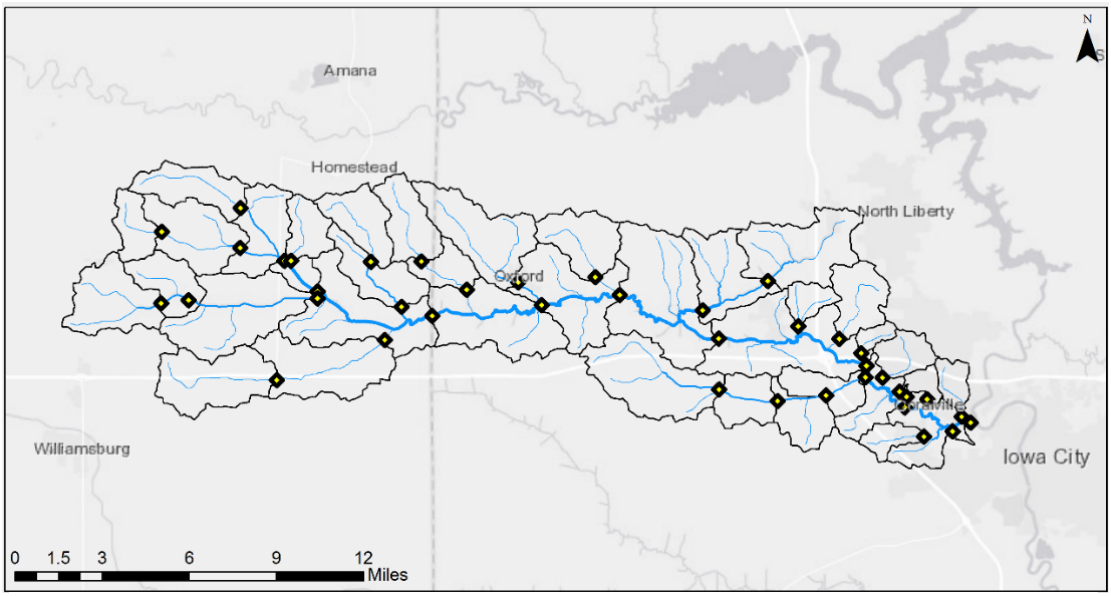

Figure 2.3: Sampling Locations in the Clear Creek Watershed and the watershed that drains into each point. Subwatersheds averaged 6.7 km^2.

We used a Nitratax Plus sc with a 1 mm path length to measure nitrate concentrations for each subsample. We measured samples in duplicate and accepted the value if the they agreed to within 0.1 mg L^{-1}. Orthophosphate concentrations were measured with a Phosphax sc Phosphate Analyzer. We measured filtered samples in duplicate and accepted them if the results agreed to within 0.02 mg L^{-1}.

We attempted to sample each watershed every two weeks. However, small changes were made due to staffing scheduling conflicts. Samples were collected on 6/2/17, 6/15/17, 6/29/17, 7/13/17, 7/27/17, and 8/10/17 on the English River and 6/22/17, 7/6/17, 7/18/17, 7/31/17, and 8/17/17 on Clear Creek. The summer of 2017 was unusually dry in Southeast Iowa, causing several of the small tributaries to stop flowing or dry completely during the late July and August samples.

2.3 Land Use and Slopes

The majority of land in the state of Iowa is devoted to corn and soy production. The production of corn and soy constitutes a large proportion of Iowa's economy, but is also associated with elevated nitrate concentrations within streams that drain this agricultural land (Schilling and Libra, 2000). Highest corn and soybean land use on the English River is in the Deer Creek Watershed and the headwaters in the western part of the watershed (Fig. 2.4). Highest corn and soybean land use on Clear Creek is in the headwaters, Deer Creek, and Buffalo Creek (Fig. 2.5). Additionally, manure from livestock can contribute nutrients to streams. Manure releases nitrate, dissolved in water, and phosphorus, often transported with soil particles (Carpenter et al, 1998). The English River has more animal feeding operations and, consequently, a greater potential for manure application in the watershed (Fig. 2.6; Fig. 2.7). Confinement density is one per 11 km^2 in the English River watershed and one confinement per 52 km^2 in the Clear Creek watershed. We assumed manure inputs to the watersheds remained within a few km radius of each confinement.

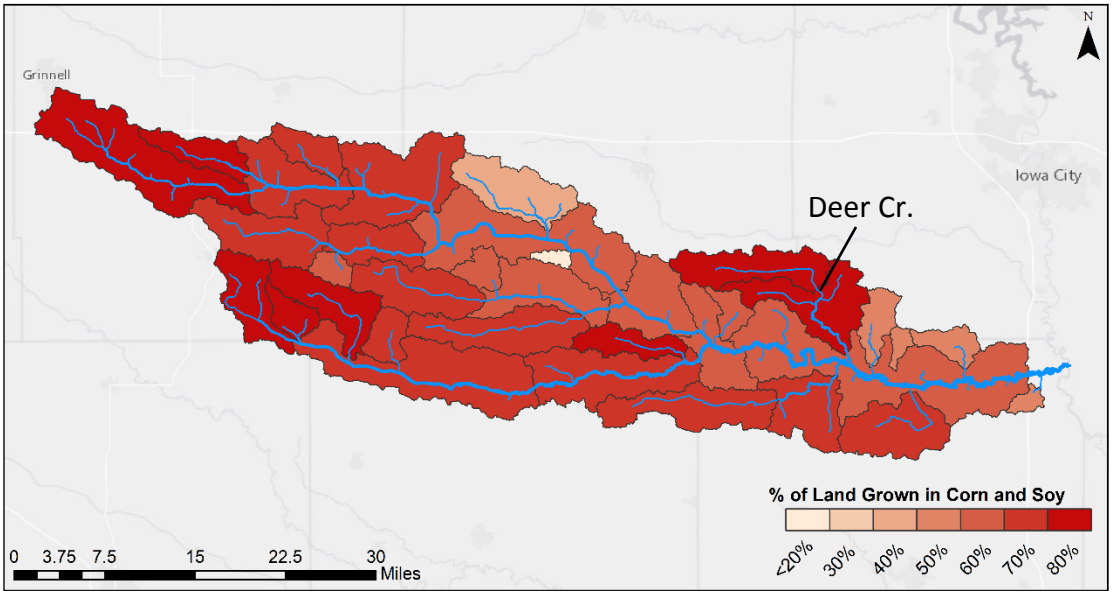

Figure 2.4: Land use in English River subwatersheds displaying the percentage of land devoted to corn and soybean production from 2009 IDNR land use data.

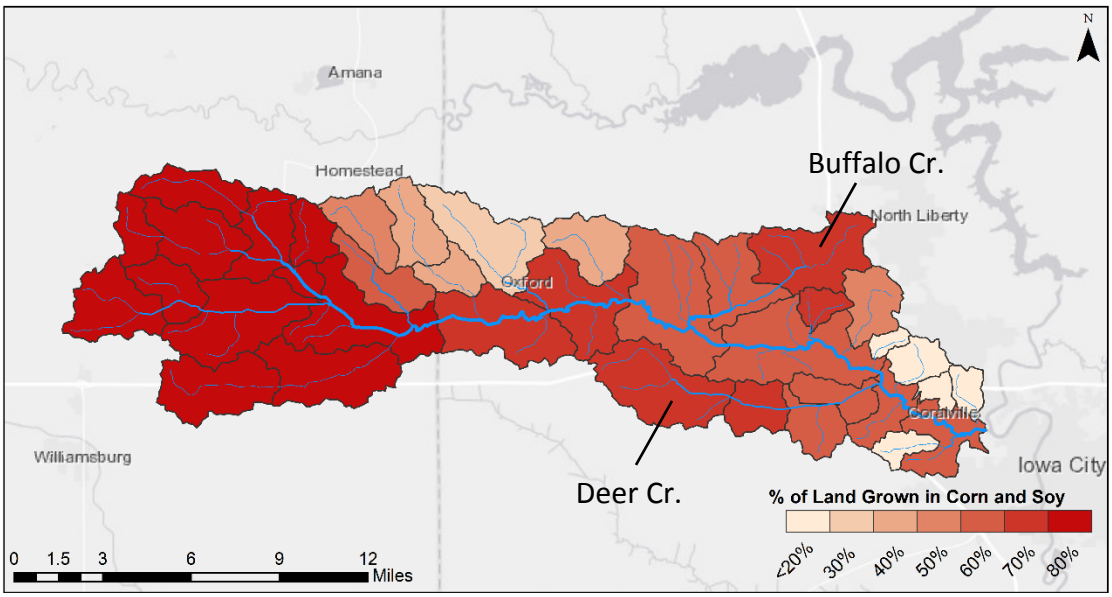

Figure 2.5: Land use in Clear Creek subwatersheds displaying the percentage of land devoted to corn and soybean production from 2009 IDNR land use data.

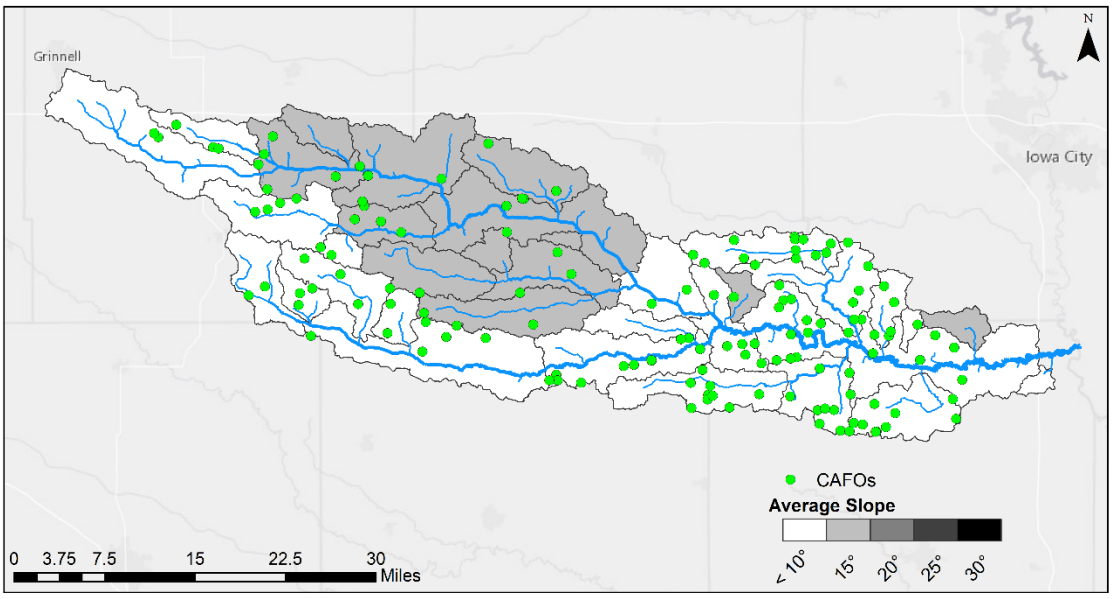

Figure 2.6: Average Slopes of English River subwatersheds and the location of permitted confined animal feeding operations (CAFOs).

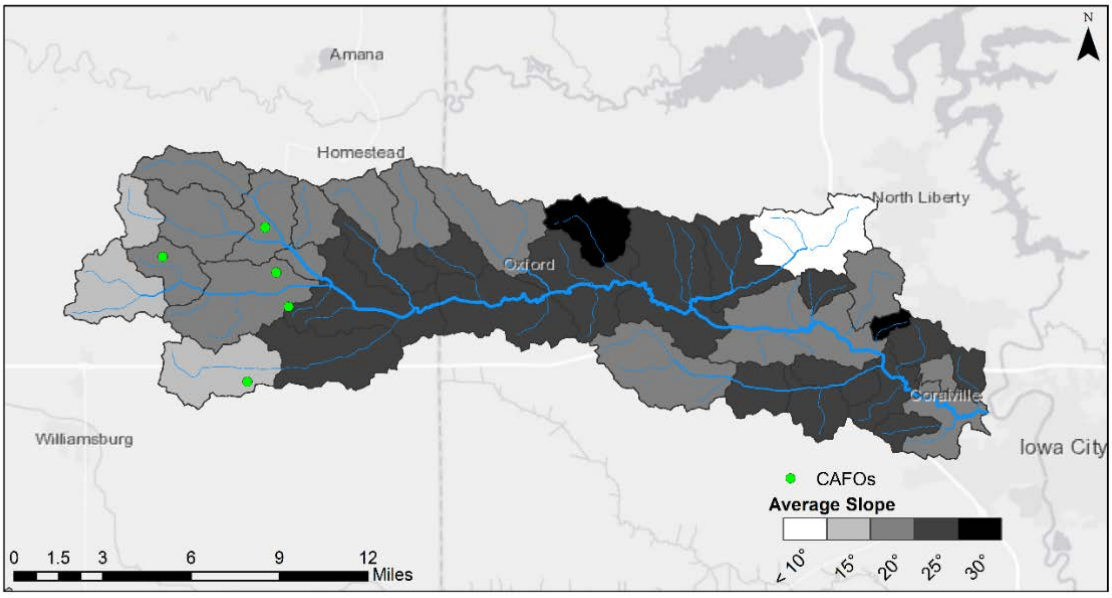

Figure 2.7: Average Slopes of Clear Creek subwatersheds and the location of permitted confined animal feeding operations (CAFOs).

2.4 Results and Discussion

English River NO_3^-N concentrations varied across the watershed (Fig. 2.8). Highest average NO_3^-N concentrations, exceeding 10 mg L^{-1}, were observed in the Deer Creek watershed and Dugout Creek, a small watershed in the headwaters of the North English River (Fig. 2.8). Higher NO_3^-N concentrations were observed across the western headwaters of the North English River and South English River, Camp Creek, and Lime Creek. Lower NO_3^-N concentrations were observed in the central portion of the watershed and in main channel subsamples. Our results suggest future nitrate reduction efforts focus on the headwaters of the North English and South English Rivers, Deer Creek, Camp Creek, where average NO_3^-N concentrations were highest.

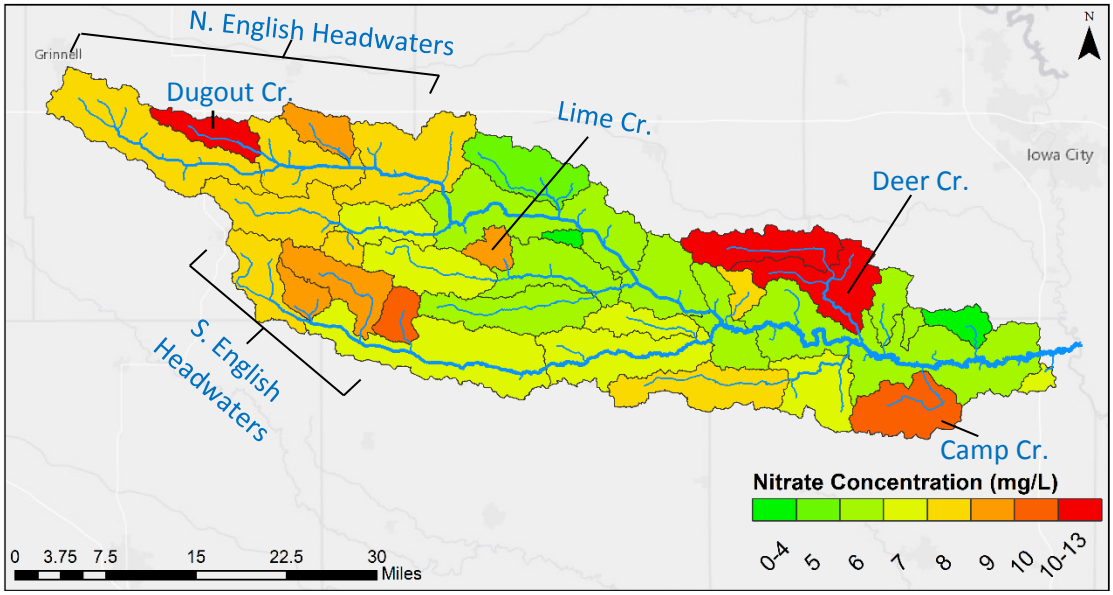

Figure 2.8*:* Average nitrate concentrations in the English River watershed from sampling on 6/2/17, 6/15/17, 6/29/17, 7/13/17, and 7/27/17. Samples collected on 8/10/17 were excluded due to the lack of flow at several locations.

High NO_3^-N concentrations were observed in the headwaters of the Clear Creek watershed (Fig. 2.9). The southwest portion of the watershed averaged over 10 mg L^{-1} NO_3^-N in July, while the tributaries on the east side of the watershed averaged less than four mg L^{-1} NO_3^-N. Deer Creek was the exception, where average NO_3^-N concentrations

were almost 9 mg L^{-1}. These observed differences in NO_3^-N concentrations follow the rural to urban gradient that is present in the Clear Creek watershed. The headwaters, to the west, are dominated by rural landscape. The cities of Tiffin, Coralville, and Iowa City occupy the eastern third of the watershed. To reduce overall nitrate loads within Clear Creek, our data suggests nutrient management efforts should focus on the land dominated by row crop production in the headwaters. Specifically, we suggest focusing efforts in Iowa County and in Deer Creek.

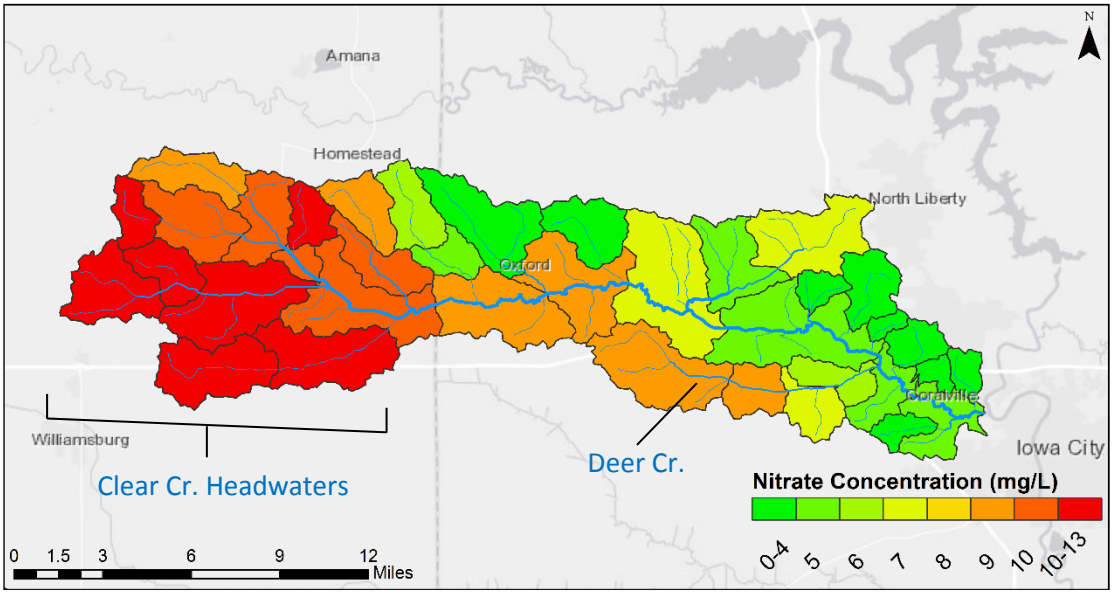

Figure 2.9: Average nitrate concentrations in the Clear Creek watershed from sampling on 7/6/17, 7/18/17, and 7/31/17. Samples collected on 8/17/17 and 8/28/17 were excluded due to the lack of flow at several locations.

Interestingly, we observed higher NO_3^-N concentrations in the Clear Creek headwaters compared to the English River headwaters. Both areas are characterized by high corn and soybean production (Fig. 2.5 & 2.6). However, we observed higher conductivity in the Clear Creek headwaters than the English River headwaters (Fig. 2.13 & 2.14). Higher SPC may indicate higher influence of tile drainage in the Clear Creek. If

so, tile drainage likely contributes to higher stream NO_3^-N in Clear Creek compared to the English River (Arenas et al. 2017)

Nitrate concentrations in Iowa streams are correlated to the proportion of the watersheds that are grown in corn and soybeans (Schilling and Libra 2000). Schilling and Libra (2000) discovered this correlation at watershed scales ranging from 47 km^2 to 2774 km^2. Our data also suggests a correlation between row crop production and riverine NO_3^-N concentrations. Our results are consistent with Schilling and Libra (2000), but at a smaller watershed scale. Our studied watersheds ranged from 1.3 km^2 to 164 km^2 with an average drainage area of 26 km^2. Despite the smaller watersheds, we observed a similar

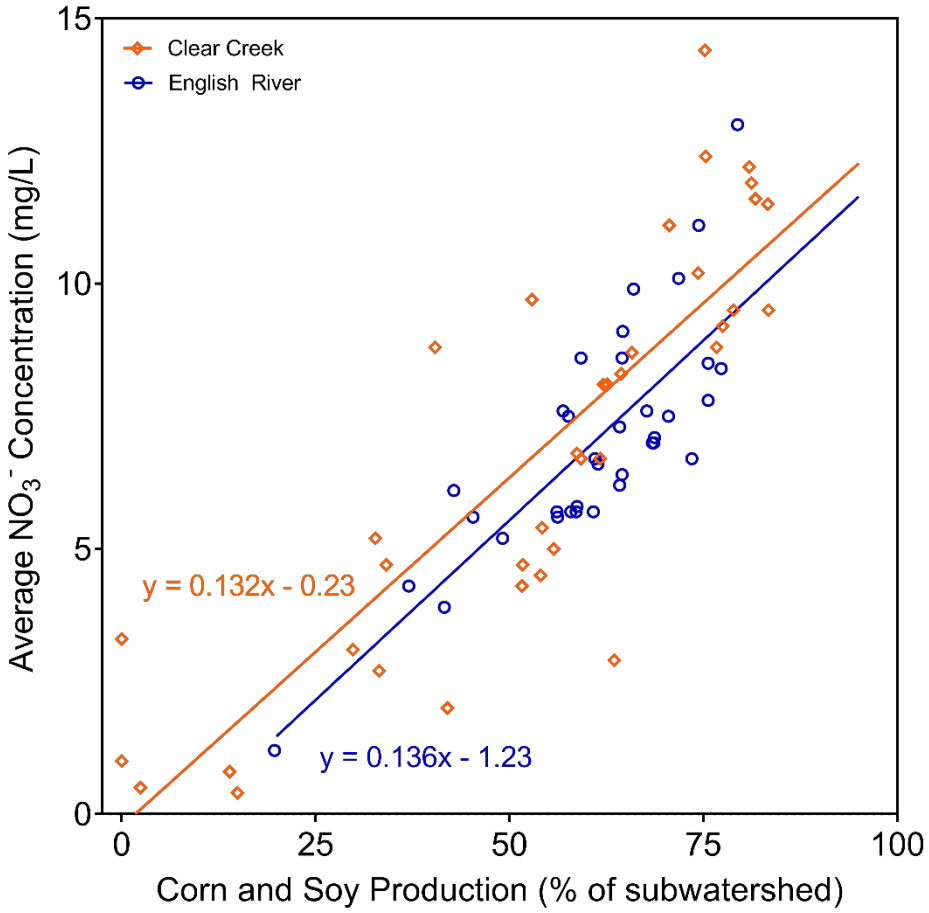

Figure 2.10: Average NO_3^-N concentrations from Clear Creek and English River subwatersheds compared to the percentage of corn and soy grown in those watersheds.

regression (slope = 0.132 and 0.136) compared to Schilling and Libra (2000) (slope = 0.1077 and 0.1113).

Dissolved phosphorus, or orthophosphate, is the only form of phosphorus available for biotic uptake, even though phosphorus attached to sediment is often more abundant (Correll, 1998). Plant available phosphorus is often the limiting nutrient for plant and bacterial growth in freshwater systems. Higher concentrations of available phosphorus allow intense freshwater algal blooms during summer months (Howarth and Marino, 2006)

Orthophosphate concentrations were similar across the English River with a few exceptions (Fig. 2.11). Three small subwatersheds on the northeast corner of the watershed had consistently high orthophosphate concentrations, while the rest of the watershed had average concentrations below 0.2 mg L^{-1}. Concentrations of CAFOs are similar in these subwatersheds compared to others (Fig. 2.6). Point sources such as the

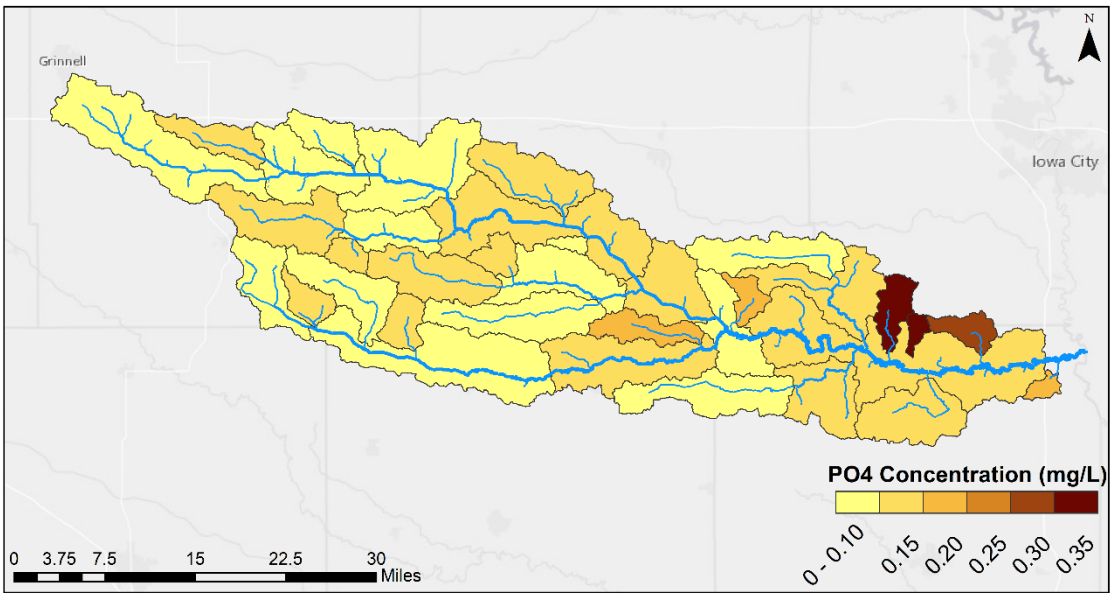

Figure 2.11: Average PO_4^- concentrations in English River subwatersheds. Samples were collected on 7/13/17, 7/27/17, and 8/10/17.

wastewater effluent from Kalona Creamery or individual septic systems may contribute to these elevated orthophosphate concentrations, but further exploration would be needed to pinpoint the exact source.

None of the Clear Creek subwatersheds exceeded orthophosphate concentrations of 0.2 mg L^{-1}, but 33/38 exceeded 0.1 mg L^{-1} (Fig. 2.12). Highest orthophosphate concentrations were scattered, but the lowest concentrations were consistently observed in small creeks draining urban watersheds in Coralville, North Liberty, and Tiffin.

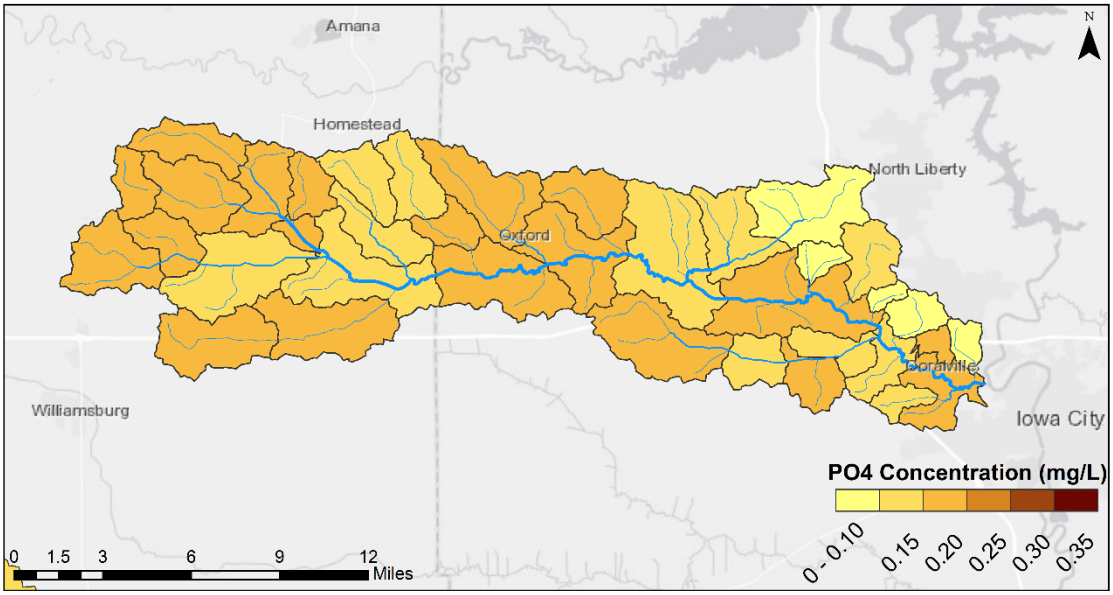

Figure 2.12: Average PO_4^- concentrations in Clear Creek subwatersheds. Samples were collected on 7/6/17, 7/18/17, and 7/31/17.

Average specific conductivity in the English River watershed was relatively consistent across all subwatersheds tested (Fig. 2.13). With the exception of Little Creek, the lowest average SPC reading was 464 µS cm^{-1} and the highest was 621 µS cm^{-1}. Little Creek had an average conductivity of 736 µS cm^{-1}. Differences between Little Creek and the rest of the watershed include two CAFOs located near the sample location and Cox Sanitation and Recycling Inc., located in the headwaters of Little Creek. If the elevated conductivity is the result of point sources, it is likely one of these few operations.

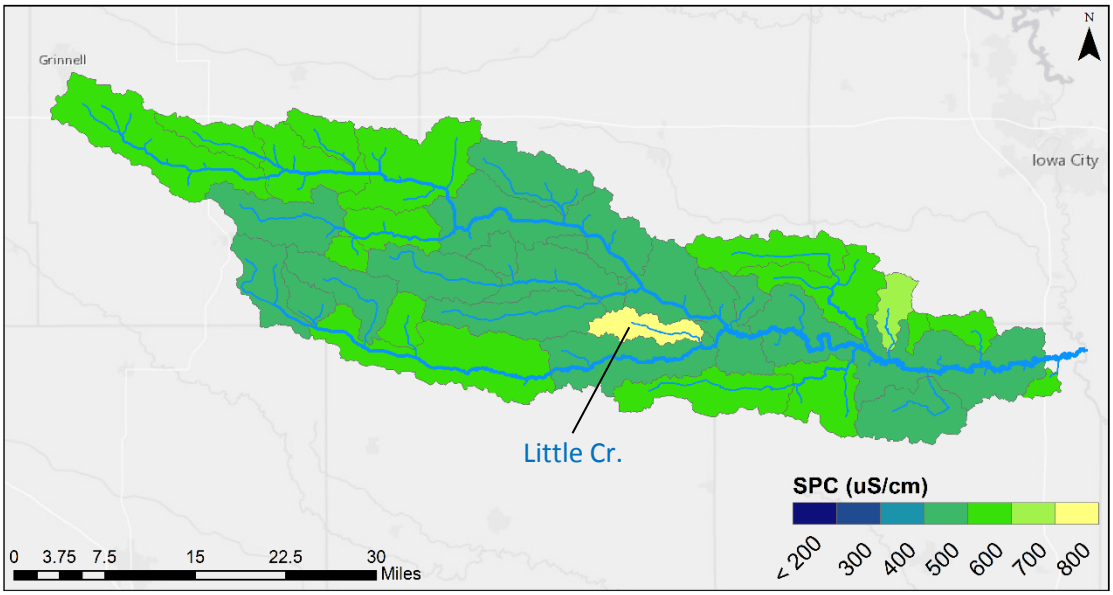

Figure 2.13: Average specific conductivity in English River subwatersheds. Samples were collected on 6/2/17, 6/15/17, 6/29/17, 7/13/17, and 7/27/17.

Highest average specific conductivity was observed in the headwaters of Clear Creek (Fig. 2.14). Conductivity was consistently above 600 µS cm^{-1} in the upstream, row crop dominated reaches of Clear Creek and below 600 µS cm^{-1} downstream of these reaches. The small urban streams varied greatly compared to the rural streams. One such stream had an average conductivity of 804 µS cm^{-1}, whereas others were below 400 µS cm^{-1}. Dr. Arthur Bettis, of the University of Iowa, mentioned there was a leaking sewage main upstream of that sample location. A point source, such as a leaking sewer, could explain high SPC observed in the stream. Our observed variable urban stream conductivity supports previous studies where urbanization increased conductivity in some streams while it decreased conductivity in others (Walsh et al. 2005). Potentially variable

point source pollutants in urban watersheds explains variable SPC we observed in urban streams in the Clear Creek watershed.

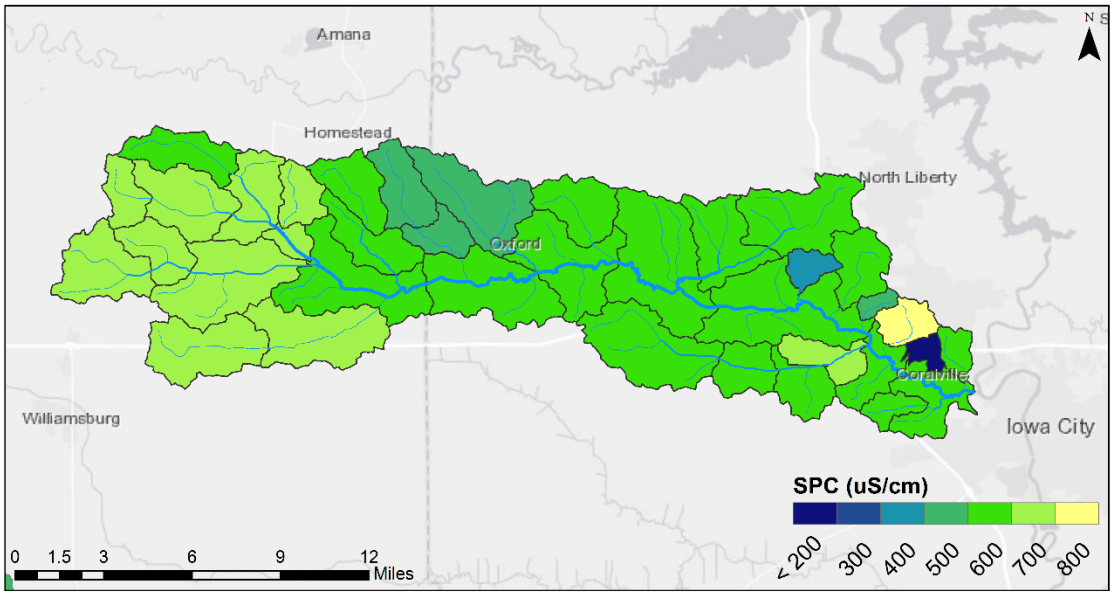

Figure 2.14: Average specific conductivity in Clear Creek subwatersheds. Samples were collected on 7/6/17, 7/18/17, and 7/31/17.

2.5 Summary

The IWA project will construct several wetlands in the English River and Clear Creek watershed by the summer of 2019. IWA watershed coordinators decided to focus efforts on the majority of the Clear Creek watershed and only a few subwatersheds of the English River (Fig. 2.15). Constructed wetlands will provide value to selected watersheds by reducing peak flows, trapping sediment, nutrient uptake, and denitrification (Cedfeldt et al. 2000; Tomer et al. 2003).

We observed low NO_3^- concentrations in the four highlighted areas in the middle of the English River watershed (Fig. 2.15), but relatively high PO_4 concentrations. Reductions of both nitrogen and phosphorus loads should result after the construction of wetlands in these areas (Cedfeldt et al. 2000; Tomer et al. 2003). The highlighted area in

the headwaters of the English River to the northwest (Fig. 2.15) will benefit from the construction of wetlands as well, because relatively high average nitrate concentrations (7.5 mg L^{-1}) were observed draining from that subwatershed in 2017. Elevated initial NO_3^- concentrations provide potential for greater nitrate reduction compared to the other watersheds in the English River where IWA wetlands will be placed.

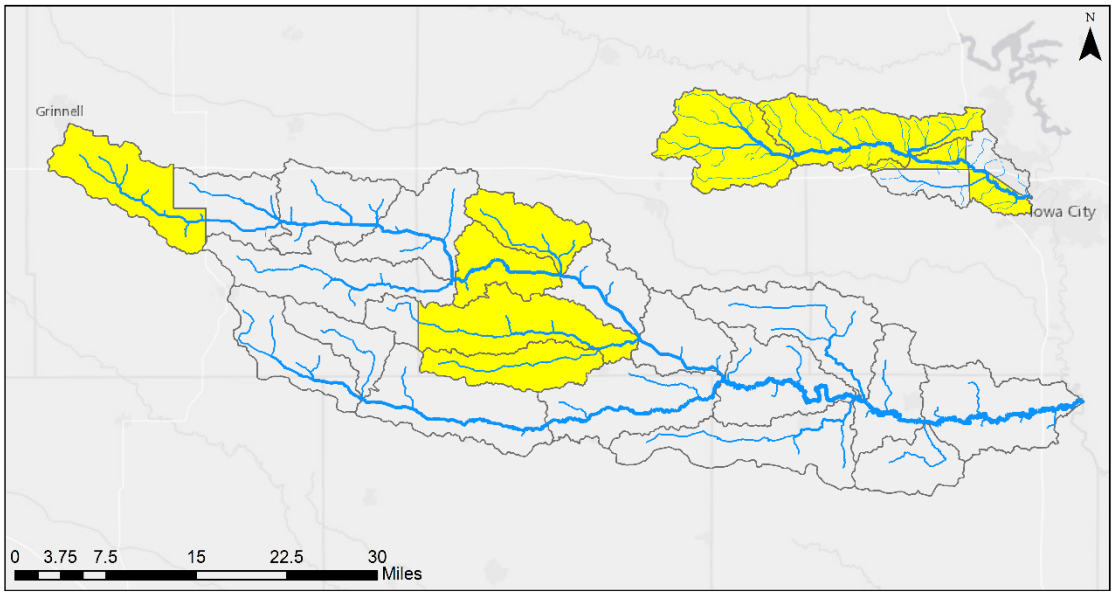

Figure 2.15: Subwatersheds where the IWA intends to create wetlands and implement other practices to hold water on the landscape and improve water quality.

Since Clear Creek is a smaller watershed than the English River, a larger proportion of the watershed will be funded through IWA. The headwaters of Clear Creek, where NO_3^-N concentrations often exceeded 10 mg L^{-1}, will benefit from denitrification as a result of installed wetlands (Schilling and Libra, 2000; Tomer et al. 2003). Furthermore, orthophosphate reductions are expected across the watershed, because biotic uptake and sedimentation in constructed wetlands will slow phosphorus transport (Cedfeldt et al. 2000).

To assess the effectiveness of IWA project implementation at a watershed scale, further sampling must occur. This study provided water quality data at high spatial

resolutions to inform decision makers, but also provides a baseline to compare NO_3^- and PO_4^{3-} concentrations after IWA project implementation.

CHAPTER 3: ERROR ASSOCIATED WITH NITRATE LOAD ESTIMATES AT VARYING TEMPORAL SCALES

3.1 Motivation

Continual monitoring of nitrate (NO_3^-N) is a vital step toward the reduction of total NO_3^-N flowing downstream. It is impossible to quantify the effectiveness of management, land use, and edge of field practices without monitoring before, during, and after practice implementation. Management practices can then be evaluated based on the results of monitoring and stakeholders can make informed decisions regarding future implementations. A movement toward high frequency measurements using *in-situ* sensors has occurred in recent years, but NO_3-N loads are also still measured traditionally with grab samples (Jones et al. 2018a.; Jones et al. 2018b.; Jones et al. 2018c.)

NO_3-N concentration and discharge must be measured if researchers wish to calculate NO_3-N load data using grab samples. Because these measurements require staffing resources, time, and money, they are often collected at coarse temporal resolutions (Bowes et al. 2009; Jones et al. 2018b.). A degree of error results when both NO_3-N concentration and discharge are measured at course temporal resolutions. Varying inputs of rainfall to the watershed alter the streamflow based on geology, drainage area, and river connectivity (Criss & Winston 2008; Higashino & Stefan 2019). Nitrate-N concentrations may vary temporally due to land use (Schilling & Libra 2000), discharge (Jones et al. 2017), density of agricultural tile drainage (Arenas et al. 2017), variable nitrogen inputs, and biotic uptake.

Our goal in this research was to determine the error resulting from NO_3-N load estimates derived from daily, weekly (every 7 days), fortnightly (every 14 days), and

monthly (every 28 days) sampling in rivers across Iowa. Iowa consists of eight distinct geological landforms varying in age, hydrology, and relief (Prior 1991). The Des Moines Lobe (DML) and Iowan Surface (IS) are rather flat, newer landscapes with less developed drainage networks compared to older glacial surfaces like the Southern Iowa Drift Plain (SIDP) and Northwest Iowa Plains (NWIP) (Prior 1991). An even steeper landscape can be found on the Paleozoic Plateau (PP), where streams have cut through porous limestone bedrock (Prior 1991). Differences in the parent material and relief of the Iowa geological regions may affect streamflow and NO_3-N variability. We made comparisons of these geological features to determine if the location of streams across Iowa's landscapes affected the error resulting from NO_3-N load estimates.

We expected streams in the IS and DML to have the lowest sampling error, because they have poor natural hydrologic connectivity and may not respond as quickly to storm events (Prior 1991). Low relief in these landforms holds storm water on the land. However, agricultural tile drainage is used on these landforms, accelerating the drainage of saturated soils. Conversely, we expected to see the highest error in the PP, where the landscape has the most relief and natural hydrologic connectivity (Prior 1991). However, stream size also affects variability of NO_3-N concentration and stream discharge. Small watersheds have greater potential for abrupt variability (Edwards et al. 2015). We anticipated larger error when estimating NO_3-N loads in smaller catchments due to faster hydrologic responses and greater temporal variability in stream flow.

We expected our results to support the error found in Bowes et al. (2009), where NO_3-N load estimate error increased with the sampling interval. However, Bowes et al (2009) did not include analysis of long-term, high temporal resolution, *in-situ* water

quality sensor data. With an increasing need for NO_3-N sampling in Iowa, this evaluation will help to quantify possible error in sampling methods so sampling protocols can be tailored to reduce error while minimizing cost.

3.2 Methods

We examined the error derived from daily, weekly, fortnightly, and monthly sampling at 17 locations (table 3.1; Fig. 3.1) across Iowa during the 2017 sampling season. Sensor deployment duration varied somewhat by location. Deployments began in January through March and, in some cases, lasted through December. The Iowa Water Quality Information System (IWQIS) measures NO_3-N concentration every 15 minutes at various locations using HACH, Nitratax Plus sc sensors. The sensors used in this study were co-located with USGS stream gauges, which provided measurements of discharge (U.S. Geologic Survey 2016). In each location, streamflow and NO_3-N concentration were continuously measured, allowing calculation of hourly NO_3-N loads.

Table 3.1: A description of location, watershed size, landform(s), and stream order where each of the 17 sensors used in this study were placed.

Location of Sensor	Watershed size (km^2)	Landform(s)	Stream Order
Clear Creek in Oxford	158	Southern Iowa Drift Plain	3
Otter Creek in Elgin	119	Paleozoic Plateau	3
Clear Creek in Coralville	254	Southern Iowa Drift Plain	4
South Fork Iowa River in New Providence	580	Des Moines Lobe	4
Squaw Creek in Ames	508	Des Moines Lobe	4
Upper Iowa River in Dorchester	2015	Paleozoic Plateau, Iowan Surface	4
Yellow River at Ion	572	Paleozoic Plateau	4
Boyer River in Logan	2201	Southern Iowa Drift Plain, Des Moines Lobe, Northwest Iowa Plains	5
Middle Raccoon River at Panora	1140	Southern Iowa Drift Plain, Des Moines Lobe	5
Soldier River in Pisgah	1049	Loess Hills, Southern Iowa Drift Plain	5
Thompson River at Davis City	1816	Southern Iowa Drift Plain	5
Wapsipinicon River in De Witt	6050	Iowan Surface	5
Cedar River in Conesville	20168	Iowan Surface, Southern Iowa Drift Plain	6
Floyd River in James	2295	Northwest Iowa Plains	6
Iowa River in Iowa City	8151	Southern Iowa Drift Plain, Des Moines Lobe	6
Skunk River in Augusta	11168	Southern Iowa Drift Plain, Des Moines Lobe	6
Des Moines River at Keosauqua	36358	Southern Iowa Drift Plain, Des Moines Lobe	7

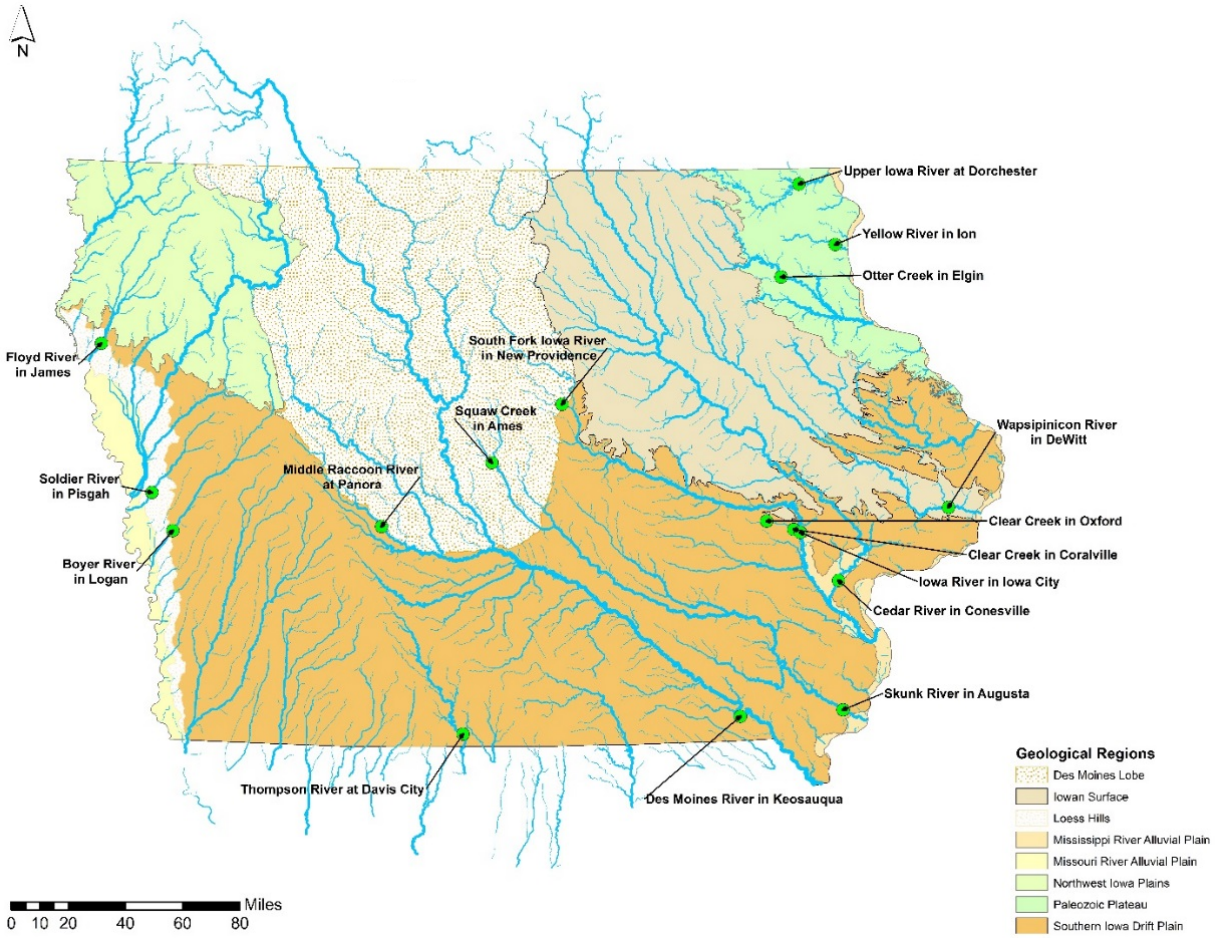

Figure 3.1: The sensor locations used for data analysis and the geologic landforms each across Iowa. All landforms are represented to some extent other than the Missouri River Alluvial Plain and a range of stream sizes are represented with these sensor locations.

Fluctuations of concentration and discharge occur at small temporal scales. However, hourly load data used in this study was the finest resolution available and was 6.5 times more frequent than the preceding United Kingdom study (Bowes et al. 2009). Similar to Bowes et al. (2009), the data was artificially dissected to simulate sampling at coarser temporal resolutions. We considered daily, weekly, fortnightly, and monthly sample protocols.

Many NO_3^- load interpolation methods exist, but we used linear interpolation. Linear interpolation is simple and was used in other similar studies (Dolan et al. 1981; Bowes et al. 2009; Schilling et al. 2017). We assumed each individual sample represented

the NO_3^- load for the entire day of sampling when we calculated NO_3^- loads using daily, weekly, fortnightly, and monthly sampling. Yearly NO_3-N load estimates were calculated for each sampling frequency (Eq. 3.1). An example of the baseline hourly data compared to daily, weekly, fortnightly, and monthly sampling estimates is shown in figure 3.2. There is potential for error with each sampling time step increase (Fig. 3.2).

Equation 3.1: $$\text{Yearly } NO_3^- \text{ Load} = \sum \left(\frac{L_t + L_{t+\Delta t}}{2} * \Delta t + \frac{L_{t+\Delta t} + L_{t+2\Delta t}}{2} * \Delta t + \cdots \right)$$

L_t = Daily NO_3^-N load at time t t = time of sample collection

Δt = time between samples

We calculated separate yearly NO_3^- load estimates for every hour of data available. For example, when we calculated NO_3^- loads with a daily sampling protocol, we calculated loads using hour 1, 2, 3, etc. every day for a total of 24 load estimates. We calculated yearly loads 24 separate times for daily samples, 168 times for weekly samples, 336 times for fortnightly samples, and 672 times for monthly samples. If the beginning or end of the sampling period did not span the entire length of the 2017 sensor deployment, we carried the first/last value until the final day of sensor deployment.

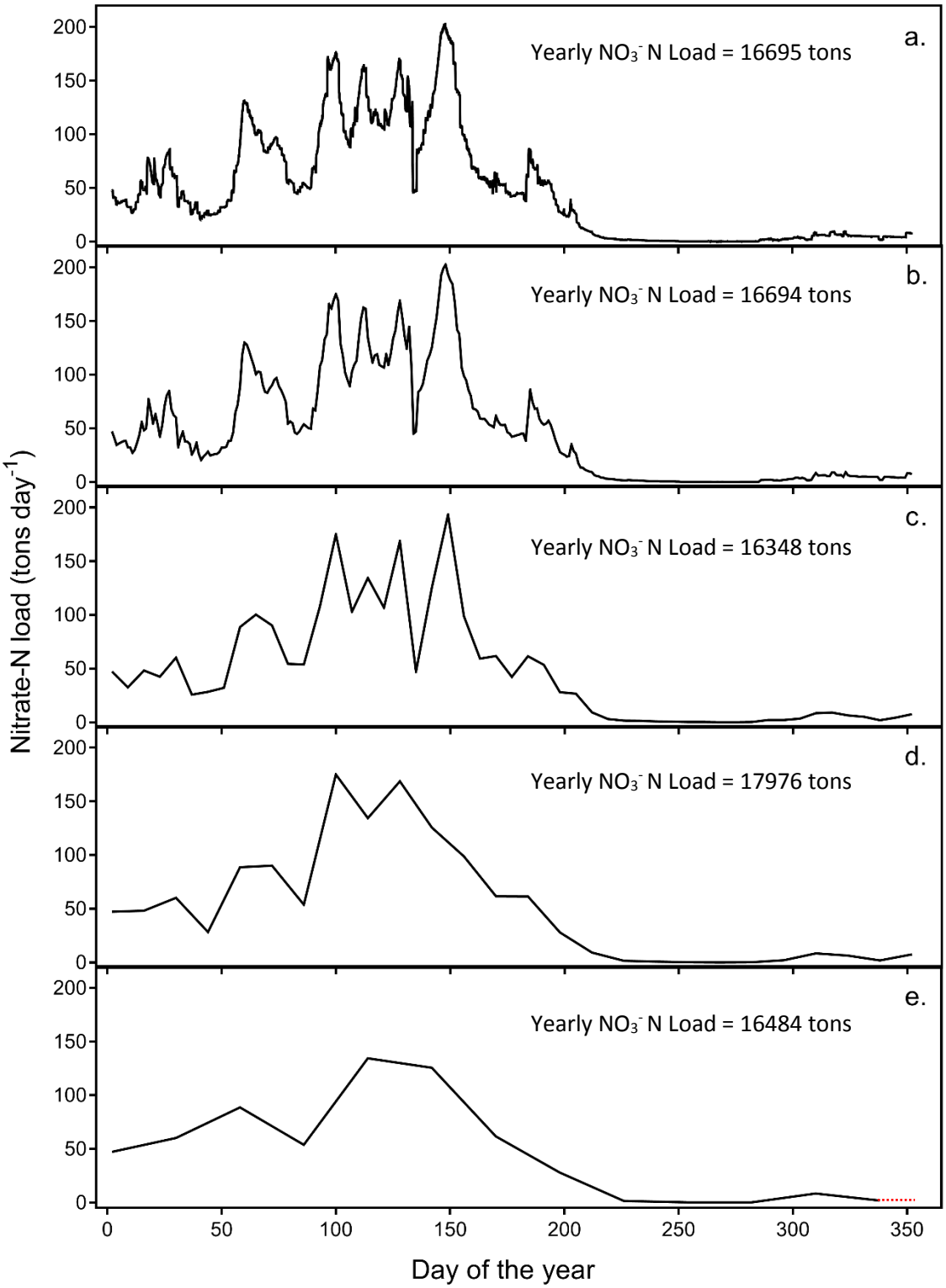

Figure 3.2: 2017 NO_3-N load measurements in the Iowa River in Iowa City displayed in terms of hourly (a.), daily (b.), weekly (c.), fortnightly (d.), and monthly (e.) collected samples. The red dashed line represents interpolated values outside the data points that match the total days sampled with hourly data.

To evaluate the precision and accuracy of the load estimates at the different sampling frequency, we used hourly load data to calculate total yearly NO_3-N load. Since hourly data was the highest temporal resolution available, we considered that the baseline. When we calculated sampling error, we assumed the baseline to be representative of the actual yearly NO_3-N load.

We calculated bias and standard deviation to evaluate how well load estimates represented the baseline load estimate, as was done in previous studies (Dolan et al. 1981; Kronvang & Bruhn 1996). Standard deviation represents the precision of each load estimate and bias shows how well the mean estimated load represents the "actual load" (Dolan et al. 1981; Kronvang & Bruhn 1996). Bias (Eq. 3.2) and standard deviation (Eq. 3.3) were used to calculate Root Mean Squared Error (R.M.S.E) (Eq. 3.4). R.M.S.E. represents how well the estimated loads represent the hourly baseline load by quantifying accuracy and precision (Dolan et al. 1981). The following equations were used to calculate standard deviation(σ), bias (β), and R.M.S.E. (L_a = Baseline load from hourly data, L_i = NO_3^- load estimate for the i^{th} estimate, and n = the number of load estimates).

Equation 3.2: $$\sigma^2 = \frac{\sum\left(L_i - \frac{\sum L_i}{n}\right)^2}{n}$$

Equation 3.3: $$\beta = \overline{L_i} - L_a$$

Equation 3.4: $$R.M.S.E.(L_i) = \sqrt{\sigma^2 + \beta^2}$$

Because baseline loads differed based on site location, we normalized R.M.S.E. by calculating the percent R.M.S.E. Percent R.M.S.E calculations allowed us to compare all locations (Eq. 3.5).

Equation 3.5: $$\%\,\mathrm{R.M.S.E.} = \frac{\mathrm{R.M.S.E.}}{\mathrm{L}_a} \times 100$$

3.3 Results and Discussion

R.M.S.E. increased as sampling frequency decreased at all sample locations (Table 2). Average R.M.S.E. greatly exceeded that found from Bowes et al. (2009). On the River Frome; fortnightly and monthly R.M.S.E. were 2.5% and 5.1%. The average fortnightly and monthly R.M.S.E. in this study was 14.0% and 24.1%, respectively. While, R.M.S.E. was not consistent across all 17 sample locations, even the location with the lowest R.M.S.E. (The Iowa River in Iowa City) had more than double the error observed in Bowes et al. (2009). Interestingly, the Iowa River in Iowa City has less variable discharge than other streams, because most of the flow is artificially controlled by the Coralville Reservoir only a few kilometers upstream.

Our results suggest the landform in which each watershed is located may influence the R.M.S.E. of NO_3-N load estimates. Highest error was observed in the PP for all sampling intervals. The SIDP and DML had comparable R.M.S.E. and the IS and NWIP had the lowest sampling error (Fig. 3.3). Flashier hydrologic regimes were observed on the steep topography in the PP compared to the other landforms. These quick responses to rain events potentially led to higher NO_3-N load estimate error, especially for daily and weekly sampling. However, streams on the PP also happened to be smaller on average compared to other landforms.

Table 3.2: % R.M.S.E. of all sensor locations at varying temporal scales.

Location of Sensor	Daily Samples	Weekly Samples	Fortnightly Samples	Monthly Samples
Clear Creek in Oxford	1.25%	9.33%	14.65%	22.28%
Otter Creek in Elgin	3.94%	16.25%	22.84%	34.71%
Clear Creek in Coralville	1.73%	11.99%	16.84%	27.75%
South Fork Iowa River in New Providence	0.42%	8.08%	28.41%	29.27%
Squaw Creek in Ames	1.22%	6.32%	18.40%	27.96%
Upper Iowa River in Dorchester	0.57%	5.43%	5.89%	15.18%
Yellow River at Ion	5.70%	19.21%	25.71%	32.32%
Boyer River in Logan	0.65%	3.57%	11.65%	20.87%
Middle Raccoon River at Panora	1.37%	6.68%	15.41%	24.88%
Soldier River in Pisgah	1.49%	6.37%	9.67%	17.11%
Thompson River at Davis City	1.80%	18.04%	31.20%	37.93%
Wapsipinicon River in De Witt	0.10%	2.26%	4.40%	20.01%
Cedar River in Conesville	0.18%	1.71%	2.66%	12.02%
Floyd River in James	0.29%	3.01%	9.59%	17.41%
Iowa River in Iowa City	0.20%	1.43%	5.07%	12.06%
Skunk River in Augusta	0.45%	4.31%	12.23%	45.11%
Des Moines River at Keosauqua	0.24%	3.05%	4.12%	13.16%
Averages	**1.27%**	**7.47%**	**14.04%**	**24.12%**

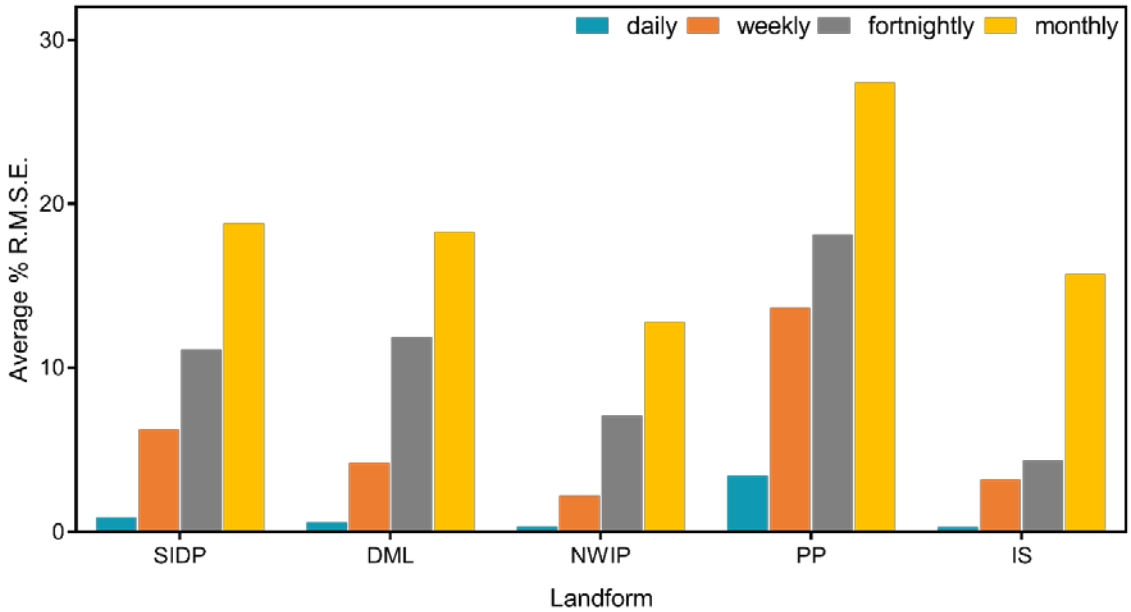

Figure 3.3: Average R.M.S.E. calculated in five major Iowa Landforms. Streams that cross boundaries of landforms were counted for every landform which it resided.

Stream size also influenced the R.M.S.E. associated with NO_3-N load estimates. Load estimate error decreased as Strahler stream order increased (Fig. 3.4) and R.M.S.E. decreased as watershed size increased (Fig. 3.5). The larger streams in this study have a slower hydrologic response to rain events (Fig. 3.6). Less error results from coarse temporal resolution sampling when there is a slower hydrologic response, because high flows are spread over the duration of days or weeks. High flows on small streams may only occur for hours (Fig. 3.6). If a sample period falls directly on a flashy peak (Fig 3.6.a.: day 176) the resulting NO_3-N load will be biased high. Slower rising and falling limbs (Fig. 3.6.b.: day148) may be captured with less loss of fidelity.

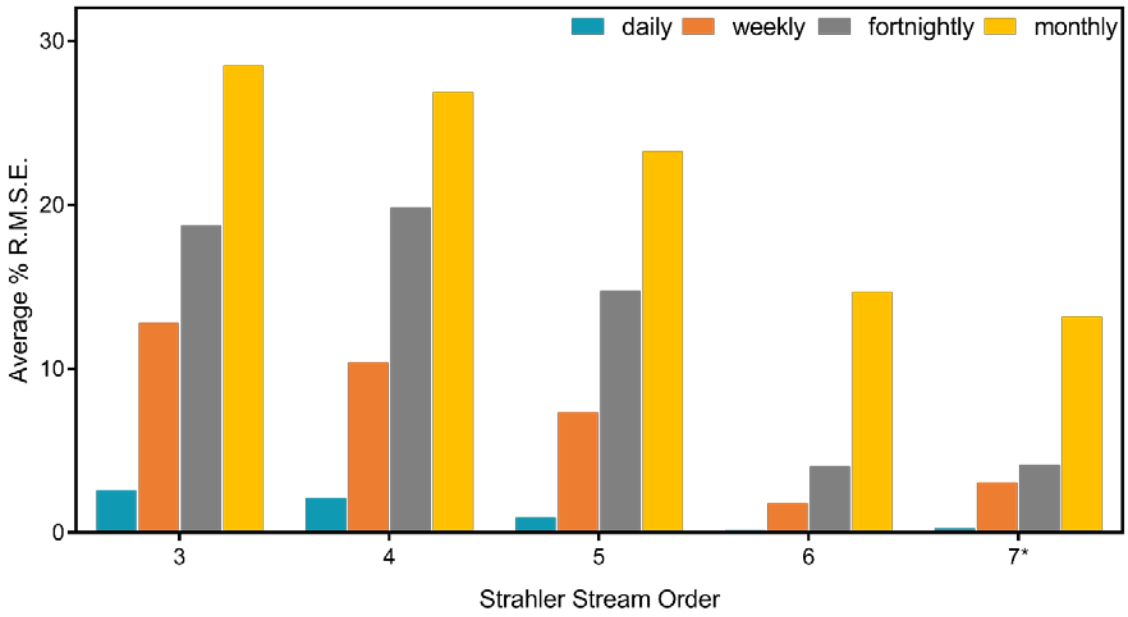

Figure 3.4: Average R.M.S.E. for daily, weekly, fortnightly, and monthly sample intervals across the various Strahler Stream Orders included in this study. Error decreased as stream order increased. Stream order = *7 is only represented by one sample.

While it is likely Iowa Landforms affect the variability of streamflow due to differences in surficial geology, stream size also impacts R.M.S.E. associated with NO_3-N load estimates. Proving one variable has a greater impact over another would require further data across geological regions and a wide range of stream sizes. However, not all landforms in Iowa host the full range of studied stream sizes.

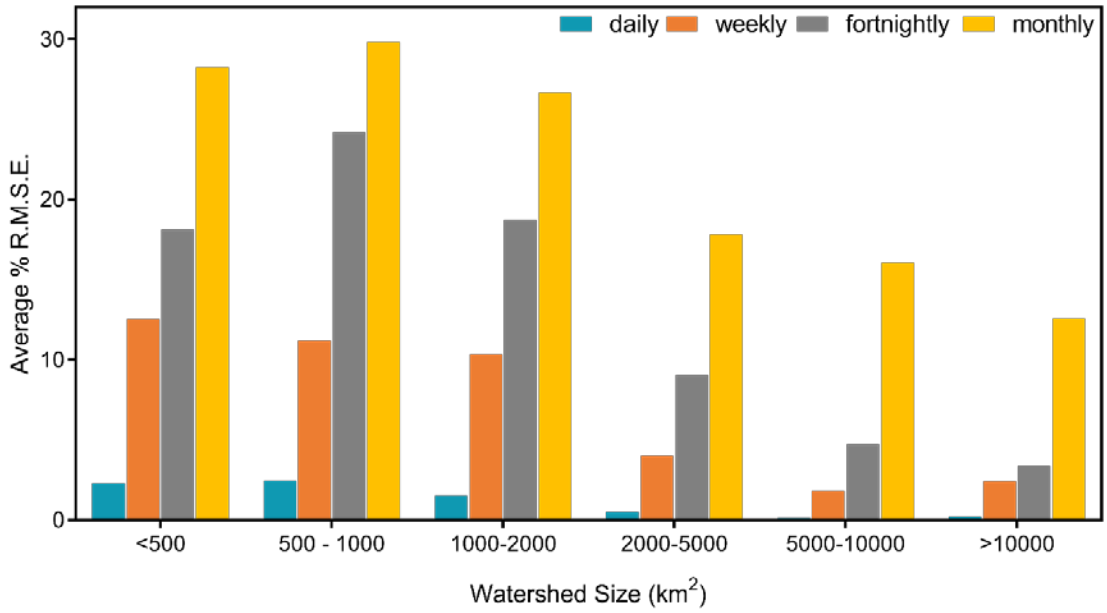

Figure 3.5: Average R.M.S.E. for daily, weekly, fortnightly, and monthly sample intervals across the various watershed sizes included in this study. Error decreased as watershed size increased.

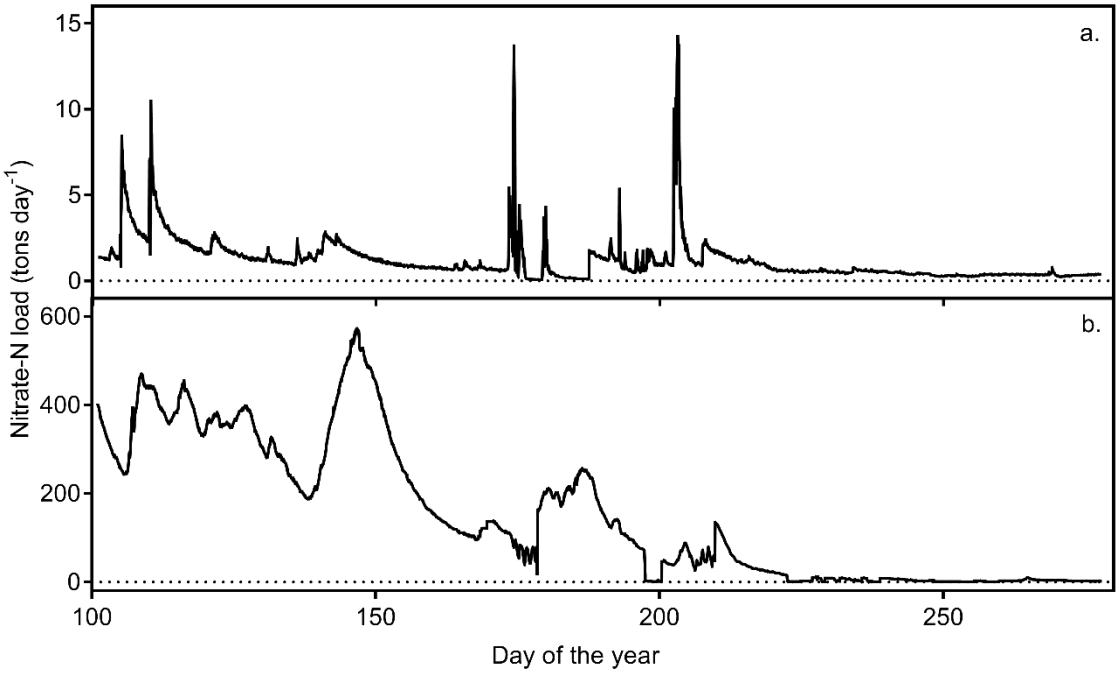

Figure 3.6: Time series of NO3-N loads produced from hourly data on a 3rd order stream (Otter Creek in Elgin (a.)) and a 6th order stream (Cedar River at Conesville (b.)) for the summer of 2017.

3.4 Summary

This study provides valuable information to those who plan to collect grab samples with the intent of calculating yearly NO_3-N loads in rivers of the Midwest United States. Collecting daily samples will provide minimal error when calculating NO_3^-N loads for all stream orders and watershed sizes. However, limited resources may not allow for daily samples to be taken. If samples are collected weekly, we recommend yearly NO_3-N loads only be calculated on streams with watersheds larger than 2,000 km^2, where our data suggests R.M.S.E. under 5%. We only recommend fortnightly sampling protocols on rivers with a drainage area larger than 5,000 km^2 if researchers wish to limit R.M.S.E. to 5%. Schilling et al. (2017) recommended monthly grab samples with linear interpolation to assess NO_3^-loads, but our data suggests high R.M.S.E. with these load estimates if samples are only collected for one year. However, monthly sampling frequency may still be sufficient if sampling duration is extended past a year as was done by Schilling et al. (2017).

CHAPTER 4: CONTINUOUS WATER QUALITY SENSOR SYSTEM DESIGN

4.1 Water Quality Sensors

Throughout most of the 20th century, researchers quantified stream pollutant loading using conventional grab sample collection followed by laboratory analysis. They then calculate pollutant loads using stream discharge measurements. In recent years, the advent of robust and accurate *in situ* nitrate sensors has generated a large body of research. Research using *in-situ* sensors has improved our understanding of stream nitrate loading (Pellerin et al. 2014; Jones et al. 2018c), in-stream processing (Heffernan and Cohen, 2010; Jones et al. 2018d), and concentration-discharge relationships (Duncan et al. 2017; Jones et al. 2017). Methods enabling continuous, boat-deployed real-time sensors to collect high spatial resolution data are an extension of these fixed, *in situ* deployments (Crawford et al 2015). This technique allows researchers to measure longitudinal water quality profiles of lotic systems. Longitudinal profiles provide insight into the sources and sinks of contaminants in streams and help us to better understand flux patterns as a whole (Crawford et al. 2015; Loken et al. 2018). The system designed by Crawford et al (2015) provided overall design concepts and methodology to create a system fit to measure water quality in Iowa's waterways.

4.2 A System Fit for Iowa

Navigating rivers in Iowa posed problems for the creation of a platform capable of collecting data with continuous boat-deployed sensors. Many of Iowa's rivers are shallow, with sand or silt substrate in the lower reaches; they are often littered with logs and rock bars in their upper reaches. Therefore, large boats cannot safely navigate stretches of Iowa's rivers and streams. We designed a sensor platform to deploy on a 14-foot jon boat equipped with a 25 hp jet drive outboard engine. This boat allows

navigation in any water deeper than 0.1 meter and is protected from impact with submerged logs and rocks. However, the vessel's small size limited the allowable weight and volume of the sensor platform.

The boat-deployed water quality measurement system included a Hach Co. Nitratax Plus sc to measure NO_3-N concentration and a Hydrolab DS5X to measure temperature, specific conductivity, pH, and dissolved oxygen. The system used a PVC intake, Tygon tubing, and a pump to deliver surface water to each sensor. The general design concept was outlined by Crawford et al (2015), but our new design remained light and compact for deployment on a small vessel. Figure 4.1 illustrates the system components and the flow of water, data, and power.

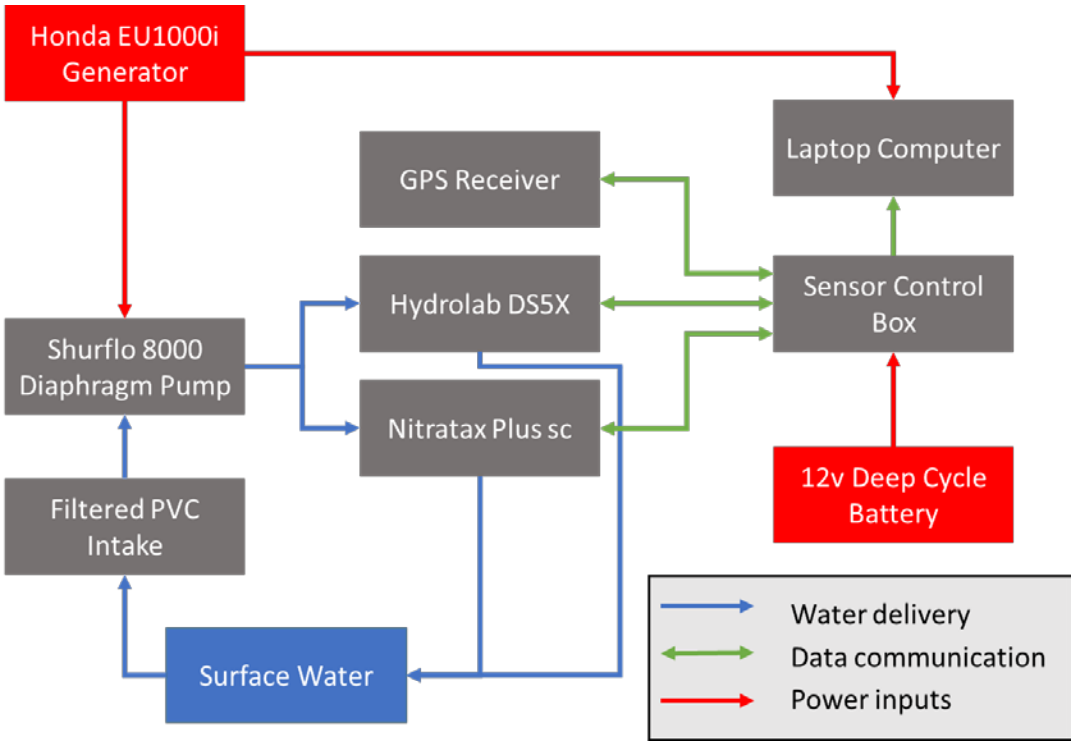

Figure 4.1: The boat-deployed water quality measurement system operates with a water-delivery system (blue), data communication system (green), and two power sources (red).

4.3 Water Delivery

We fabricated a mounting bracket using slotted strut channel to support the Nitratax Plus sc, Hydrolab DS5X, and Shurflo 8000 diaphragm pump (Fig. 4.2). The bracket held the sensors over the edge of the boat, freeing up space for the boat driver and other gear. We designed and built a water intake with PVC tubing and mounted it on the stern (Figs. 4.2 &4.3). The intake rested just below the bottom of the boat and wire mesh prevented large debris from entering the system intake (Fig. 4.3).

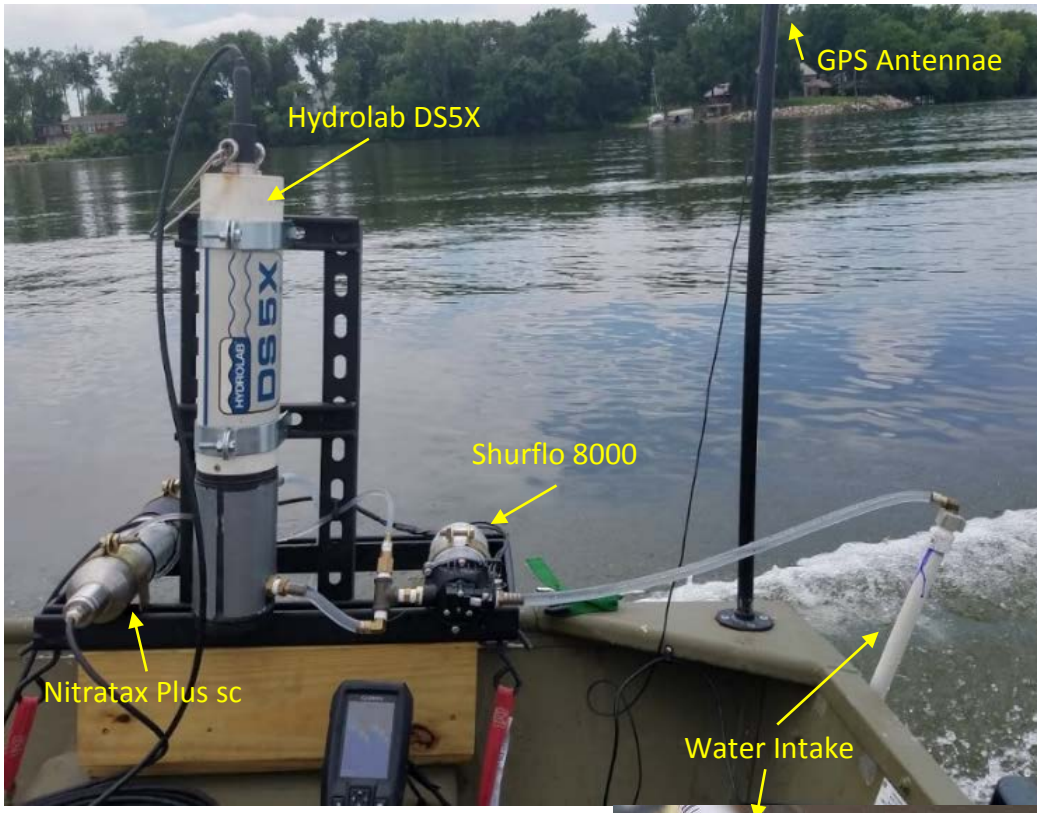

Figure 4.2: (Left) The Shurflo 8000 diaphragm pump pulls surface water through a PVC intake to the Nitratax and Hydrolab through a network of Tygon tubes. The GPS antenna is positioned directly above the intake.

Figure 4.3: (Right) The PVC intake faces forward to push water into the system at high speeds. Wire mesh protects the pump and sensors from debris. We used PVC for its elasticity, and to prevent damage from impacts with logs or rocks.

We diverted flow from the diaphragm pump into a Ø4.76 mm tube flowing to the Nitratax and a Ø12.7 mm diameter plastic tube flowing to the Hydrolab. We inserted the Ø4.76 mm tube into the factory-designed flow-through hole on the Nitratax Plus sc to create the Nitratax flow-through element (Fig. 4.4). We created a flow-through cell for the Hydrolab DS5X by installing two hose barb fittings on a standard Hydrolab calibration cup (Fig. 4.5). Water enters through the lower hose barb and exits the flow-through cell through a hose barb fitting near the top of the calibration cup.

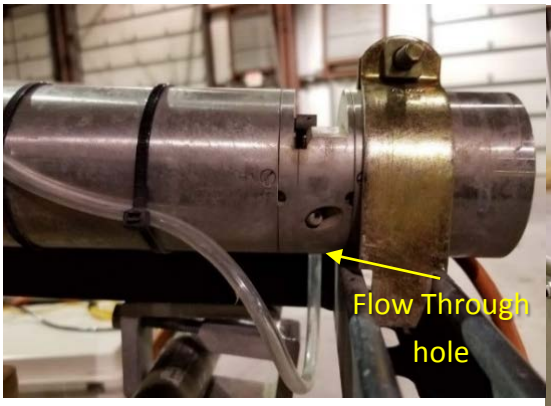

Figure 4.4: (Above) A Ø4.76 mm tygon tube was inserted into a factory designed flow through hole in the Nitratax to deliver water.

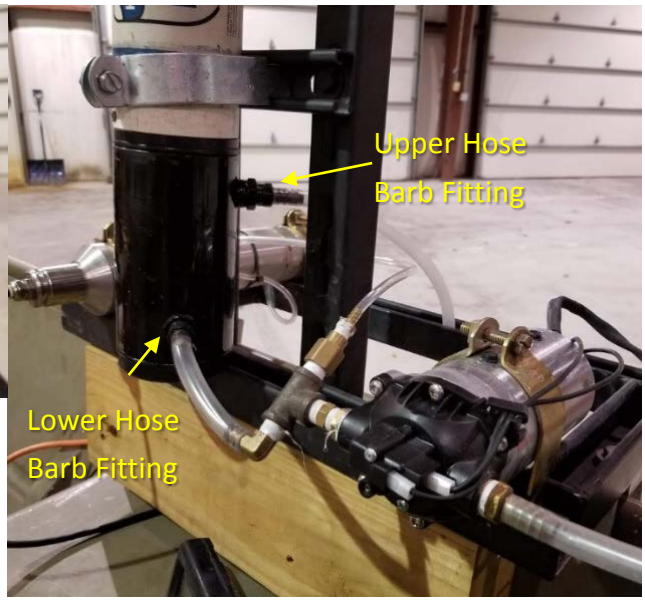

Figure 4.5: (Right) A Hydrolab flow through cell was created by inserting hose barbs into a factory issued calibration cup. Water was delivered to the lower barb and forced out of the upper barb.

4.4 Data Communication

Our system automatically stored and displayed sensor data in real time. Electrical engineers at the University of Iowa designed a control box for the sensors, which provided power to the Nitratax, Hydrolab, and a Trimble Copernicus® II GPS. Every five seconds, the control box commanded a sensor measurement and recorded the data to a micro-SD card as GPS-NEMA strings in a text file. The GPS-NEMA strings were also streamed to HYPACK software on a laptop computer, providing real-time raw NO_3^-N concentrations on a map.

4.5 Power Input

Two separate sources provided power to the system. A Honda EU1000i generator powered the Shurflo 8000 pump and laptop computer. The sensor control box used a 12v deep cycle marine battery, which was already on board, to be used as starter battery for the outboard engine. The 12v battery offered superior electrical surge protection compared to the generator.

4.6 Residence Time of the Flow-through System

In situ water-quality sensors make direct measurements as water flows by. The boat-deployed system differs from this traditional use, because water is pumped from the source through a network of tubing before entering flow-through cells around the sensors. Lag time exists between the moment water is captured and when the water-quality measurement is taken because of the network of tubing. We used residence time calculations to determine the travel time of water through our system (Crawford et al, 2015).

We calculated residence time using Equation 4.1 as performed by Crawford et al, (2015) where $\tau_w = \text{residence time}, V = \text{volume of the system}, \text{and } q = \text{the system flow rate.}$

Equation 4.1: $$\tau_w = \frac{V}{q}$$

We estimated flow rate using the average of three measurements of discharge received from the outflow pipe over time. We measured the volume of the system using the following methods; (1) We first primed the system and shut it off; (2) we then forced water through the system using compressed air and collected it; (3) we next measured the

collected water using a graduated cylinder; and (4) we used the recorded volume and estimated flow rate to calculate residence time using Equation 4.1. Flow rates, volume, and residence times for each test are shown in Table 4.1. The average residence time of the system was 7.74 seconds with a standard deviation of 0.05 seconds.

Table 4.1: Flow rate (q), volume (V), and residence time (τw) of the flow through system.

	q (L s^{-1})	V (L)	τ_w (s)
test 1	0.103	0.798	7.78
test 2	0.104	0.798	7.67
test 3	0.103	0.796	7.76
average	**0.103**	**0.797**	**7.74**

4.7 Sensor Response Time

We programmed the data logger to record measurements every five seconds even though the fastest sample rate possible for the Nitratax Plus sc is every 15 seconds. The Hydrolab DS5X, on the other hand, records the average T, SPC, DO, and pH over the period of those five seconds. Sensor lag time results from the temporal resolution of measurements and the time taken for water delivery and mixing (Crawford et al., 2015). We conducted experiments to determine lag times of the Nitratax Plus sc and Hydrolab DS5X.

We determined the response time of the Nitratax Plus SC using source water containing NO_3^- concentrations of 1.9 mg L^{-1} and 23 mg L^{-1}. We primed the flow through system with source water at 1.9 mg L^{-1} NO_3^-N. The pump delivered water through the system for several minutes. We then switched the water to the 23 mg L^{-1} NO_3^- concentration source. We recorded the time it took for the Nitratax to read the correct value. We repeated the above mentioned process, alternating source waters a total of 17

times (Table 4.2). The average response time of the Nitratax Plus sc was 21.2 seconds. The standard deviation was 6.3 seconds and the 95% confidence interval ranged from 8.6 seconds to 33.8 seconds. We used this information, during post processing, to match nitrate concentration data to location data collected approximately 20 seconds prior, which best represented the average Nitratax response time of 21.2 seconds.

Table 4.2: Response times of the Nitratax Plus sc after switching source water from 1.9 mg L^{-1} to 23 mg L^{-1} nitrate.

Test #	Response time (s)	Change in source water
1	22	low concentration to high
2	14	high concentration to low
3	28	low concentration to high
4	11	high concentration to low
5	31	low concentration to high
6	25	high concentration to low
7	29	low concentration to high
8	19	high concentration to low
9	11	low concentration to high
10	12	high concentration to low
11	23	low concentration to high
12	20	high concentration to low
13	19	low concentration to high
14	21	high concentration to low
15	23	low concentration to high
16	25	high concentration to low
17	27	low concentration to high
Average	**21.2**	

We used similar methods to determine the response time of the Hydrolab DS5X. The Hydrolab was equipped to measure temperature, dissolved oxygen, specific conductivity, and pH. We tested only one parameter for lag time since all of the probes measure at intervals <5 seconds. We used source waters at temperatures of 13°C and 32°C and alternated similar to the NO_3^- experiment. The 15 tests for lag time are shown in Table 4.3. The average response time for the Hydrolab was 18.1 seconds. The standard deviation was 1.4 seconds and the 95% confidence interval was between 15.3 and 20.9

seconds. We used this information during post processing, to match Hydrolab measurements to locations collected approximately 20 seconds prior. Location data 20 seconds prior best represented the average Hydrolab response time of 18.1 seconds.

Table 4.3: Response times of the Hydrolab DS5X after switching source water from 13°C to 32°C.

Test #	Response time (s)	Change in source water
1	18	low temp to high temp
2	17	high temp to low temp
3	19	low temp to high temp
4	18	high temp to low temp
5	17	low temp to high temp
6	19	high temp to low temp
7	15	low temp to high temp
8	18	high temp to low temp
9	18	low temp to high temp
10	20	high temp to low temp
11	16	low temp to high temp
12	20	high temp to low temp
13	18	low temp to high temp
14	20	high temp to low temp
15	18	low temp to high temp
Average	**18.1**	

4.8 Sensor Calibration

The Nitratax Plus sc and Hydrolab DS5X were calibrated differently. The Nitratax has a very long calibration life because it uses UV light absorbance. We conducted a simple experiment to compare Nitratax readings with standard solutions to verify calibration (Fig. 4.6). Recorded concentrations were within the error limitations listed by HACH and accepted for use without recalibration. During deployment, we periodically compared Nitratax readings to other sensor measurements and grab sample test results from the Iowa State Hygienic Lab to confirm proper function (Fig 4.7).

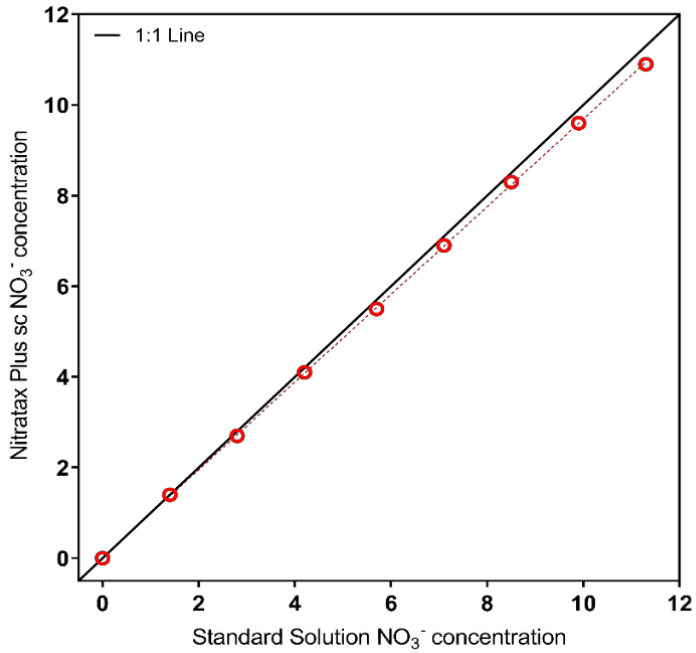

Figure 4.6: Recorded nitrate concentrations using a Nitratax Plus sc compared to standard solutions. Nitratax measurements agreed with standard solutions for all dilutions of the standard solution.

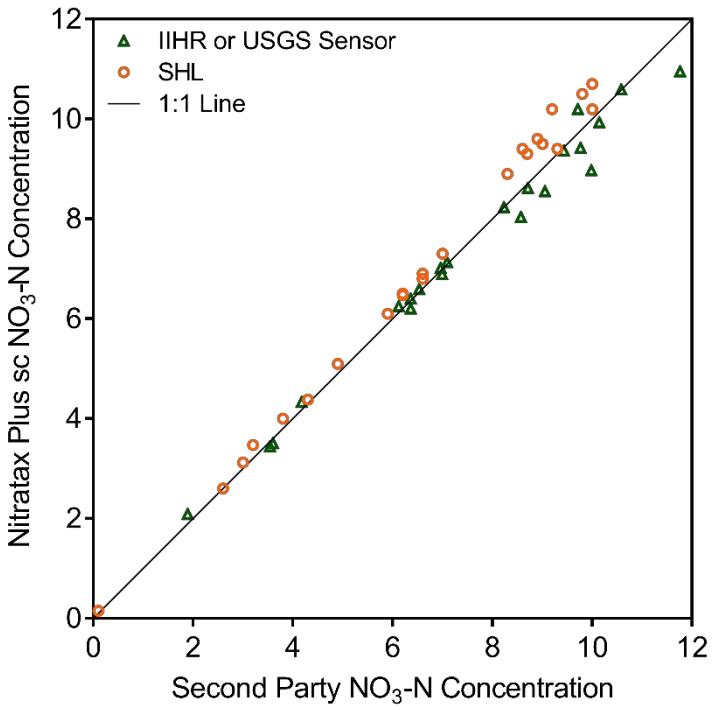

Figure 4.7: Comparison of observed NO_3-N concentrations using the boat-deployed Nitratax to NO_3-N concentrations from the Iowa State Hygienic Lab (SHL) and to IIHR and USGS in situ NO_3-N sensors. The boat-deployed sensor agreed well for all concentrations tested.

The Hydrolab DS5X needed more frequent calibrations. The manufacturer, HACH Co., recommends calibrations of SPC, DO, and pH prior to each sensor deployment. Prior to each campaign, we calibrated SPC, pH, and D.O. using OTT: Hydras 3LT software. Hydras 3LT allowed us to program the calibrated values compared to standard solutions as recommended by the manufacturer.

During SPC calibration, we first calibrated the sensor to an SPC reading of 0 µS cm^{-1}. We used air for the standard of 0 µS cm^{-1} as recommended by the manufacturer. Then we calibrated the sensor to a high standard value of 2060 µS cm^{-1}. Lastly, we checked the linearity of sensor measurements, comparing sensor readings to a standard of 445 µS cm^{-1}. If the reading was within 20 µS cm^{-1}, we accepted the sensor calibration. If linearity could not be achieved, we calibrated the upper measurement to 700 µS cm^{-1} and checked the linearity measurement again.

The Hydrolab DS5X is equipped with a temperature compensated pH probe. During pH calibration, we first calibrated the sensor to a standard solution of 7.00 pH units. Then we calibrated the sensor to 4.01 and 10.01 pH units in that order. Finally, we checked the linearity of pH measurements using a pH = 7.00 standard solution. If the linearity check agreed within 0.10 pH units, we accepted the calibration.

To calibrate D.O., we shook room temperature water for at least 60 seconds, fully saturating the water as recommended by the manufacturer. In Hydras 3LT, we typed in the measured barometric pressure at our location and calibrated the dissolved oxygen to 100% saturation.

We logged all measured values before calibration (Appendix: A1) for every calibration date. Additionally, we checked to ensure that the sensors did not drift between calibrations (Appendix: A2). We compared SPC to standards of 445 µS cm^{-1} and 700 µS cm^{-1}. If they disagreed by more than 20 µS cm^{-1}, we would have recalibrated the SPC sensor. We compared pH measurements to standards of 7.00 and 10.01 pH units. If they disagreed by more than 0.10 pH units, we would have recalibrated the pH sensor. We compared D.O. measurements to saturated solutions. If they disagreed by over 4% saturation, we would have recalibrated the D.O. sensor.

CHAPTER 5: OBSERVED LONGITUDINAL NITRATE, TEMPERATURE, SPECIFIC CONDUCTIVITY, AND PH TRENDS IN THE IOWA RIVER BASIN

5.1 Motivation

The magnitude of NO_3^-N delivery to Iowa streams is spatially variable and, at the landscape scale, largely dependent upon landform features, cropping intensity, and the cropping system. The recently glaciated Des Moines Lobe (DML) landform (Prior 1991) in north-central Iowa has low relief, extensive networks of constructed tile drainage, and constructed drainage channels to lower the water table and optimize soil moisture conditions for corn and soybean production. Loss of NO_3^-N through these drainage systems is substantial. NO_3^-N losses range from 20 to more than 60 kg ha^{-1} yr^{-1} in the DML (Tomer et al. 2003; Jones et al. 2019; Schilling and Walter 2005; Ikenberry et al. 2014). The Iowan Surface (IS) is an erosional surface and, like the DML, has low relief and is extensively tiled (Prior 1991). Yield of NO_3^-N from this area varies from 22 to 41 kg ha^{-1} yr^{-1} (Jones et al. 2018c; Schilling and Walter 2005; Drake et al. 2018). The Southern Iowa Drift Plain (SIDP) is an older, pre-Illinoisan glacial landscape with well-developed natural drainage and fewer areas that require tile drainage for crop production (Prior 1991). SIDP nitrate yields have been reported to be about half that of yields in the DML and IS (Schilling and Walter 2005; Jones et al. 2018c). Although generalities exist that well-predict NO_3^-N yield at large scales in these landforms, variable losses at small scales within these land areas occur (Schilling and Spooner 2006; Tomer et al. 2003).

Water quality samples are often collected at coarse spatial resolutions that do not capture small spatial variabilities of NO_3^-N fluxes. Rather, they capture an average contribution of the upstream watershed. Boat-deployed water quality sensors allow measurements at finer spatial scales than previously attainable (Crawford et al. 2015).

One such system was used to identify the Iowa/Cedar River Basin as a significant contributor of NO_3-N to the Upper Mississippi River (Loken et al. 2018). Due to the size and spatial heterogeneity of landforms and land use in the Iowa/Cedar Basin, all areas in the watershed should not be considered to equally contribute to NO_3^- loading at the outlet.

In this chapter, our objectives were to explore spatial (across differing landforms) and temporal (across months) differences in NO_3-N flux (concentrations, loads, and yields), temperature (T), specific conductivity (SPC), and pH in the Iowa and Cedar Rivers using novel monitoring techniques described in Chapter 4. These objectives included; (1) use of continuous, boat-deployed, real-time sampling to characterize the patterns of nitrate delivery to the Iowa-Cedar River basin (ICRB); (2) identify potential land use influences in these basins that may be affecting nitrate flux; (3) determine if nitrate is being retained in impounded areas within the basin's stream network; (4) identify longitudinal T, SPC, and pH trends in the main channels of the ICRB; and (5) identify target areas for water quality improvements with the focus on NO_3-N reduction.

5.2 Study Area

Spanning 32,506 km^2, the Iowa/Cedar River Basin (ICRB) covers approximately 20% of the land area of the State of Iowa and is the state's second-largest interior watershed (Fig. 5.1). The basin is situated across several landforms including the SIDP, DML, IS, and the Iowa Cedar Lowland (ICL) (Fig. 5.1). Most of the Cedar River watershed resides within the IS, while the Iowa River begins in the DML and flows through the SIDP. The two rivers combine near Columbus Junction and flow 47 km

through the Iowa-Cedar River Lowland, eventually discharging into the Upper Mississippi River.

Figure 5.1: The Iowa and Cedar River Basins (outlined in bold black), major tributary watersheds (outlined in thin grey), and Iowan Landforms (colored in the background) which the watersheds reside. Sampling on the Iowa River occurred from Wapello to Eldora and the Cedar River was sampled from Columbus Junction to Charles City.

5.3 Land Use

Corn and soy production dominates both the Iowa River Basin (12,100 km^2) and Cedar River Basin (20,200 km^2), with 68.1% and 76.6% of the land areas, respectively, dedicated to this crop rotation (Homer et al. 2015). Over 80% of the land is dedicated to

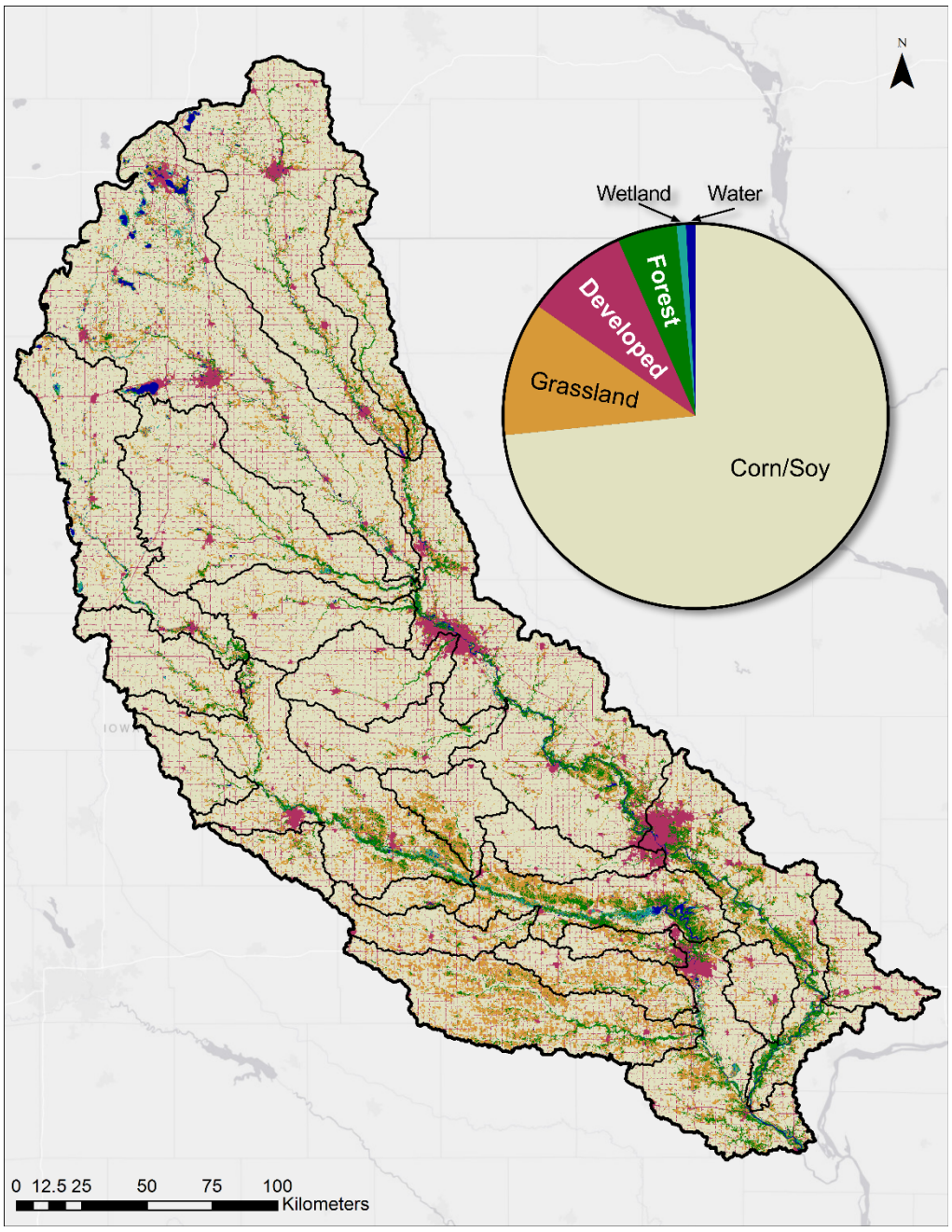

Figure 5.2: Major categories of land use in the Iowa and Cedar Rivers. This map was generated from the National Land Cover Database (Homer et al. 2015)

row crop production in the headwaters of the Iowa River as well as the South Fork of the Iowa River and Minerva Creek (Fig. 5.2). Every major tributary on the Cedar River has over 80% of the land dedicated to row crop production except the Shell Rock River and the Little Cedar River (Fig. 5.2). Less row crop land use exists in the SIDP whereas more corn and soybeans are grown in the DML and IS (Fig. 5.2).

5.4 Water Quality Data Collection

We used a boat-deployed water quality sensor system (Ch. 4) for the first time to measure water on the Iowa and Cedar Rivers. The system automatically collected NO_3^-N concentration with a Nitratax Plus sc and temperature (T), dissolved oxygen (DO), specific conductivity (SPC), and pH with a Hydrolab DS5X every five seconds as we drove a 14 ft. Jon boat upriver. We drove the safest apparent route of navigation on the rivers, which was most often the main channel of flow. Measurements were taken at speeds ≈ 24 km hr^{-1}, or one measurement every 33 meters. We also measured tributary plumes by slowing down and zigzagging laterally across the channel to capture mixing. Dense sampling near tributary plumes was only possible with moderate water depth and, if depth permitted, we navigated up tributaries beyond the influence of the main channel. Real time display of NO_3^-N concentration on the laptop was helpful, because we could identify differing plumes of water while driving and we were reassured that data were streaming in properly.

We sampled the Iowa and Cedar River four times each (Table 5.1). We sampled the Iowa River from Wapello, IA to Eldora, IA (435 river-km) while navigation on the Cedar River allowed us to sample from Columbus Junction to Charles City, IA (440 river-km) (Fig. 5.1). Three dams on the Iowa and seven on the Cedar required us to

remove and relaunch the boat using a vehicle and boat trailer. We collected measurements from sunrise to sunset on each day of sampling to minimize expected temporal changes in water quality (Brauer et al. 2009; Drake et al. 2017; Jones et al. 2018d) while maintaining safe boating conditions.

Table 5.1: Sample dates on the Iowa and Cedar Rivers for each month of sampling.

River	May	June	July	August
Iowa River	5/14/18-5/17/18	6/6/18-6/8/18	7/10/18-7/11/18	8/6/18-8/8/18
Cedar River	5/29/18-5/31/18	6/28/18-6/30/18	7/16/18-7/17/18	8/9/18-8/10/18

5.5 Discharge, NO_3-N Load, and NO_3-N Yield Estimation

We estimated discharges for over 123,000 water quality measurements collected on the Iowa and Cedar Rivers. Nine United States Geological Survey (USGS) stream gauges were located on the Iowa River and 11 on the Cedar River, providing known discharges for water quality observations made at these discrete sites (U.S. Geological Survey 2016). We estimated discharges for measured points between USGS gages using linear interpolation based on contributing drainage area of each measured point of water quality data (Eq. 5.1). We calculated NO_3^-N loads at each point based on the product of concentration and either measured or estimated discharge (Eq. 5.2). We divided NO_3^-N loads by drainage area to calculate NO_3^-N yields for each point (Eq. 5.3).

Eq. 5.1 $$Q_{est.} = Q_{USGS,US} + \frac{Q_{USGS,DS} - Q_{USGS,US}}{DA_{USGS,DS} - DA_{USGS,US}} \times (DA_n - \text{US } DA_{USGS})$$

Eq. 5.2 $$NO_3\_N \text{ Load} = [NO_3^-] \times Q_{est.}$$

Eq. 5.3 $$NO_3\_N \text{ Yield} = \frac{[NO_3^-] \times Q_{est.}}{DA_n}$$

$Q_{est.}$ = Estimated discharge at each point

DA_n = Drainage area at each point

$Q_{USGS,US}$ = Discharge at the nearest upstream USGS gauge at the time of each measurement

$Q_{USGS,DS}$ = Discharge at the nearest downstream USGS gauge at the time of each measurment

$DA_{USGS,US}$ = Drainage area at the nearest upstream USGS gauge

$DA_{USGS,DS}$ = Drainage area at the nearest downstream USGS gauge

5.6 Rainfall Quantification

Rainfall directly influences discharge and is related to stream NO_3^-N concentrations (Jones et al. 2017). We assessed rainfall on each watershed using precipitation data from PRISM Climate Group ten days prior to the second day of sampling (PRISM Climate Group 2018). We considered a ten-day period of antecedent rainfall prior to the second day of sampling, because surface water travel time for each river to the starting sampling points is approximately 9-10 days (Krajewski & Mantilla 2010). Our consideration of extended rainfall took into account travel time and the likely NO_3^-N contribution from agricultural tile drainage after a rain event (Arenas Amado et al, 2017). We chose to consider rainfall before the second day of sampling, because precipitation occurred during our first sampling day on a few occasions.

5.7 Iowa River Results

Precipitation and Discharge

Accumulated 10-day rainfall varied in time and space across the Iowa River watershed. Highest average 10-day rainfalls (38.7mm and 37.8mm) were observed in August and July and lowest average rainfall (12.8 mm) was observed in early June (Fig.

5.3). The majority of the rainfall fell on the lower half of the watershed in May and the upper half of the watershed in July and August (Fig. 5.3).

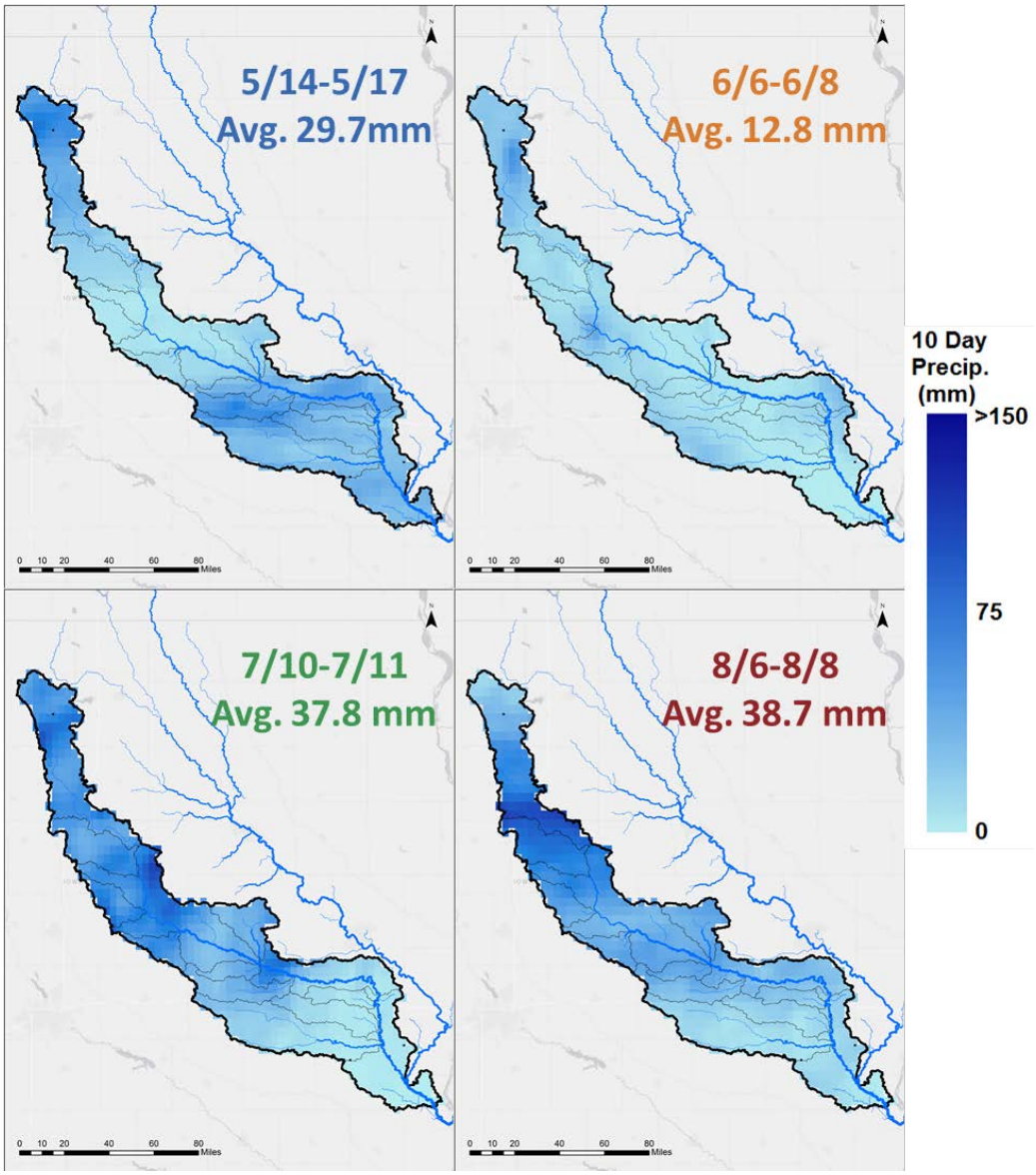

Figure 5.3: Accumulated Rainfall over the Iowa River watershed 10 days prior to the second day of sampling. Accumulated daily radar rainfall estimates in a 4 km grid from PRISM Climate Group were used to generate these four figures.

Discharge along all reaches of the Iowa River also varied in time and space. Discharge was highest in May and July and increased steadily along the length of the river (Fig. 5.4). Discharge was lowest during June and August sampling despite high rainfall in early August. During August sampling, a pop up thunderstorm dropped

significant rain near Marshalltown on 8/7/18 (Fig. 5.3). Flow nearly doubled overnight around Belle Plaine, IA because of that thunderstorm (Fig. 5.4: 225 km).

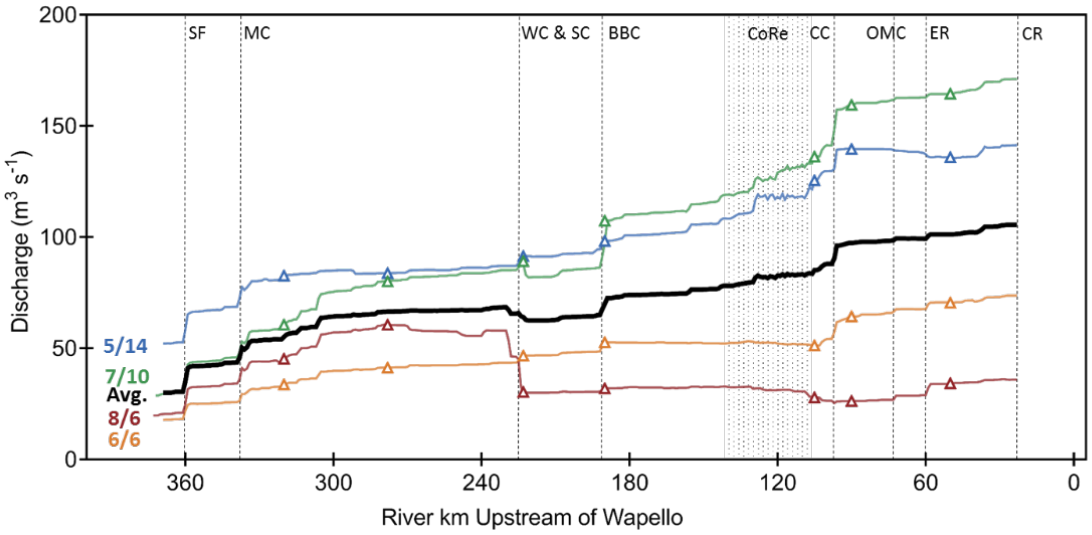

Figure 5.4: Iowa River discharge generated from interpolation of known discharges at USGS gauges along the Iowa River during sampling. Colored lines represent each sample period and the black line represents the average discharge. Dashed lines indicate tributary confluences and the dotted rectangle represents the Coralville Reservoir. Triangles represent observed discharges at USGS gauges.

Main Channel Nitrate

Highest average NO_3^-N concentrations (9.3 mg L^{-1}) and yields (11.7 kg km^{-2} day^{-1}) were observed below the South Fork confluence (Fig. 5.6) where majority of the watershed resides within the DML (Fig. 5.1). Average NO_3^-N concentration and yields decreased moving downstream through the SIDP and remained constant as the river flowed through the Iowa-Cedar Lowland (ICL). Average NO_3-N yields decreased at the confluences of Walnut and Salt Creek, Old Man's Creek, and the English River despite minimal changes in NO_3-N concentration from these tributaries. Iowa River average NO_3^-N loads remained relatively constant between the City of Tama and the confluence of Big Bear Creek and in the Coralville Reservoir. Continual NO_3^-N load increases indicate NO_3^-N inputs were present from all areas of the watershed, but the rate of NO_3^-N load increases was fastest >300 km upstream of Wapello. Major tributaries included in this

reach were the South Fork and Minerva Creek, which added NO_3-N loads of 9.7 Mg day^{-1} and 5.0 Mg day^{-1} on average (Fig 5.6).

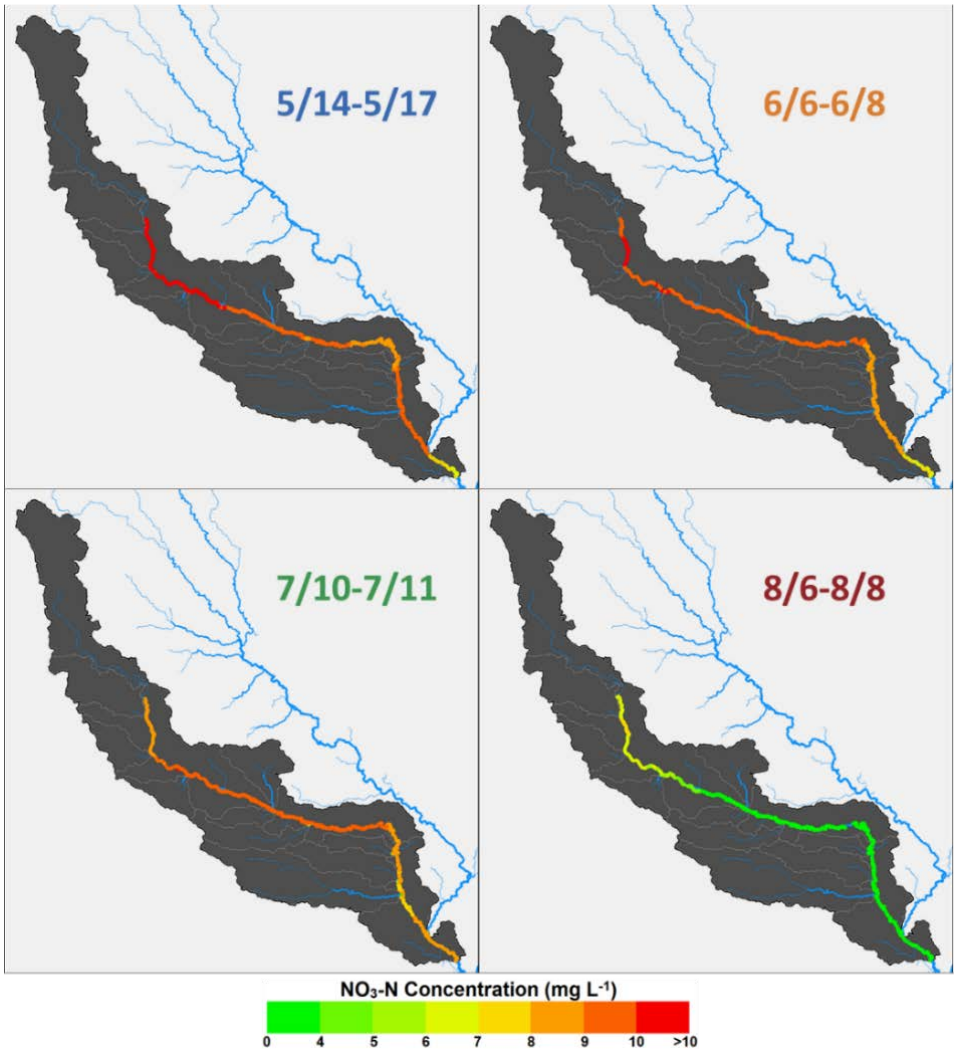

Figure 5.5: Observed NO_3-N concentrations along the Iowa River using the boat-deployed Nitratax Plus sc. Highest NO_3-N concentrations were consistently found at the upstream end of the watershed and August concentrations were lowest in all reaches.

Nitrate concentrations on the Iowa River decreased as the growing season progressed from May to August (Fig. 5.5). This trend was especially distinct in the headwaters and below the Coralville Reservoir, but less pronounced between Walnut Creek (Fig 5.6: 225 km) and the Coralville Dam (Fig 5.6: 109 km). Low NO_3-N concentrations were observed in August compared to other months sampled, especially

downstream of Minerva Creek. Nitrate-N yields were also lowest in August due in part because of low NO_3-N concentrations (Fig. 5.6) and low flow (Fig. 5.4).

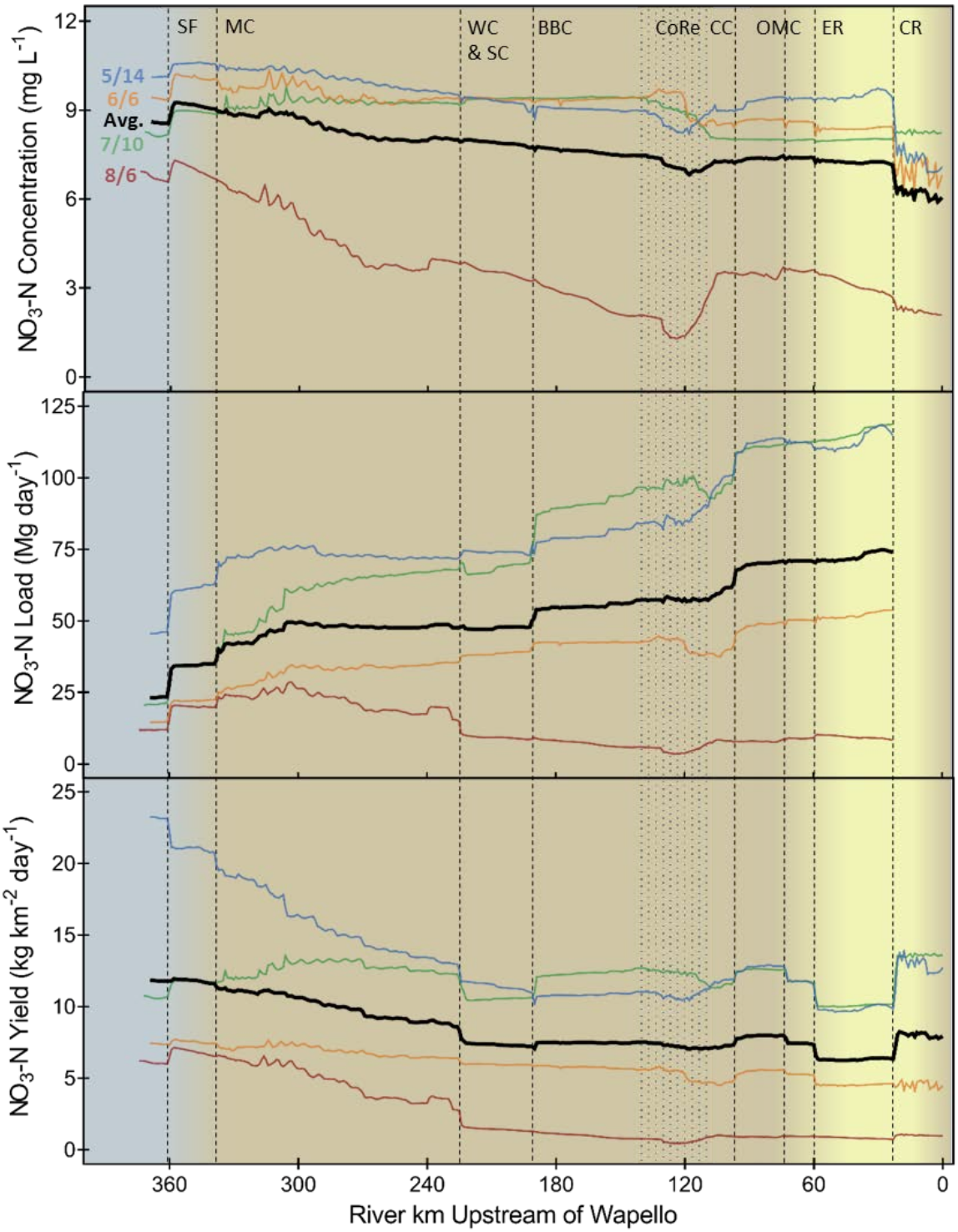

Figure 5.6: Longitudinal profiles of average NO_3-N concentration, load, and yield for every km upstream of Wapello, IA. Dashed lines represent major confluences (CR: Cedar R., ER: English R., OMC: Old Man's Cr., CC: Clear Cr., BBC: Big Bear Cr., WC: Walnut Creek, SC: Salt Creek, MC: Minerva Cr., SF: South Fork Iowa R.), the dotted area represents the Coralville Reservoir, and shaded colors represent landforms (DML, SIDP, ICL).

Tributary NO_3-N concentrations

The concentration of NO_3^-N was lower in the major tributaries than it was in the main stem of the Iowa River with a few exceptions. NO_3^-N concentrations in South Fork of the Iowa River exceeded the Iowa River NO_3^-N concentrations on all occasions and NO_3^-N concentrations in Minerva Creek and Big Bear Creek exceeded the Iowa River NO_3^-N concentrations on one occasion (Fig. 5.7). The tributaries furthest upstream had the highest NO_3^-N concentrations in general (Fig. 5.7).

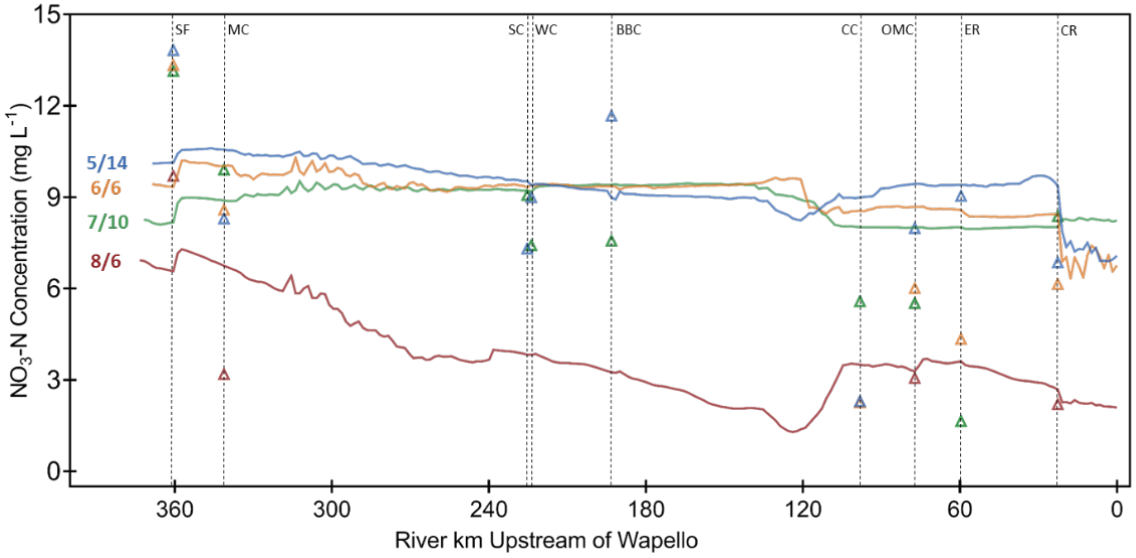

Figure 5.7: Longitudinal profiles of average NO_3-N concentrations every km upstream of Wapello, IA (colored lines) and NO_3-N concentrations of major tributaries (colored triangles). Dashed lines represent major confluences (CR: Cedar R., ER: English R., OMC: Old Man's Cr., CC: Clear Cr., BBC: Big Bear Cr., WC: Walnut Creek, SC: Salt Creek, MC: Minerva Cr., SF: South Fork Iowa R.).

Iowa and Cedar River Mixing

Limited mixing occurred downstream of the Iowa and Cedar River confluence. A USGS nitrate sensor measuring the total NO_3^-N load of the ICRB is located 22.5 km downstream of the Iowa/Cedar confluence on the west side of the river. The rivers had not yet mixed at this location on 5/14/18, 6/6/18, and 7/10/18. The unmixed plumes from each river may bias yearly NO_3^-N load estimates when the NO_3^-N concentrations of the Iowa and Cedar River differ. We observed the greatest difference on 6/6/18, when Iowa River NO_3^-N concentrations were 8.45 mg L^{-1} compared to 6.15 mg L^{-1} on the Cedar

River. NO_3^-N concentrations still differed by 0.63 mg L^{-1} laterally at the USGS NO_3^-N sensor (Fig. 5.8). Nitrate measurements from the *in-situ* sensor were biased toward Iowa River concentrations, because the sensor is located on the west side of the river. Researchers could consider different sensor placement such as mid-stream or on the east side of the river to reduce this bias.

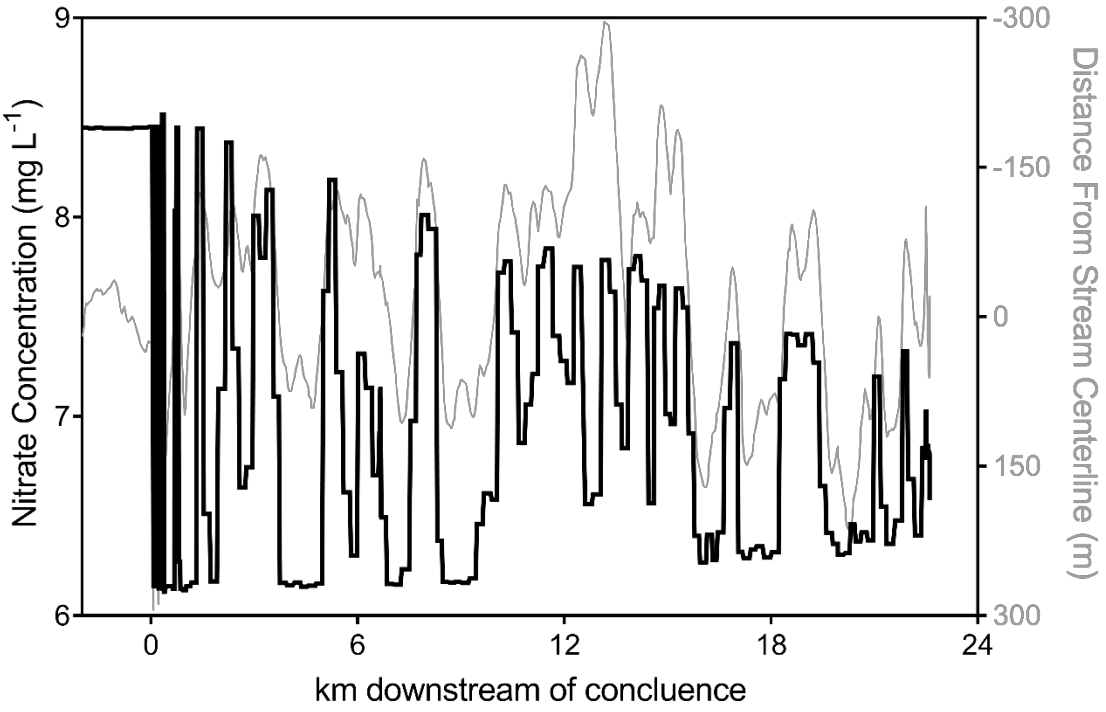

Figure 5.8: Observed NO_3^-N concentrations downstream of the Iowa/Cedar River Confluence (black line). The grey line represents the boat's distance from the stream centerline for each sample point. Positive distances from the stream centerline favor the Cedar River plume and negative distances favor the Iowa River plume.

Temperature

On average, temperatures along the Iowa River increased as the water moved downstream. Longitudinal temperature gradients were mild, with some notable exceptions (Fig. 5.8). Exceptions occur at locations where sampling ended one evening and restarted the next morning. The river cooled overnight, causing a sharp temperature drop upstream of the last recorded temperature the night before. High surface water temperatures were observed in the Coralville Reservoir in every month sampled.

Specific Conductivity

SPC varied monthly along the Iowa River. The river's SPC remained constant and slowly declined from upstream to downstream in May and July, when discharge was highest (Fig. 5.9). Conductivity of the river varied greatly in August, when discharge was the lowest (Fig. 5.9). Overall, the highest SPC recorded in the main channel was 667 µS cm^{-1} in the headwaters on 6/8/18 and the lowest was 405 µS cm^{-1} around Chelsea, IA on 8/8/18.

pH

The pH of the Iowa River remained steady longitudinally and in time. Overall, pH values ranged from 7.8 at 200 km (Fig. 5.9) on 5/16/18 to 8.6 on 8/6/18 at 40 km upstream of Wapello. This range of pH values indicates the river remains slightly basic and the concentration of H_3O^+ ions did not vary beyond one order of magnitude temporally or spatially on the Iowa River. However, rapid pH swings were observed in the Coralville Reservoir. On 8/6/18, the pH changed as much as 0.65 in only a few kilometers in this impoundment, likely a result of the biotic uptake of CO_2 (Fig. 5.9: 124 km).

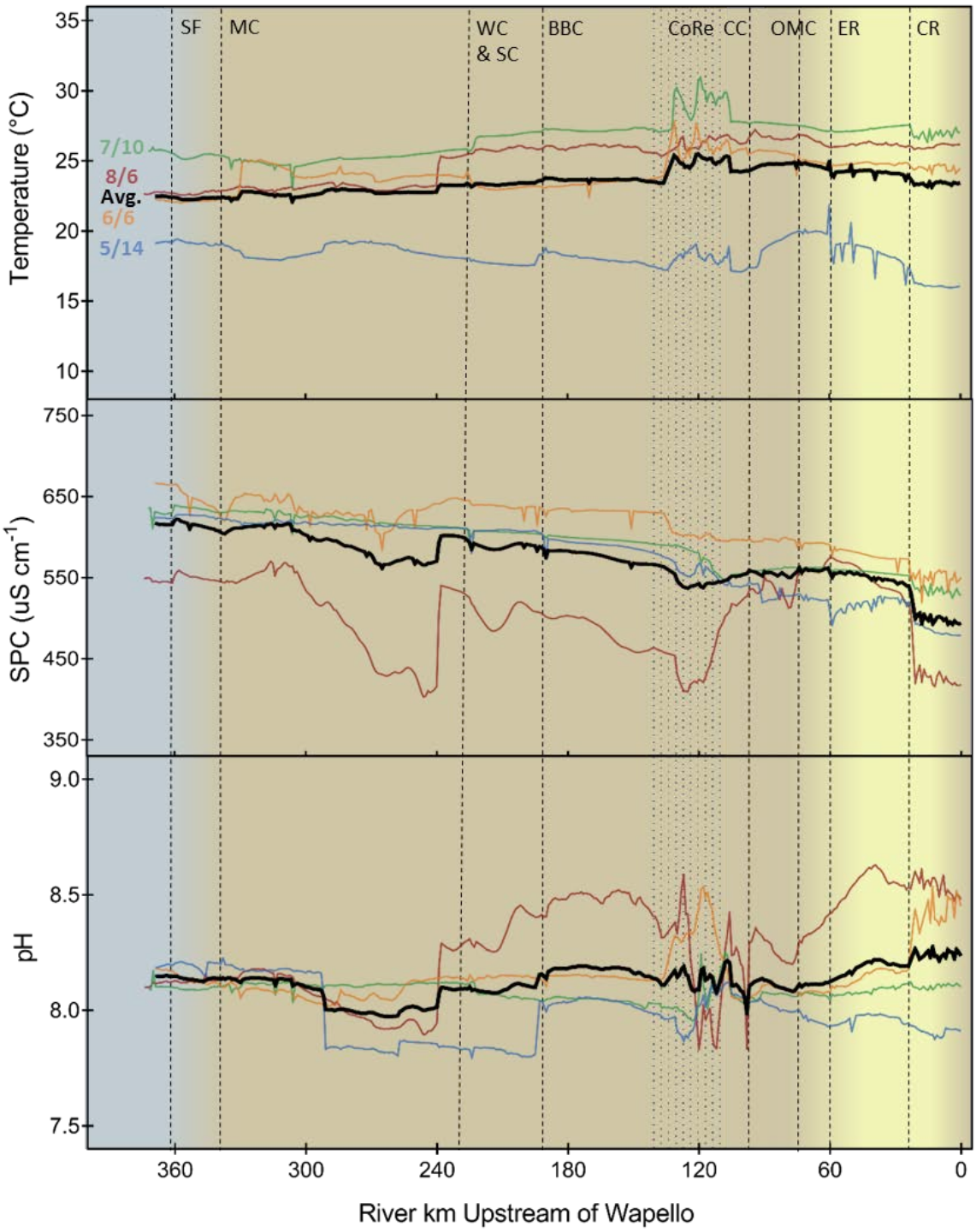

Figure 5. 9: Longitudinal profiles average Temperature, Specific Conductivity, and pH for every km upstream of Wapello, IA. Dashed lines represent major confluences (CR: Cedar R., ER: English R., OMC: Old Man's Cr., CC: Clear Cr., BBC: Big Bear Cr., WC: Walnut Creek, SC: Salt Creek, MC: Minerva Cr., SF: South Fork Iowa R.), the dotted area represents the Coralville Reservoir, and shaded colors represent landforms (DML, SIDP, ICL).

5.8 Cedar River Results

Precipitation and Discharge

Accumulated 10-day rainfall varied significantly time and space across the Cedar River watershed. Highest average 10-day rainfalls (91.9mm and 64.8mm) were observed in June and August and lowest average rainfall (21.9 mm) was observed in July (Fig. 5.10). Relatively even dispersal of rainfall fell across the watershed in May, June, and July (Fig. 5.10). However, heavy rainfall occurred in August mostly in the central parts of the watershed including the West Fork, Beaver Creek, Black Hawk Creek, Wolf creek, and several small watersheds along the Middle Cedar River (Fig. 5.10).

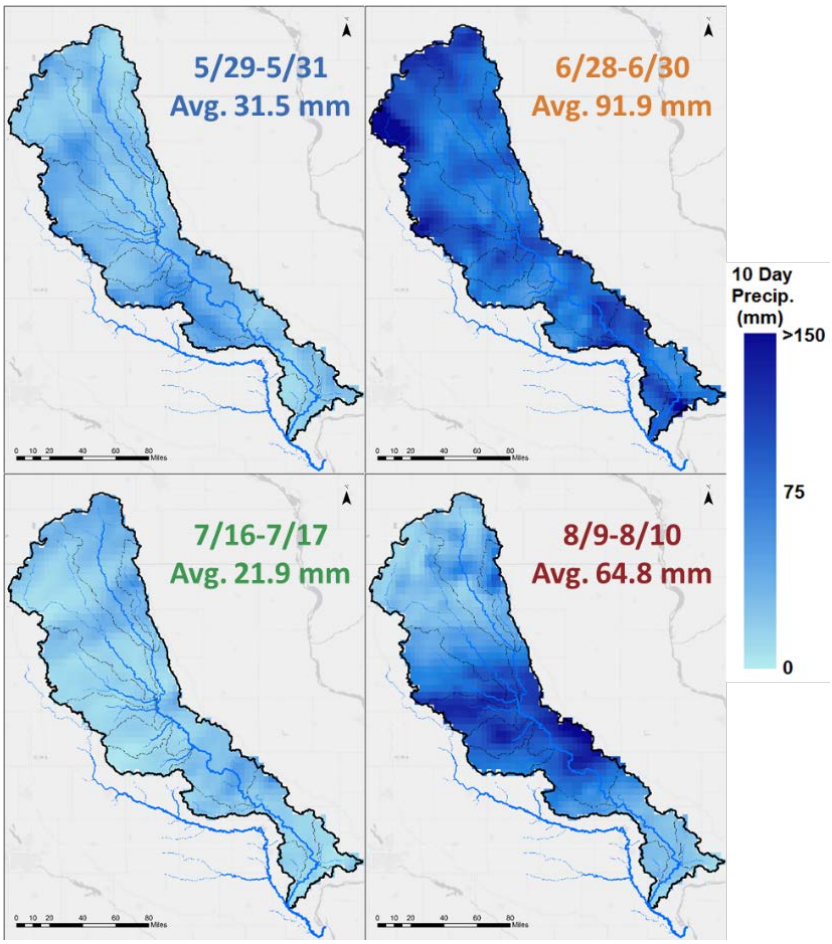

Figure 5.10: Accumulated Rainfall over the Cedar River watershed 10 days prior to the second day of sampling. Accumulated daily radar rainfall estimates in a 4 km grid from PRISM Climate Group were used to generate these four figures.

Discharges in May, July, and August were comparable for all river reaches (Fig. 5.11). Heavy rainfall in June, however, led to elevated discharges during that sample period (Fig. 5.11). The observed river stages were near or above bank full in all reaches south of the West Fork confluence, where the West Fork and Shell Rock River feed into the main stem of the Cedar, tripling the Cedar River discharge (Fig. 5.11: 286 km). Upstream of the West Fork confluence, discharge was considerably low on 8/10/18 and highest on 6/30/18.

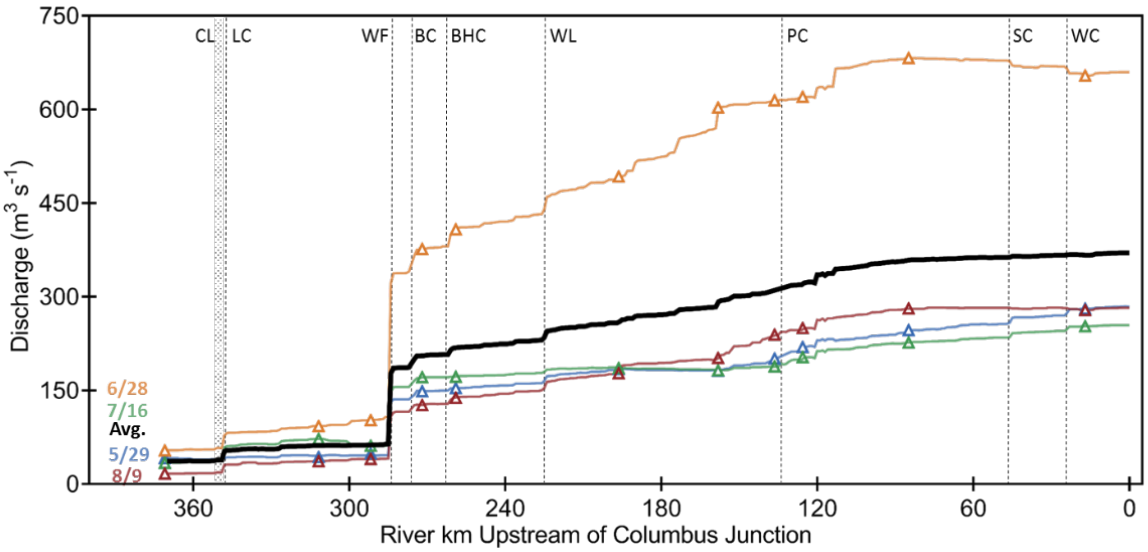

Figure 5.11: Cedar River discharge generated from interpolation of known discharges at 11 USGS gauges along the Cedar River during sampling. Colored lines represent each sample period and the black line represents the average discharge. Dashed lines represent major tributary confluences. Triangles represent observed discharge at USGS gauges.

Main Channel Nitrate

Cedar River average NO_3^-N concentrations remained relatively steady along the length of the sampled reaches. Average NO_3^-N concentrations declined from 7.4 mg L^{-1} to 6.2 mg L^{-1} at the West Fork Confluence, which includes the Shell Rock River (Fig. 5.13). However, the influence of Beaver Creek, Black Hawk Creek, and Wolf Creek increased average NO_3^-N concentrations to 7.3 mg L^{-1} in the main channel. Average NO_3^-N yield increases were observed in the lower reaches of the IS and at the Little Cedar

River, Beaver Creek, and Wolf Creek confluences (Fig. 5.13). The only two tributaries to decrease NO_3^-N yields were Sugar Creek and Wapsinonoc Creek. The SIDP and ICL occupy areas inside both of these tributaries. They have high proportions of row crop agriculture, but exist in landforms that do not require extensive tile drainage (Prior 1991). Average NO_3^-N yields leveled off in the SIDP and began to decline after the river entered the ICL. Cedar River average NO_3^-N loads also increased throughout the IS before

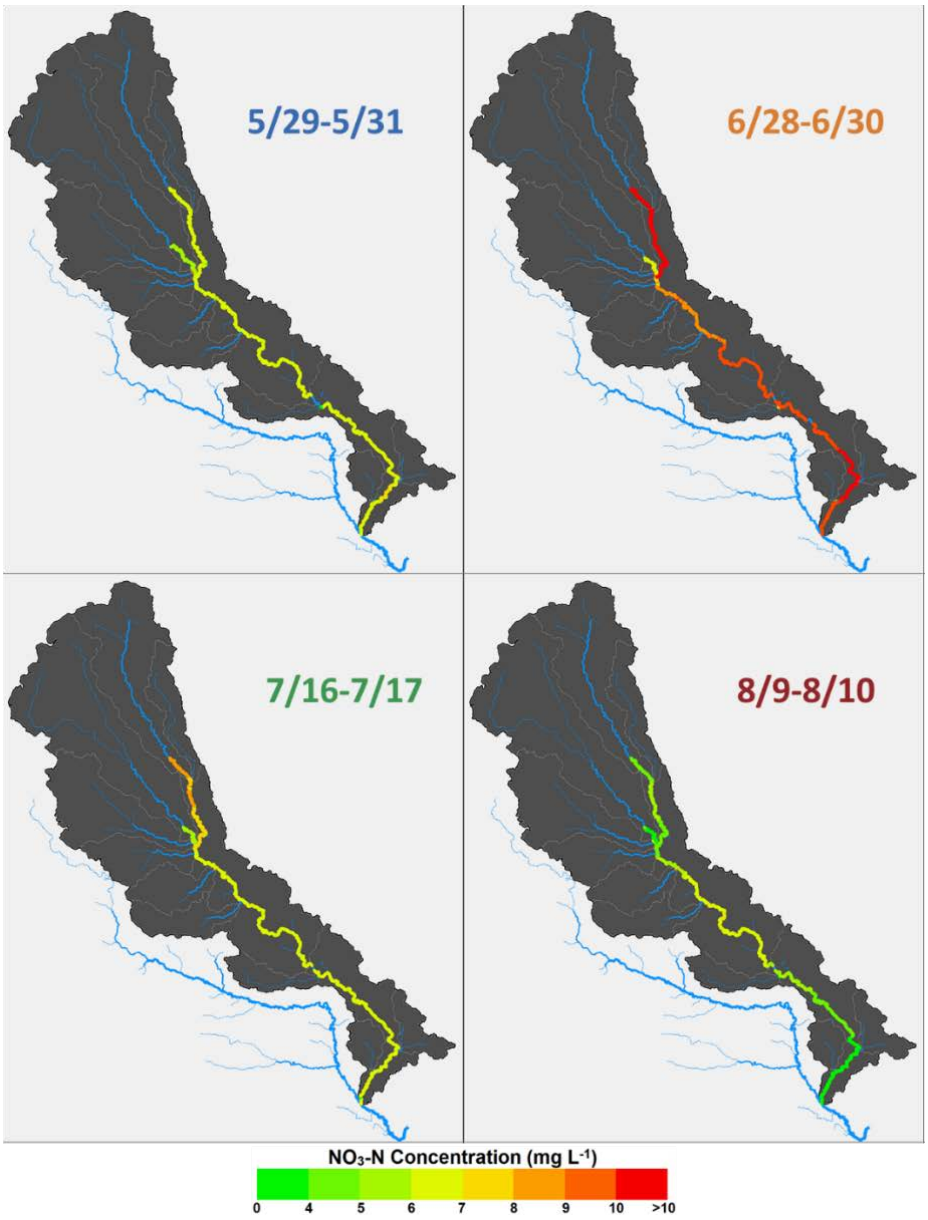

Figure 5.12: Observed NO_3-N concentrations along the Cedar River using the boat-deployed Nitratax Plus sc. Nitrate-N concentrations varied spatially by month.

leveling off in the SIDP and declining as water traveled through the ICL. A substantial NO_3^-N load increase occurred at the West Fork confluence, where the West Fork and Shell Rock River nearly triple discharge in the Cedar River.

The highest NO_3^-N concentrations, load, and yield were observed in June in all river reaches (Fig. 5.12: Fig. 5.13). Sampling in May and July resulted in similar NO_3^-N concentrations, loads, and yields downstream of the West Fork confluence, but higher NO_3^-N concentrations, loads, and yields were observed upstream of this confluence in July. Lowest NO_3^-N concentration, load, and yields were observed in August in the upper and lower river reaches (Fig. 5.12: fig. 5.13).

Tributary NO_3-N Concentrations

Tributary NO_3^-N concentrations varied spatially along the Cedar River. Observed Nitrate-N concentrations in Prairie Cr., Sugar Cr., and Wapsinonoc Cr. were consistently lower than the main channel of the Cedar River (Fig. 5.14). NO_3^-N concentrations were consistently higher in tributaries of the Middle Cedar River compared to the main channel (Fig. 5.14). These tributaries include Wolf Cr., Black Hawk Cr., and Beaver Creek. Lower NO_3^-N concentrations were observed in the Shell Rock River and high NO_3^-N concentrations were observed in the West Fork. The two rivers mix over a short distance before spilling into the Cedar River with observed NO_3^-N often below concentrations of the main stem. Observed NO_3^-N concentrations were consistently higher in the Little Cedar River than the channel of the Cedar River (Fig. 5.14).

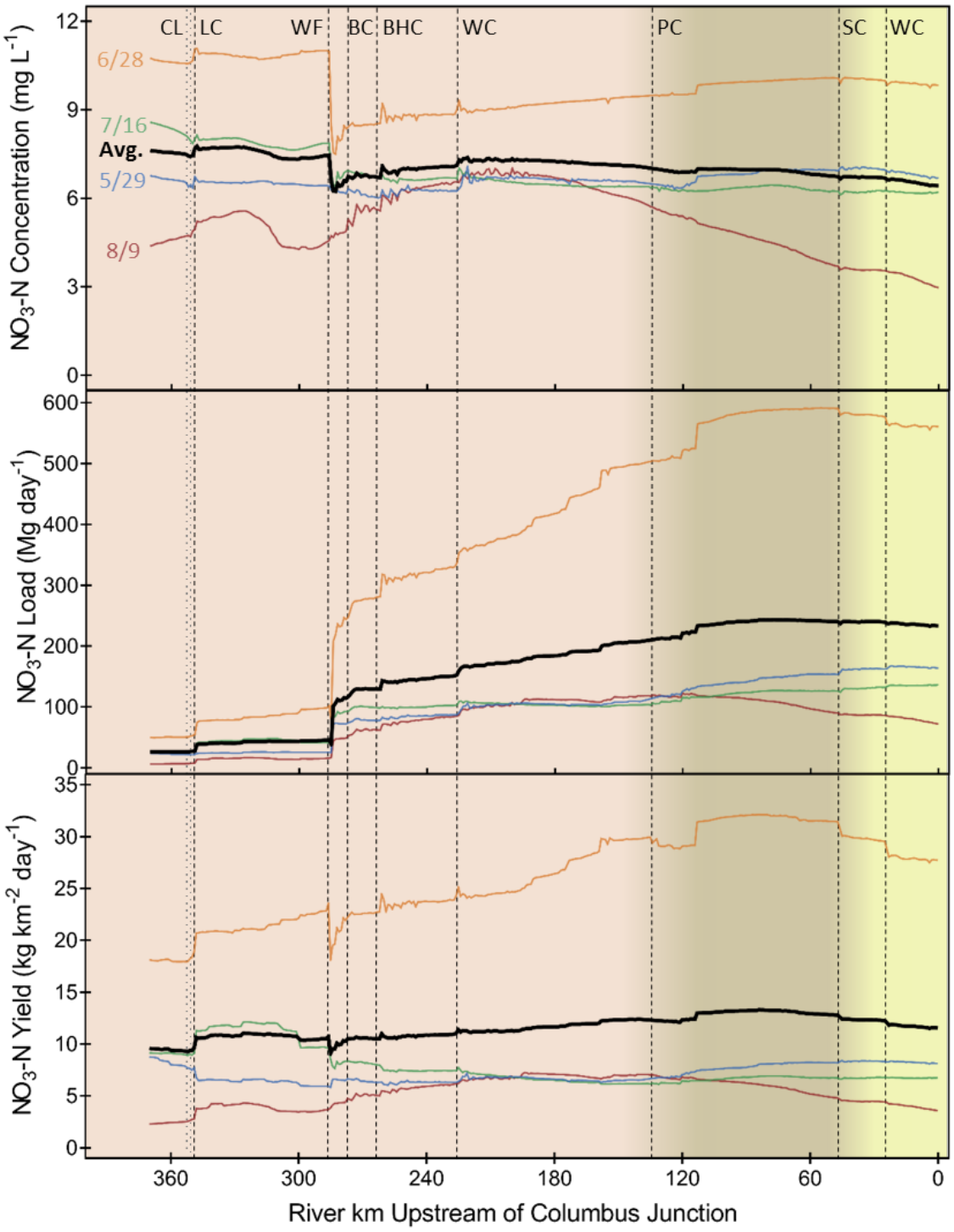

Figure 5.13: Longitudinal profiles of average NO_3-N concentration, load, and yield for every km upstream of Columbus Junction, IA. Dashed lines represent major confluences (WC: Wapsinonoc Cr., SC: Sugar Cr., PC: Prairie Cr., WL: Wolf Cr., BHC: Black Hawk Cr., BC: Beaver Cr., WF: West Fork/Shell Rock R., LC: Little Cedar R.), the dotted area represents the Cedar Lake (CL), and shaded colors represent landforms (IS, SIDP, ICL).

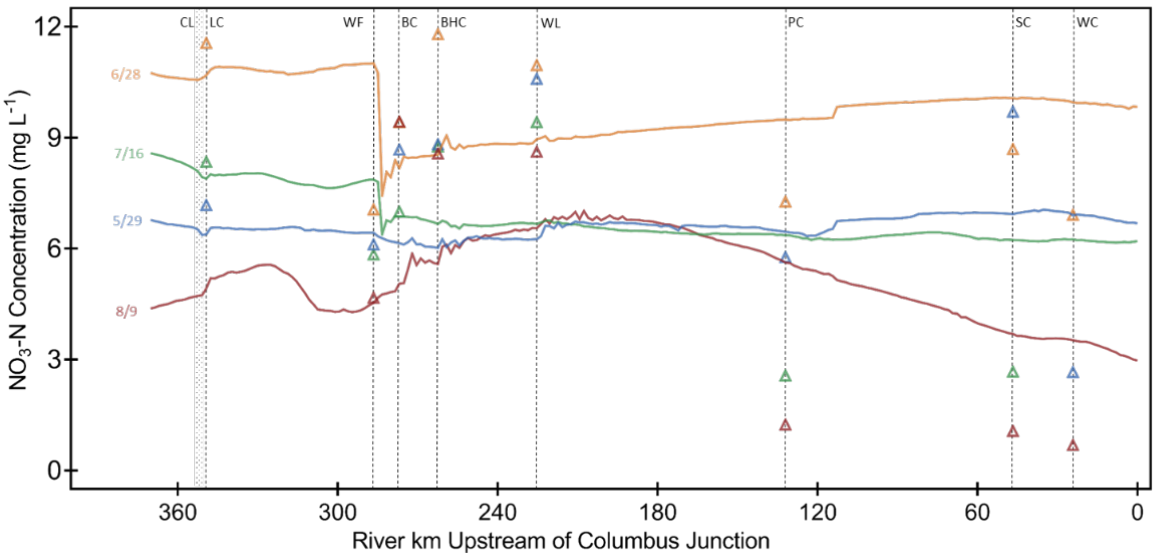

Figure 5.14: Longitudinal profiles of average NO_3-N concentrations for every km (colored lines) and NO_3-N concentrations of major tributaries (colored triangles). Dashed lines represent major confluences (WC: Wapsinonoc Cr., SC: Sugar Cr., PC: Prairie Cr., WL: Wolf Cr., BHC: Black Hawk Cr., BC: Beaver Cr., WF: West Fork/Shell Rock R., LC: Little Cedar R.).

Temperature

Surface water temperatures slowly increased on the Cedar River from Charles City to Columbus Junction. Average summer temperatures were around 25°C and varied <6°C in all river reaches and months (Fig. 5.15). Spikes in surface water temperature were observed in Cedar Lake (Fig. 5.15: 353 km) and drops in temperature were observed at the West Fork Confluence (Fig. 5.15: 286 km), indicating cooler water delivered from the West Fork and Shell Rock Rivers.

Specific Conductivity (SPC)

Average specific conductivity declined from upstream to downstream in general. The influence of the Little Cedar River greatly decreased SPC in the headwaters, but average SPC increased again with the influence of the West Fork and Shell Rock River (Fig. 5.15). Small variations in SPC were observed at other major tributaries, but consistent spikes were observed at the Cedar Rapids wastewater effluent (Fig. 5.15: 125km). The highest recorded SPC was 573 µS cm^{-1} on 7/16/18 (Fig. 5.15: 77km) and the

lowest was 390 µS cm^{-1} on 8/9/2018 (Fig. 5.15: 53 km). In general, observed SPC on the Cedar River was lower than SPC on the Iowa River.

pH

The pH of the Cedar River remained constant longitudinally and in time. A range of pH values were observed between 7.8 on 6/28/18 (Fig. 5.15: 3km) and 8.7 on 7/16/18 (Fig. 5.15: 124km). Slight changes in pH were observed at the Little Cedar River and West Fork confluences, but nothing to dramatically change the H_3O^+ concentrations. The Cedar River remained slightly basic during every sample period in the summer of 2018.

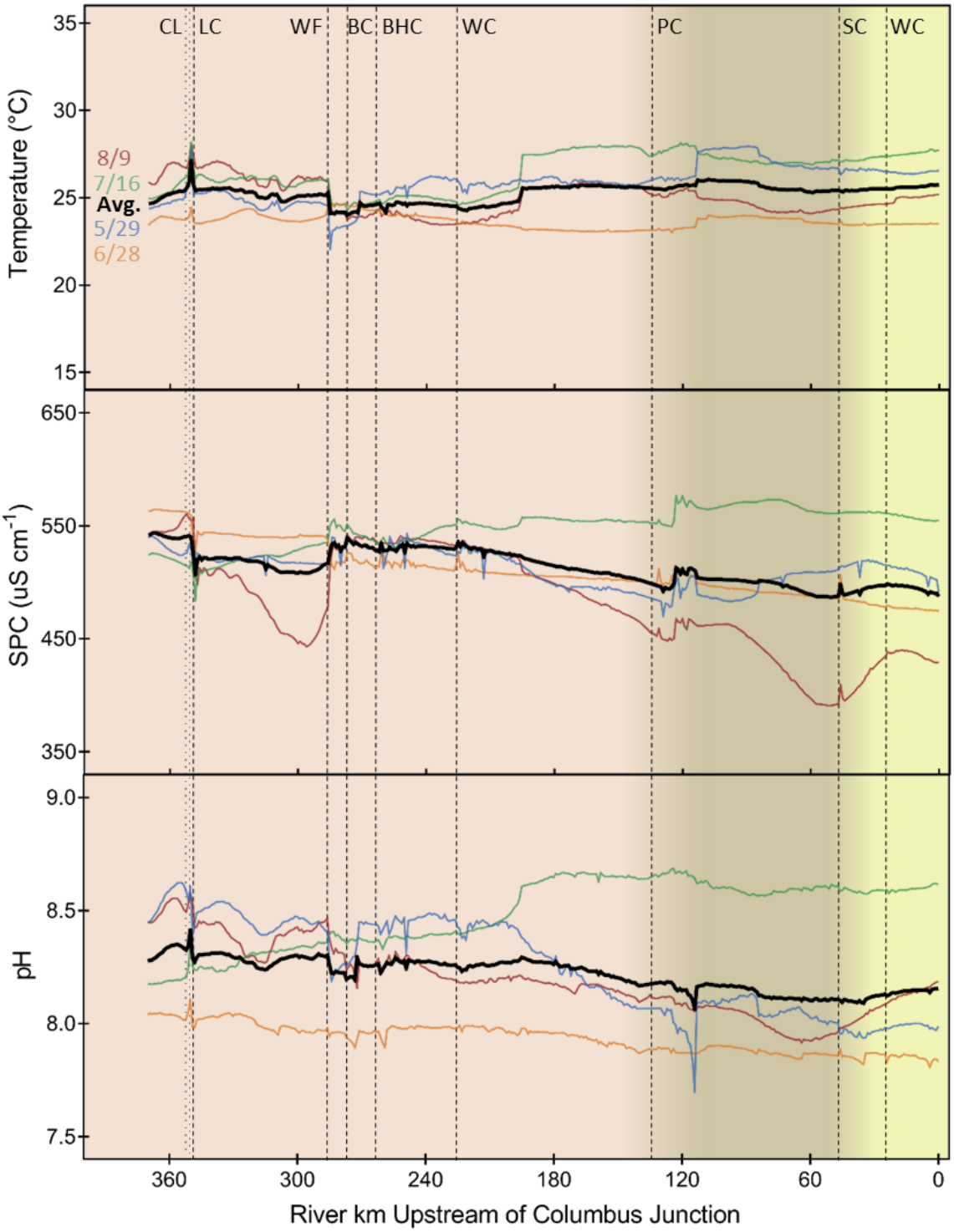

Figure 5.15: Longitudinal profiles of average Temperature, SPC, and pH for every km upstream of Columbus Junction, IA. Dashed lines represent major confluences (WC: Wapsinonoc Cr., SC: Sugar Cr., PC: Prairie Cr., WL: Wolf Cr., BHC: Black Hawk Cr., BC: Beaver Cr., WF: West Fork/Shell Rock R., LC: Little Cedar R.), the dotted area represents the Cedar Lake (CL), and shaded colors represent landforms **(IS, SIDP, ICL)**.

5.9 Discussion

Nitrate Yields and Concentrations

Average NO_3^-N yields observed in this study are comparable to those found previously, however, dense measurements of NO_3^-N yields in rivers as they flow across Iowan Landforms have never previously been collected. Average NO_3^-N losses nearest the DML were 11.7 kg km^{-2} day^{-1} in this study. Previously, NO_3^-N yields of 5.5-16.4 kg km^{-2} day^{-1} have been observed in the DML (Tomer et al. 2003; Jones et al. 2019; Schilling and Walter 2005; Ikenberry et al. 2014). NO_3^-N yields declined as the Iowa River flowed through the SIDP, especially at the confluence of the English River and Old Man's Creek. Observed NO_3^-N losses in the SIDP have previously been about half the losses in the DML, which is consistent with this study. Average NO_3^-N yields declined from 11.7 kg km^{-2} day^{-1} at the South Fork confluence to only 6.2 kg km^{-2} day^{-1} downstream of the English River confluence. On the Cedar River, average NO_3^-N yields increased from 9.6 kg km^{-2} day^{-1} to over 13.0 kg km^{-2} day^{-1} across the IS. The NO_3^-N losses found in this study compared to the high end of previous studies, where IS NO_3^-N losses were between 6.0 and 11.2 kg km^{-2} day^{-1} (Jones et al. 2018c; Schilling and Walter 2005; Drake et al. 2018). The NO_3^-N yield increase on the Cedar River occurred as the West Fork, Beaver Creek, Black Hawk Creek, and Wolf Creek entered the river. All of these watersheds are in the IS (Fig. 5.1) and corn and soy production occupies over 80% of their land area (Fig. 5.2). Average NO_3^-N yields then leveled off and began to decline in the downstream reaches as the Cedar River watershed entered the IS and ICL despite high corn and soy production in Prairie Creek, Sugar Creek, and Wapsinonoc Creek.

The DML and IS have lower relief than the SIDP (Prior 1991), have a larger proportion of cultivated crop production (Fig. 5.2), and likely require more tile drainage

for agricultural production (Prior 1991). Increased NO_3^-N losses were observed where watersheds of highest row crop production flowed from the IS or DML into the Iowa and Cedar Rivers. However, no average NO_3^-N yield increases were observed as SIDP tributaries with intense row crop production flowed into the rivers. Agricultural production combined with dense tile drainage likely contribute to the higher observed NO_3^-N losses in the DML and parts of the IS (Schilling and Libra 2000; Arenas et al 2017).

Observed seasonal changes in NO_3^-N concentration and yield were also consistent with previous studies. May, June, and July NO_3^-N concentrations were higher than August NO_3^-N concentrations on both the Iowa and Cedar Rivers. Declines in NO_3-N concentration during late summer occurred in previous studies as well (Drake et al 2018; Arenas et al 2017; Jones et al. 2017). NO_3^-N yields also decreased in August, not only due to decreased NO_3^-N concentrations (Fig. 5.6), but also decreased discharge (Fig. 5.4). Average annual discharge over the past 30 years supports observed declining streamflow in the Iowa/Cedar Rivers in 2018 (Fig. 5.16). Increased crop leaf area and root depth may have lead to higher transpiration and lower observed streamflow in August (Arnold et al. 2000).

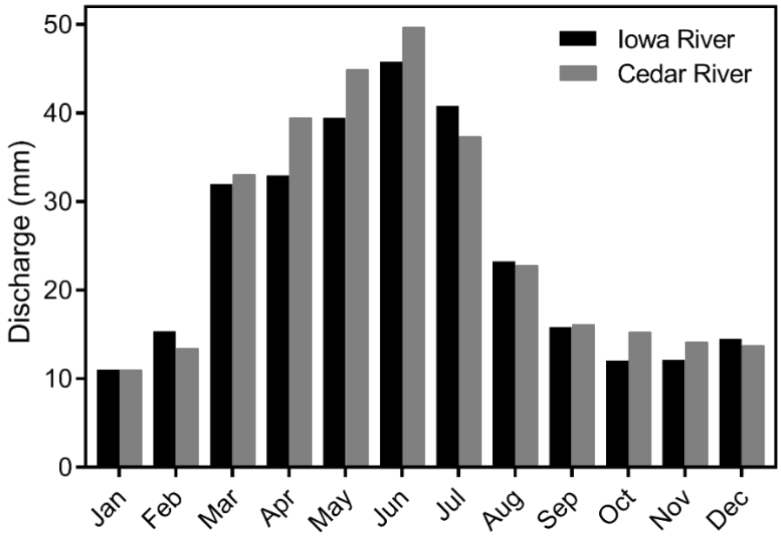

Figure 5.16: Average monthly discharge normalized to drainage area on the Iowa River @ Lone Tree and on the Cedar River @ Columbus Junction. USGS stream gauge data from 10/1/1987 to 9/30/2017 was considered for long the reported long term averages (U.S. Geological Survey, 2016).

Nitrate Load Reductions

Average NO_3^-N load reductions were observed in the Coralville Reservoir on the Iowa River (Fig. 5.6) and on the Lower Cedar River from 80-0 km upstream of Columbus Junction (Fig. 5.13). Calculated Nitrate-N loads decreased in June and July in the Coralville Reservoir. Reduction in NO_3-N loads were also observed in May and August initially but NO_3^-N increases midway through the reservoir resulted in net NO_3-N load increases. Reductions in NO_3-N load and concentration were observed in June and August and slight NO_3^-N load increases were observed in May and July despite decreasing NO_3^-N concentrations.

NO_3^-N load reductions calculations cannot reasonably be used to calculate reductions in the Coralville Reservoir with the data collected. A previous study showed NO_3^-N load reductions on the order of 4.9% in similar flood control reservoirs in Iowa (Stenback et al 2014). That study included monthly samples over decades to ensure average reductions were representative of reality (Stenback et al 2014). There would be

high uncertainty if NO_3^-N load reductions were calculated from only four samples collected on the Coralville Reservoir in 2018. However, this site was identified as an area where overall load reductions occurred during two sample runs. More frequent sampling over a longer time span must occur to quantify NO_3^-N load reductions in the Coralville Reservoir to account its long residence time. We did, however, identify NO_3^-N concentration reductions in the reservoir (Fig. 5.6). Along with NO_3^-N concentration decline, we observed pH increases in the reservoir, indicating biota may be using available NO_3^- (Fig. 5.9).

The lower Cedar River differs from the Coralville Reservoir, because the water is not detained. Daily NO_3^-N load reductions were calculated in this river reach (table 2). Nitrate-N load declines existed when discharge was highest on 6/28/2018 and when discharge was lowest on 8/9/2018. The channel had escaped its banks and connected to a wide floodplain on 6/28/2018. Nitrate reduction in the floodplain may have occurred on that day. On 8/9/2018, low observed discharge did not increase over the duration of the 80 km reach we assessed. Sandbars extended from inside bends, but also altered the water flow path where sand bars extended laterally across the river. These exposed sandbars likely increased water travel time, allowing more time for denitrification as shallow water interacted with the riverbed.

NO_3^-N load measurements occurred over four distinct days and vary between a 34% load reduction and an 11% load increase. Our results suggest an average load reduction in the lower 80 km of the Cedar River, but we hesitate to quantify NO_3^-N load reductions during the entire summer of 2018 because sampling at monthly resolution over a short duration generates high uncertainty (Ch. 3).

Table 5.2: Nitrate-N load reductions or increases observed in the Lower Cedar River.

Date	Nitrate Load 80 km upstream of Columbus Jct. (Mg/day)	Nitrate Load at Columbus Jct. (Mg/day)	Change in Nitrate Load (Mg/day)	% Nitrate Load Change
5/29/2018	148	164	+16	+11%
6/28/2018	588	560	-28	-4.8%
7/16/2018	127	137	+10	+7.9%
8/9/2018	110	72.4	-38	-34%
Average	243	233	-10	-4.1%

Temperature

Stream surface water temperature observed on the Iowa and Cedar Rivers increased from upstream to downstream as expected. Greater stream surface area exposed to solar radiation increases stream temperatures during summer months (Beschta 1997). Stream widths on the upper reaches of the Iowa and Cedar are narrower than downstream and riparian vegetation is able to shade more of the river from solar radiation.

Cedar and Iowa River temperatures may effect game fish species important for recreation within the rivers. Previous studies report critical thermal maxima for walleye (*Stizostedion vitreum*), white bass/striper hybrid (*Marone crysops* x *Marone saxatilis*), smallmouth bass (*Micropterus dolomeiu*), largemouth bass (*Micropterus salmoides*), northern pike (*Esox lucius*), muskellunge (*Esox masquinongy*), and flathead catfish (*Pylodictis olivaris*) (table x). Surface water temperatures nearly reached the critical thermal maximum for northern pike and muskellunge (table 5.3) in May and July on the lower Cedar River (Fig. 5.15) and in July on the Iowa River in the Coralville Reservoir (Fig. 5.9). Management for species with lower critical thermal maximum temperatures such as walleye, smallmouth bass, northern pike, and muskellunge should focus on the cooler waters in the upstream reaches of the Iowa and Cedar River. Predators with higher

critical thermal maxima will survive better in the lower reaches, where water temperatures are a few degrees warmer.

Table 5.3: Critical thermal maximum (Ctmax) for several important game fish species in the Iowa and Cedar River watershed.

Species	Ct_{max}°C	Reference
Stizostedion vitreum	34.8-35	Peterson (1993)
Marone crysops x Marone saxatilis	28-39.2	Woiwad & Adelman (1992)
Micropterus dolomeiu	34.8-36.9	Smale & Rabeni (1995); Lutterschmidt & Hutchinson (1997)
Micropterus salmoides	36.7-40.1	Smith & Scott (1975); Smale & Rabeni (1995)
Esox lucius	29.4	Neumann et al (1994)
Esox masquinongy	30-36	Bonin & Spotila (1978)
Pylodictis olivaris	34.2-41	Cheetham et al (1976); Smale & Rabeni (1995)

Specific Conductivity

The specific conductivity observed along all reaches of the Iowa/Cedar Rivers was representative of previous findings for surface water in Iowa. The majority of the electrical conductivity in Iowan surface waters draining agricultural land is generated from HCO_3^- , Ca^{2+}, NO_3^- , and Mg^{2+} (Zimmerman & Kaleita 2017). These ions contribute to conductivity reading generally between 300 and 760 µS cm^{-1} (Zimmerman & Kaleita 2017). Cedar and Iowa River SPC fell inside the range observed by Zimmerman & Kaleita (2017) with August concentrations being the most variable (Fig. 5.9: Fig. 5.15). There were no SPC readings above 700 µS cm^{-1} on either river, indicating safe quantities of salt were present for freshwater biota (Weber et al. 2015).

pH

Changes of pH were minimal spatially and temporally on the Iowa and Cedar Rivers. Both rivers had slightly basic pH values for all months and in all reaches.

Consistent, slightly basic, pH does not hinder the growth of many aquatic macroinvertebrates or fish species (Allard & Moreau 1987; Courtney & Clements 1998; Mount 1973). No notable issues were identified from longitudinal profiles of pH measurements. The increased pH observed in the Coralville Reservoir is possibly due to biotic uptake of CO_2 from rooted aquatic vegetation and algae in the slow moving water of the reservoir (Seitzinger 1991). Free carbon dioxide in water is acidic and rapid CO_2 uptake increases pH (Maberly & Spence 1983). The U.S. EPA suggests freshwater organisms need pH values between 6.5 and 9.0. Despite increased observed pH in the Coralville Reservoir, the pH remained in the tolerable range of aquatic life for all sampled months.

Study Limitations

Conducting a water quality study with boat-deployed water quality sensors has a few limitations worth mentioning. First, measurements were collected ≈0.1 m below the water surface. Complete vertical mixing in the rivers was assumed, but may not be the case in the large impoundments like the Coralville Reservoir and Cedar Lake. Next, the study lacks high resolution temporal data. Our intent was to collect high resolution spatial data, but, as demonstrated in Chapter 3, monthly frequency is insufficient to quantify nitrate load over short durations. However, a combination of high spatial resolution data and high temporal resolution data from *in-situ* water quality sensors can help to better estimate contaminant quantity (in situ sensor) and contaminant sources (boat-deployed sensor). Finally, diurnal variations were unavoidable with our sampling methodology. We attempted to capture longitudinal profiles as quickly to reduce temporal changes. The alternative would be to travel downstream, approximately the same speed as the current.

This alternative method would capture water quality influences on a single control volume as inputs of water enter the stream, but would dramatically lengthen the duration of each trip.

5.10 Summary

The maiden voyage of a novel, boat-deployed water quality sensor system was successful in characterizing NO_3^-N delivery patterns in the Iowa/Cedar River Basin. Highest NO_3^-N yields came from the South Fork and headwaters on the Iowa River and from several large tributaries on the middle Cedar River including the West Fork, Beaver Creek, Black Hawk Creek, and Wolf Creek. Our data suggests low relief topography found on the IS and DML and high proportions of corn and soybean production relates to high observed NO_3^-N delivery to the Iowa and Cedar Rivers.

Two river reaches were identified as potential areas of the watershed where NO_3^-N was retained in the watershed. We observed NO_3^-N load reductions in the Coralville Reservoir and an 80 km stretch of the Lower Cedar River two out of four sample days. More sampling, perhaps *in situ* sensor deployed upstream and downstream, must be done if we wish to quantify the yearly load reduction that occurs in these locations. However, our longitudinal profiles showed reductions on daily scales.

There were no alarming findings through analysis of observed longitudinal patterns of T, SPC, and pH. Temperatures were warm in the rivers, however, possibly leading to implications of game fish species as climate changes moving forward. Specific Conductivity and pH were representative of Iowan streams in all reaches and across the four summer months sampled.

Nitrate load reduction efforts should focus on the areas of highest NO_3^- losses first. Nearly all land areas in the watershed contributed NO_3^- to the river, but watersheds with low relief and intense row crop agriculture contributed more NO_3^- per km^2. These watersheds include the Iowa River watershed upstream of Eldora, the South Fork, Minerva Creek, West Fork, Beaver Creek, Black Hawk Creek, and Wolf Creek watersheds. The Iowa Nutrient Reduction Strategy suggests several management practices (N rate reduction, nitrification inhibitor, side dressing N, cover crops, and reduced tillage), land use practices (extended crop rotations, energy crops replacing row crops) and edge-of-field practices (wetlands, bioreactors, buffers, saturated buffers) to reduce NO_3^- loading to streams (Iowa nutrient reduction strategy 2012). Nutrient removal wetlands have proven results (Drake et al. 2018; Tomer et al. 2003; Cedfeldt et al. 2000) but require significant capital cost and land. Management practices may be equally effective at the cost of labor, updated equipment, or seed costs.

The Iowa Watershed Approach (IWA) focusses on implementing management strategies to reduce flooding, improve water quality, and establish habitat in eight large watersheds across Iowa. They selected HUC 12 watersheds in larger watersheds for practice implementation. The English River, Clear Creek, and Middle Cedar watersheds were three large basins included in the IWA and HUC 12s included are parts of Wolf Creek, several small watersheds around Vinton, Clear Creek, and parts of the English River in Iowa and Poweshiek counties (Fig. 5.17). Nitrate load reductions are expected in these watersheds after management practices are implemented (Drake et al. 2018). Future studies that replicate methods in this chapter will help determine if the accumulation of small scale management practices reduces NO_3^- loads in the entire Iowa/Cedar River Basin.

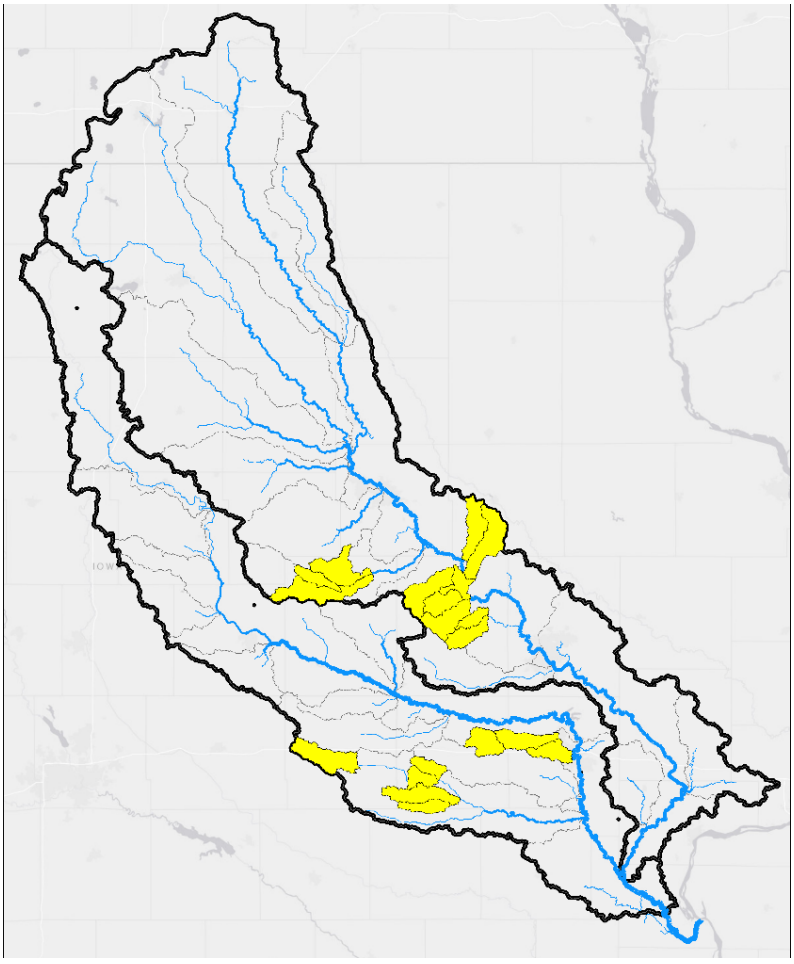

Figure 5.17: The location of HUC 12 watersheds (highlighted in yellow) where management practices such as constructed wetlands will be placed as part of the IWA project.

CHAPTER 6: SPATIAL OF STORM LAKE, IOWA WITH A CONTINUOUS BOAT-DEPLOYED SENSOR SYSTEM

6.1 Introduction

Storm Lake, including Little Storm Lake (Fig. 6.1), is a 3097 acre glacial lake located south of the City of Storm Lake in Buena Vista County, Iowa. Recreation related to Storm Lake generates an economic boost for the local economy. The Iowa Lakes Valuation Project estimated 172,032 families make trips to Storm Lake on an average year, traveling a mean of 39.7 miles to get there, and spending over $28,500,000 (Jeon et al, 2016). This spending generates over $7 million in annual income and supports an estimated 348 jobs (Jeon et al, 2016).

Storm Lake is located in the headwaters of the Raccoon River watershed and has a drainage area of 17,800 acres. Corn and Soybeans are grown on 58% of the watershed and surface water constitutes 18% of the basin (Fig. 6.2). However, corn and soybeans are grown on 78% of the 9,800 acre Powell Creek watershed (Iowa DNR High Res., 2009). The Powell Creek watershed occupies the majority of the Storm Lake watershed and contributes the most water to the lake. Corn and soybean production also dominates in the small tributaries south and west of Storm Lake including West Creek (Fig. 6.2). Runoff from the City of Storm Lake enters the north end of the lake as well. Incoming water resides in Storm Lake an average of 2.6 years before spilling over a weir into Outlet Creek on the southeast end of the lake (Iowa DNR, 2005).

The City of Storm Lake has invested in management practices to reduce nutrients flowing to the lake with hopes of reduced algal blooms and cleaner water. The first project was the restoration of Little Storm Lake Wildlife Management Area. Modifications were made to slow flow coming from Powell Creek. Increased residence

time in Little Storm Lake allowed more nutrient reductions to occur before the water flowed to Storm Lake. Other nutrient management practices implemented on the land include the construction of a wetland treating water from over 100 acres flowing into Little Storm Lake, several constructed bio-reactors, permeable paver installation, and updated city storm sewers (Storm Lake Green Infrastructure Plan 2015). Dredging has occurred in the lake since 2003 with the goal of water quality improvements. 4.75 million cubic meters of sediment were removed from the lake during the 10 year project, increasing lake volume, depth, and residence time (Storm Lake Dredging 2018).

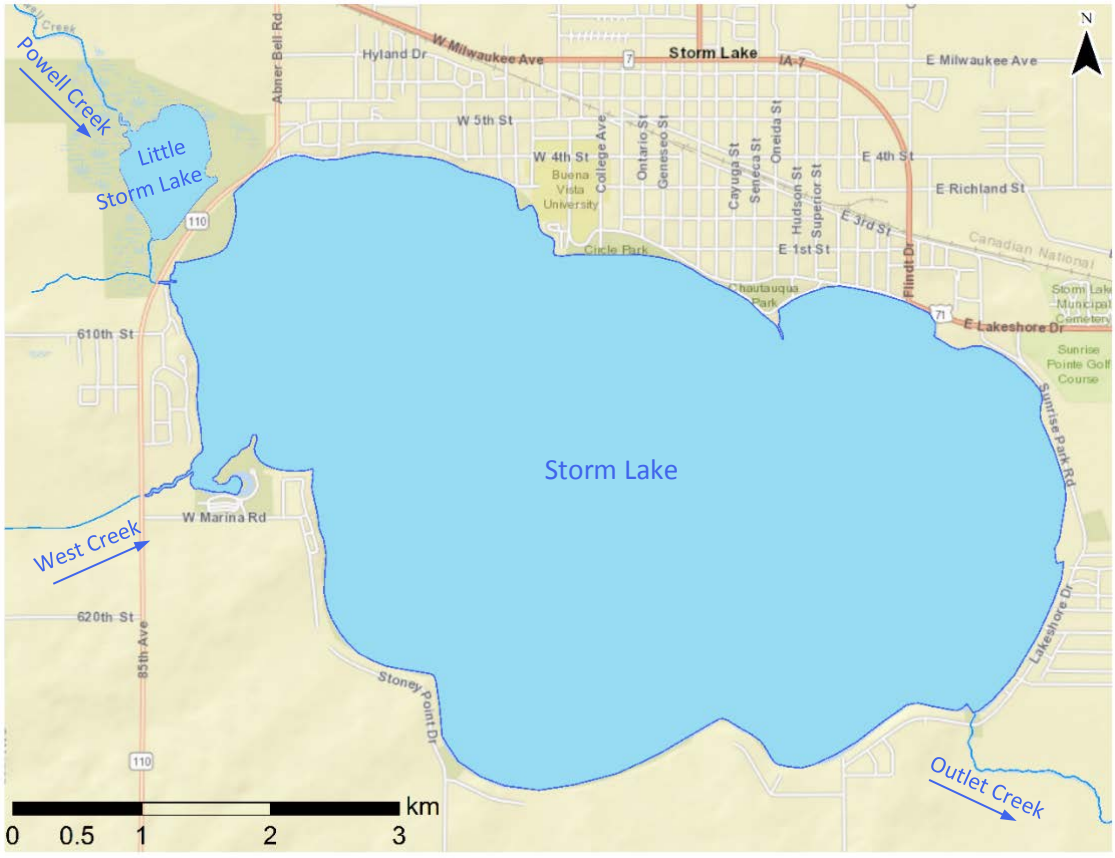

Figure 6.1: Storm Lake is located just south of the City of Storm Lake. Powell Creek and West Creek are major tributaries feeding this large, glacial lake. Water from Storm Lake flows to Outlet Creek and, eventually, the Raccoon River.

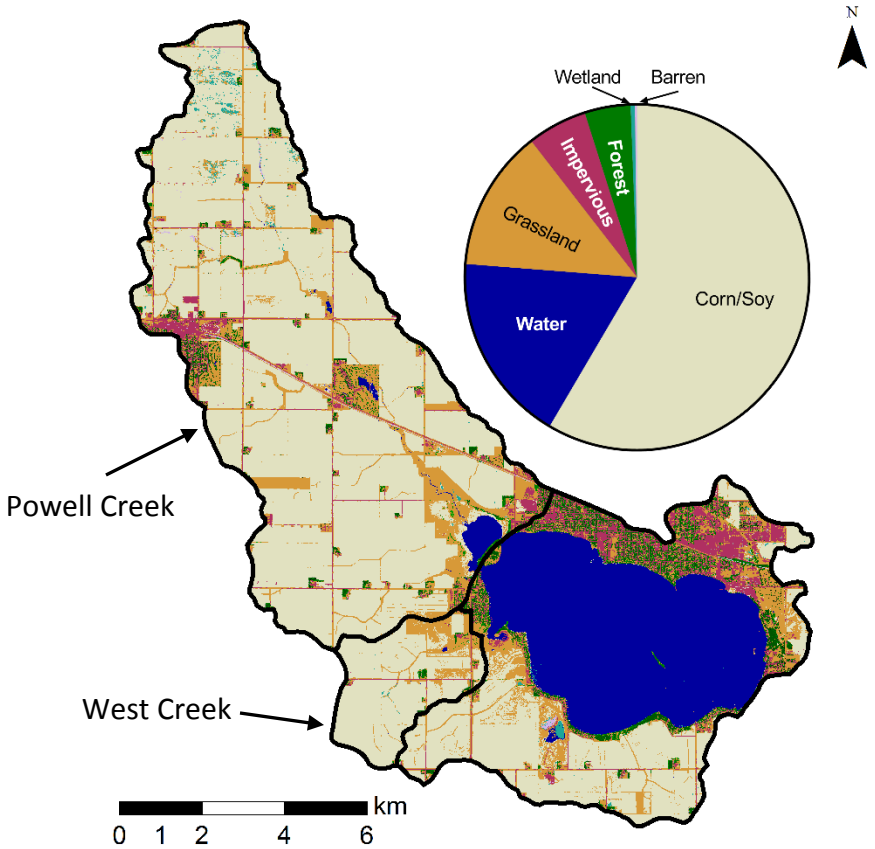

Figure 6.2: One meter, high resolution land use in the Storm Lake watershed (Iowa DNR High Res., 2009). Watersheds of the two largest tributaries, Powell Creek and West Creek, are outlined in black.

6.2 Motivation

The City of Storm Lake and Dr. Ben Maas, of Buena Vista University, expressed interest in spatial water quality sampling to visualize impacts that management practices have on nitrate concentrations in Storm Lake. We used a continuous boat-deployed water quality sensor system (Ch. 4) to measure the spatial distribution of nitrate, conductivity, temperature, dissolved oxygen, and pH in the lake and investigated causes of any observed heterogeneity.

6.3 Methodology

We used the continuous boat-deployed sensor system (Ch. 4) to measure water quality in Storm Lake, Little Storm Lake, Outlet Creek, West Creek, and Powell Creek at a depth between 0.1 and 0.2 meters. The system collects NO_3^-N concentration using a Nitratax Plus sc and temperature, specific conductivity, pH, and dissolved oxygen using a Hydrolab DS5X. Sampling occurred at an average speed of 18.4 km hr^{-1}, providing a Hydrolab measurement every 26 meters and a Nitratax measurement every 77 meters on average. However, sampling density was higher near the shorelines than in the open water. A zigzag pattern was driven across the lake (Fig. 6.3). 2,637 measurements were collected on Storm Lake and 379 measurements were collected on Little Storm Lake.

Weather

Sampling occurred on Wednesday, June 27, 2018 from 10:30 until 15:50. A small front moved through that morning driving SE winds at 5-10 mph. This led to waves in the NW end of the lake reaching about 0.5 meters. However, the front passed around 11:20, overcast conditions transitioned to sun, and wind died to light and variable. By 11:30, waves were <0.1 meters. Air temperatures steadily rose from 20°C to 29°C from 10:30 to 15:50.

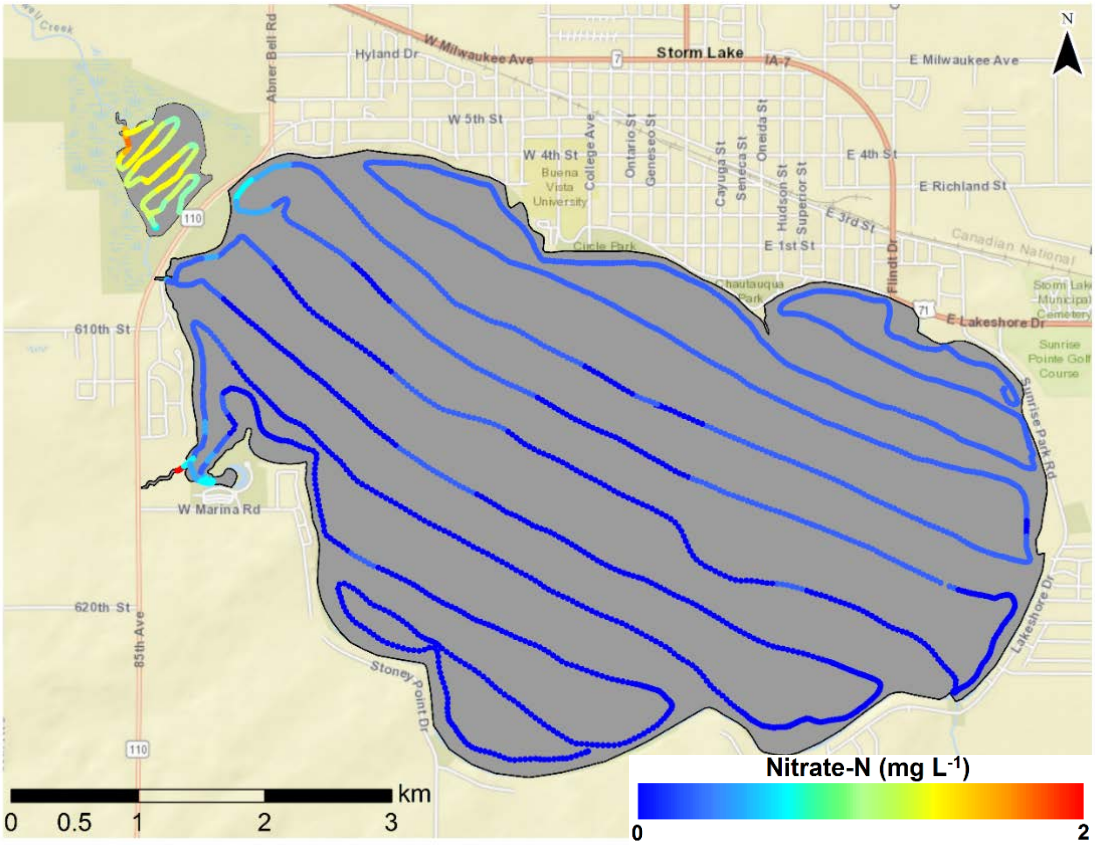

Figure 6.3: The sampling route driven across Storm Lake and Little Storm Lake displayed as dense lines of measured point data. Sampling began on Storm Lake in the NE corner and ended in the south bay and then Little Storm Lake was sampled from south to north. These point data shown were used for kriging interpolation.

Data Processing

Data was stored as a text file on a microSD card in the sensor's control box. These data were transferred into a table in Microsoft Excel. The sensor response times observed in Chapter 4 were used to match water quality measurements with corresponding GPS coordinates. The data were then imported into ArcMap 10.1 and used to generate two shapefiles. The Storm Lake shapefile and Little Storm Lake shapefile shown in Figure 6.3 were used for kriging interpolation to generate a raster displaying interpolated surface water quality values at all locations.

6.4 Results and Discussion

Nitrate

NO_3^-N concentrations in Storm Lake were low (<0.75 mg L^{-1}) compared to Powell Creek and West Creek (10.2 mg L^{-1} and 12.8 mg L^{-1}) (Fig. 6.4). NO_3^-N concentrations were highest along the western shore of Storm Lake (0.70 mg L^{-1}) and lowest near Outlet Creek (0.14 mg L^{-1}). West Creek is small, draining only 1,170 acres. Nitrate loads coming from West Creek quickly dilute upon entering the lake (Fig. 6.4). Powell Creek has a drainage area of 9,800 acres, suggesting higher flow volumes and nitrate loads are transported into Storm Lake from Powell Creek. However, Little Storm Lake intercepts the majority of water from Powell Creek before it enters Storm Lake.

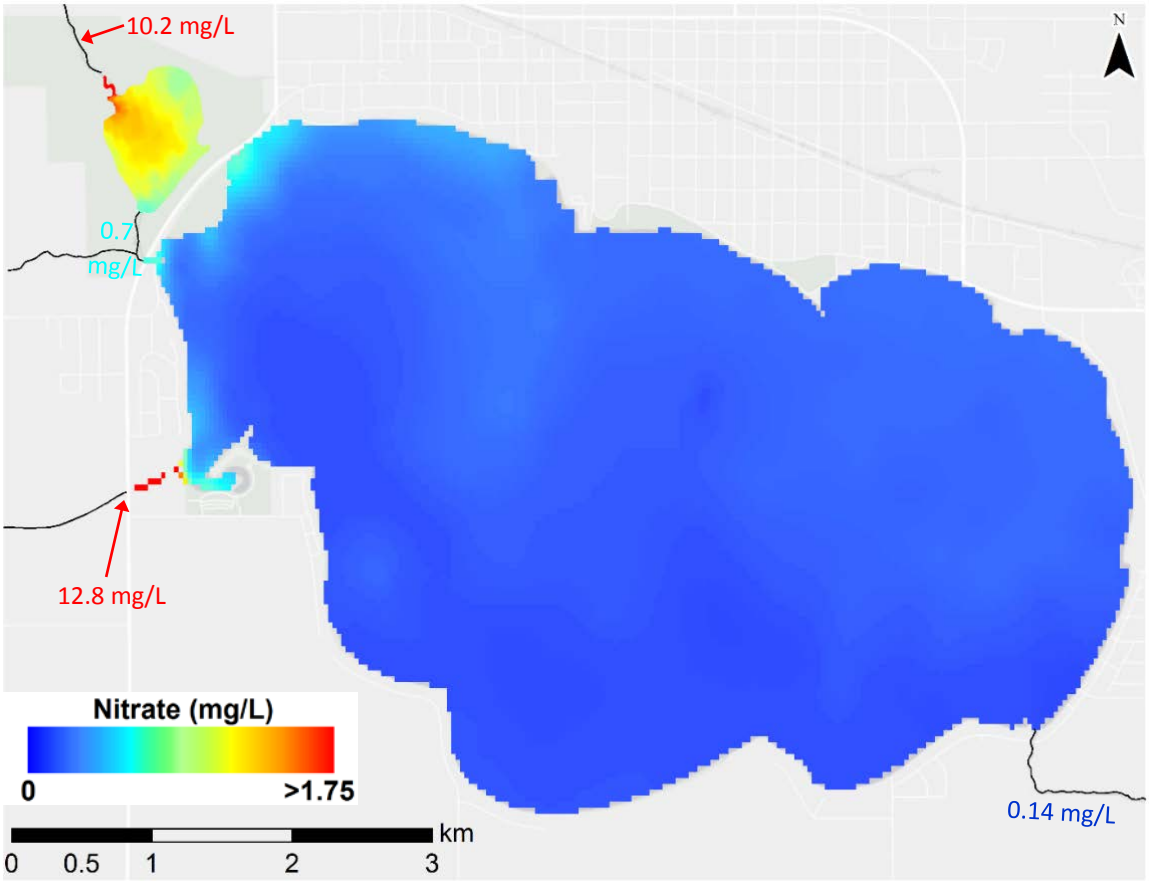

Figure 6.4: Nitrate concentration in Storm Lake and Little Storm Lake.

Significant NO_3^- reduction occurred in Little Storm Lake before the water flowed into Storm Lake (Fig. 6.4; Fig. 6.5). At the nearest upstream road, NO_3^-N concentrations measured 10.2 mg L^{-1} in Powell Creek. NO_3^-N concentrations were reduced below 1.0 mg L^{-1} in Little Storm Lake (Fig. 6.5). Incoming NO_3^-N concentrations were diluted to 1.6 mg L^{-1} upon entering Little Storm Lake. A plume of higher NO_3^- extended to the southeast, but we measured declining NO_3^-N concentrations around it (Fig. 6.5). Denitrification and plant uptake both likely played a role in the observed NO_3^- reduction in Little Storm Lake. High observed temperature (Fig. 6.8) promotes accelerated denitrification in the wetland. Additionally, we observed emergent vegetation in a growth phase, so the growing plants likely were absorbing available NO_3^-.

NO_3^-N concentrations in Storm Lake were low, but showed small variations. NO_3^-N concentrations <0.2 mg L^{-1} were located along the south and eastern portions of the lake. NO_3^-N concentrations 0.2 – 0.7 mg L^{-1} were found on the north and west portions of the lake. This spatial pattern corresponded to the wind direction on June 27 suggesting waves may have been responsible for increased mixing, drawing nutrients closer to the measured surface water. Also, urban areas are situated predominantly to the north and west on the lake. There is potential for increased NO_3^- from the small urban drainages that flow into the north end of the lake (Hobbie et al, 2017).

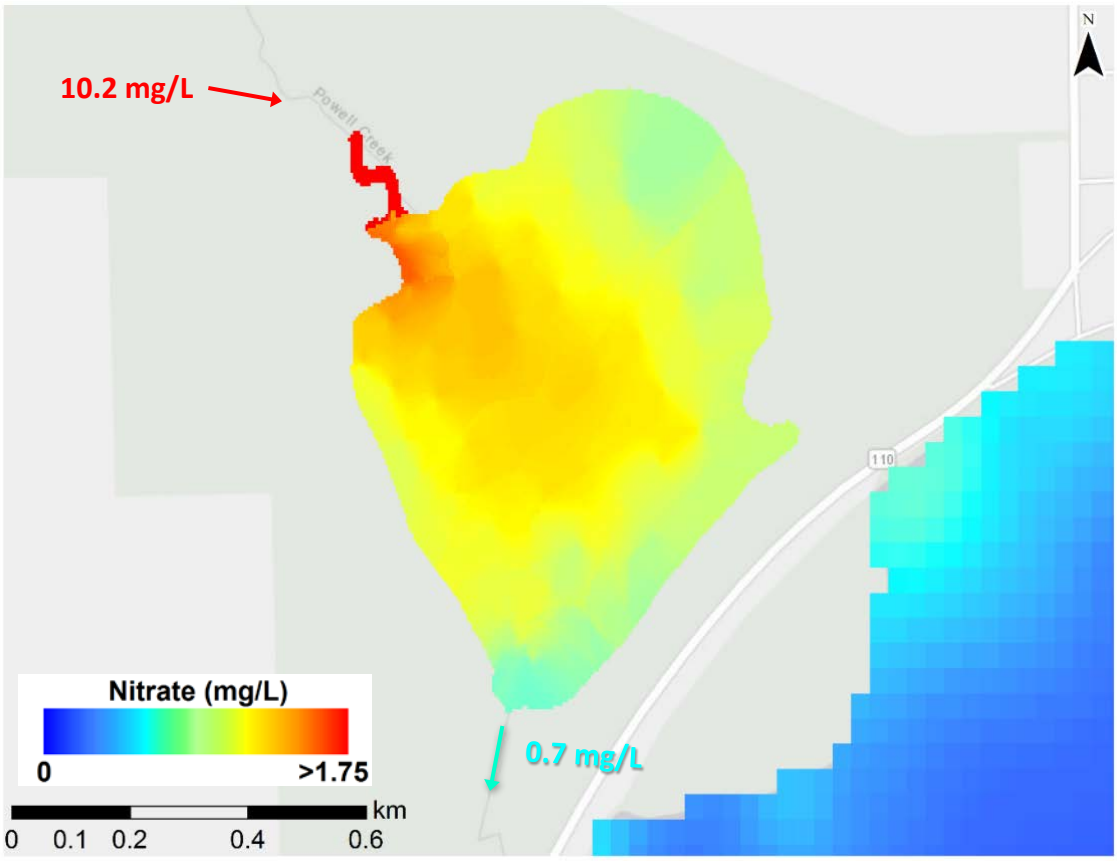

Figure 6.5: NO_3^- reductions visualized in Little Storm Lake, which intercepts water from Powell Creek before entering Storm Lake.

Specific Conductivity

The SPC of Storm Lake remained consistent across the lake despite higher conductivity observed in Powell Creek and West Creek. SPC in the main lake was near 420 µS cm^{-1} and 500 µS cm^{-1} in Little Storm Lake despite conductivities over 600 µS cm^{-1} in Powell Creek and West Creek (Fig. 6.6). The uniform conductivity indicates lateral mixing across the surface of the lake. No potential source pollutants were identified because there were no noticeable areas with significantly higher or lower conductivity.

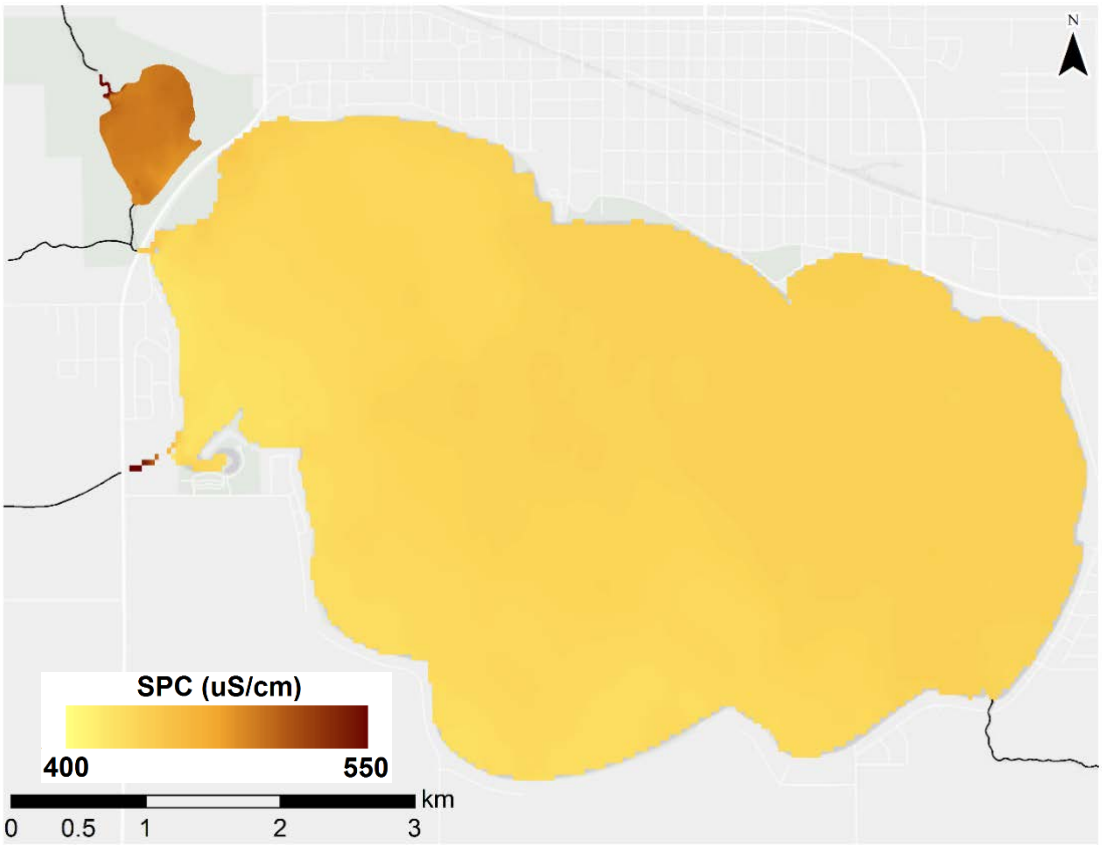

Figure 6.6: Specific Conductivity (SPC) in Storm Lake and Little Storm Lake.

pH

The pH values in Storm Lake varied from 8 to 9 (Fig. 6.7). Highest pH values were on the west and south ends of Storm Lake and lowest pH values were to the north and east. Both tributary creeks were closer to neutral, with pH values around 7.5. The pH in Little Storm Lake was consistent with that of Storm Lake. Like conductivity, no pollutant sources were identified using pH as an indicator. One possible reasoning for pH variation is biotic uptake of CO_2 occurring in space and/or the time it took to measure the entire lake. Aquatic vegetation and algae that uptake CO_2 over a few hours could have increased the pH between the beginning and end of sampling (Seitzinger 1991; Maberly & Spence 1983)

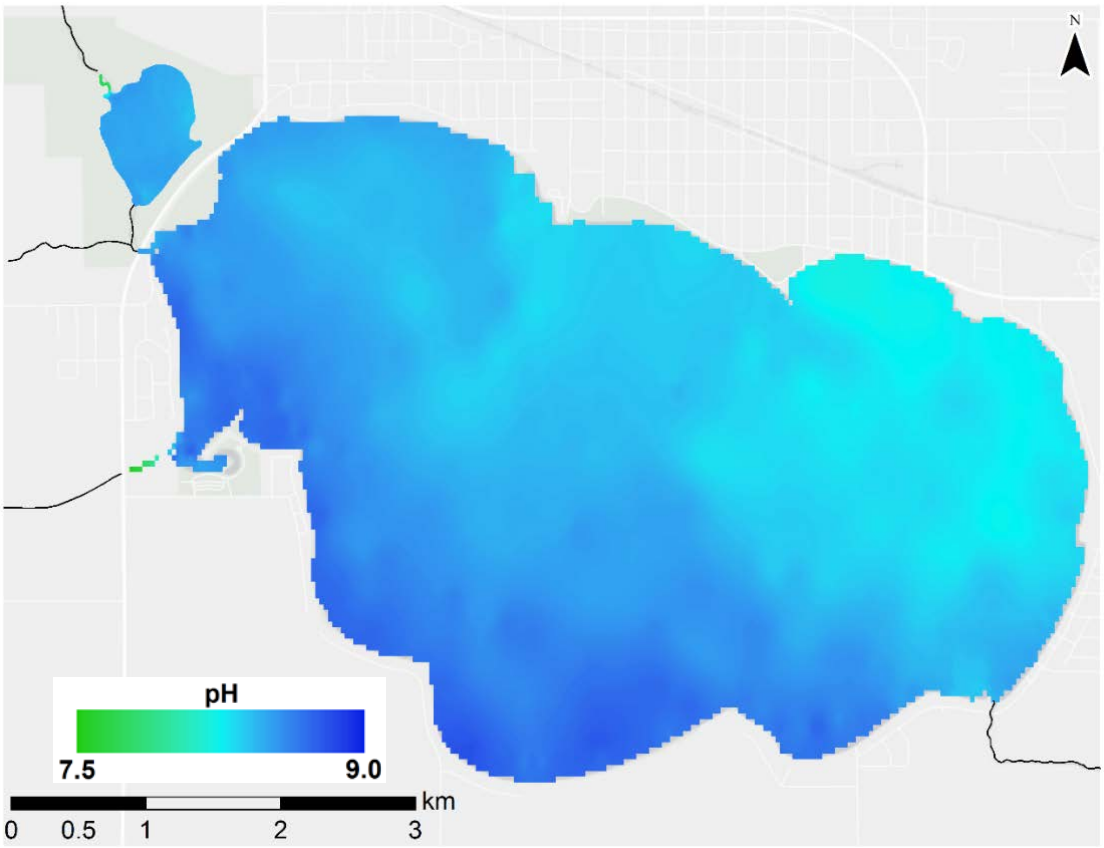

Figure 6.7: pH of Storm Lake and Little Storm Lake.

Temperature

Temperatures across Storm Lake varied across the lake. Temperatures as low as 23°C to the north and as high as 26°C to the south were observed (Fig. 6.8). Observed variability was likely a result of surface water heating as the day progressed. Air temperatures rose from 20°C to 29°C during the sample period. Little Storm Lake was warmer than Storm Lake. Temperatures in the wetland were as high as 28°C, despite incoming water from Powell Creek being 7°C cooler. The warm waters in Little Storm Lake increase denitrification rates and likely helped the wetland achieve 93% NO_3^-N reduction (Willems et al, 1997) (Fig. 6.5).

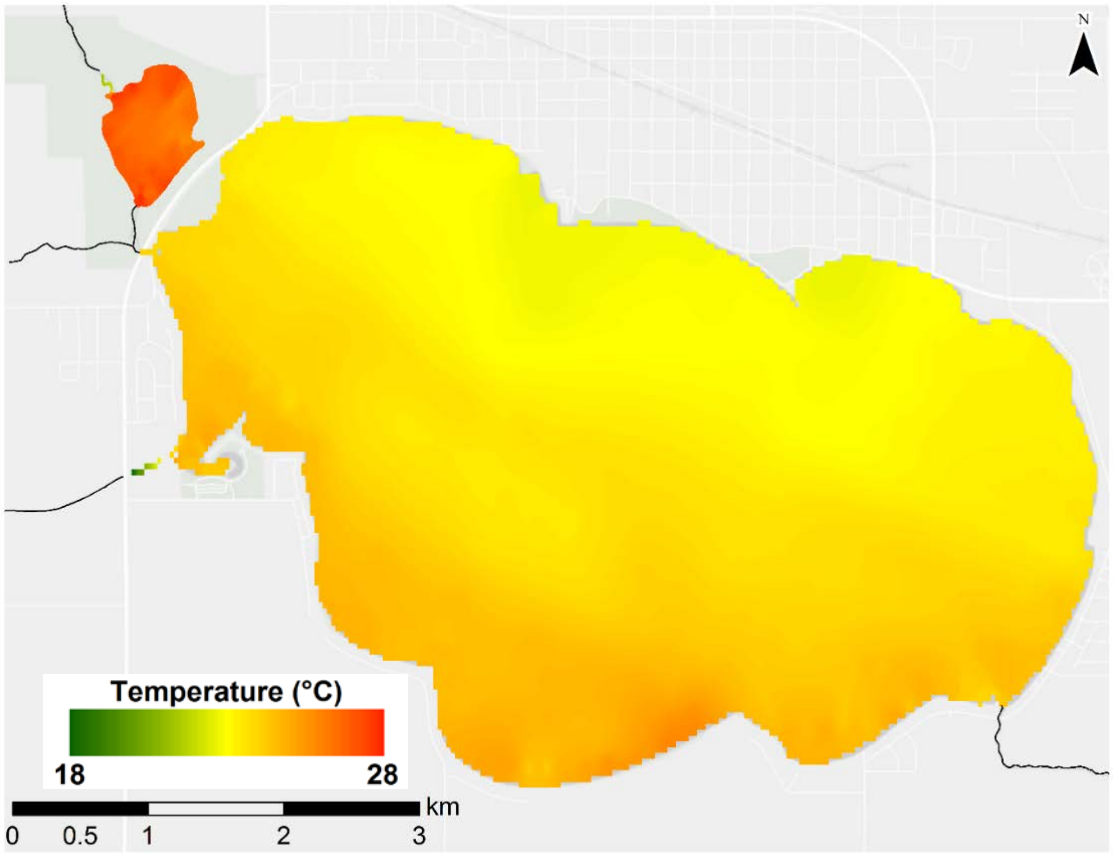

Figure 6.8: Temperatures in Storm Lake and Little Storm Lake.

Dissolved Oxygen

Dissolved oxygen measurements were above saturation in the south end of Storm Lake and in Little Storm Lake. Oxygen concentrations measured as high as 16 mg L^{-1}. Saturation occurs around 8 mg L^{-1} with water temperature, pressure, and conductivity representative of the conditions during sampling (USGS DOTABLES, 2018). Unreasonable sensor measurements occurred along the south shore of Storm Lake and continued throughout the end of sampling in Little Storm Lake. Possible causes for faulty luminescent dissolved oxygen measurements could be the influence of direct sunlight or debris interfering with the measurement probe.

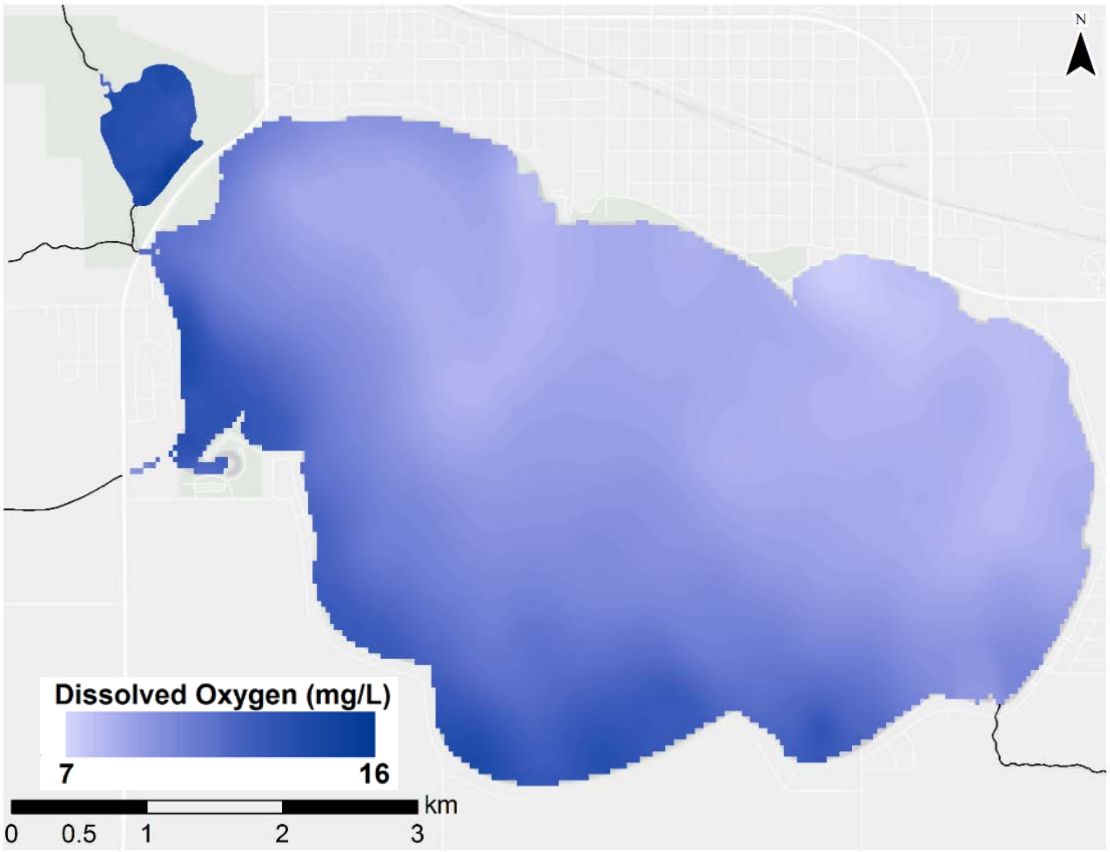

Figure 6.9: Dissolved oxygen concentrations in Storm Lake and Little Storm Lake. Faulty readings from the Hydrolab DS5X sensor likely led to concentrations well above saturation.

6.5 Summary

The continuous, boat deployed sensor system effectively measured NO_3^-N concentration, SPC, and pH, allowing visualization of spatial surface water quality of Storm Lake and Little Storm Lake. No notable point sources of pollutants were identified from these data, but significant NO_3^- reduction was observed in Little Storm Lake. The nutrient removal efforts the City of Storm Lake have invested in were successful in reducing NO_3^- transport into Storm Lake on June 27, 2018.

Continued studies should be conducted to investigate year round NO_3^- removal success. Nitrate removal is highest when flows are low and temperature is high (Willems

et al, 1997). Exploration into inputs directly after storm evens or during colder months of the year could result in different findings and should be considered before arriving at any definite conclusions.

Future studies may also benefit from the addition of more water quality parameters. Water clarity, bacteria, and algae, are important factors people use to decide whether or not they will use a lake for recreation (Jeon et al, 2016). Addition of a turbidity sensor, chlorophyll a sensor, and/or a blue green algae sensor would provide data on spatial heterogeneity of turbidity and algal blooms. These sensors are available attachments for the Hydrolab DS5X. A dissolved phosphorus sensor would also provide valuable data, as phosphorus is often the limiting nutrient for plant growth in freshwater systems (Howarth et al, 2006). However, the technology is not yet available for rapid and accurate measurement of dissolved phosphorus.

CHAPTER 7: RESEARCH SUMMARY AND IMPLICATIONS FOR FURTHER RESEARCH

We collected data to explore spatial and temporal trends in water quality in the Iowa/Cedar River Basin and in Storm Lake, IA. We initially conducted traditional grab samples to assess spatial NO_3^-, PO_4^{3-}, and SPC trends in the Clear Creek and English River Watersheds (Ch. 2). We investigated the influence of sample frequency on NO_3^- load estimates using traditional grab sample methodology (Ch. 3). Over the winter of 2017-2018, we developed a novel platform to measure spatial water quality using a boat-deployed Nitratax Plus sc and Hydrolab DS5X (Ch. 4). We used this system on the Iowa and Cedar River (Ch. 5) and Storm Lake, IA (Ch. 6) to explore spatial water quality trends and determine the merits of the sampling platform we designed.

The boat-deployed water quality system provides opportunities for future research. Analysis of surface water quality variability in lentic systems is easily achievable with the system. Nitrate removal by wetlands (Ch. 6) can be observed spatially. Algal blooms may be measured with addition of available attachments for the Hydrolab DS5X to achieve a better understanding their spatial variability of lentic systems. Opportunities to research lotic systems exist as well. High-resolution longitudinal trends in water quality are easily measured and may pinpoint sources of pollutants such as NO_3-. High-resolution longitudinal trends provide decision makers the data to prioritize water quality mitigation efforts based the water quality variable of interest. The system also easily captured plumes from tributaries and point sources before they fully mixed. Future efforts could use the system to determine the mixing efficiency of point sources such as wastewater effluent plumes to ensure regulatory compliance is met or to determine if *in-situ* sensors are located where rivers are laterally mixed.

The work done in this thesis is a small step forward to achieve the goals of the USEPA, which were a 45% reduction in the NO_3^- flowing to the Gulf of Mexico (USEPA 2008). Progressive steps toward this goal include focusing on management, land use, and edge-of-field practices on small watersheds in the U.S. Corn Belt (Tanner & Kadlec 2013; Tomer et al. 2003; David et al. 2010). More high spatial resolution NO_3^- monitoring needs to occur to identify small watersheds contributing highest NO_3^- yields. Both methods used in this thesis (grab samples and boat-deployed sensors) help provide the data necessary for nutrient management decisions to be made across varying watershed scales.

Our collected data will assist local and regional decision makers who wish to reduce watershed NO_3- loading to the Gulf of Mexico and inform them of threats to drinking water locally. High NO_3- concentrations were observed in areas with high row crop agriculture in Clear Creek and the English River (Ch. 2). Highest NO_3- yields in the ICRB were identified in area of intense row crop agriculture *and* low relief landforms (Ch. 7). We recommend local nutrient removal efforts focus on small watersheds in the DML or IS that have over 80% corn and soybean land use. We recommend regional nutrient removal efforts in the US Corn Belt also focus on low relief watersheds with high corn and soy production and potentially tile drained soils. A greater reduction of surface water NO_3- may be achieved by focusing efforts on integrated management, edge-of-field, and land use practices in these identified NO_3- hotspots.

REFERENCES

Allard M. & Moreau G. 1987. Effects of experimental acidification on a lotic macroinvertebrate community. *Hydrobiologia*. 144(1): 37-49.

Arenas Amado A., Schilling K. E., Jones C. S., Thomas N., and Weber L. J. 2017. Estimation of tile drainage contribution to streamflow and nutrient loads at the watershed scale based on continuously monitored data. *Environmental Monitoring and Assessment.* 189:426. https://doi.org/10.1007/s10661-017-6139-4

Arnold J.G., Muttiah R.S., Srinivasan R., and Allen P.M. 2000. Regional estimation of base flow and groundwater recharge in the Upper Mississippi river basin. *Journal of Hydrology.* 227(1-4): 21-40.

Beschta R. L. 1997. Riparian Shade and Stream Temperature: An Alternative Perspective. *Rangelands* 19(2): 25-28.

Bonin, J.D. & J.R. Spotila. 1978. Temperature tolerance of larval muskellunge (Esox masquinongy Mitchill) and F1 hybrids raised under hatchery conditions. *Comp. Biochem. Physiol.* 59A: 245–248.

Bowes, Michael, Smith, T. and Neal, C. (2009). The Value of High-Resolution Nutrient Monitoring: A Case Study of the River Frome, Dorset, UK. *Journal of Hydrology.* 378: 82-96.

Brauer N., O'Green A.T., and Dahlgren R.A. 2009. Temporal variability in water quality of agricultural tailwaters: Implications for water quality monitoring. *Agricultural Water Management.* 96(6): 1001-1009.

Carpenter S. R., Caraco N. F., Correll D. L., Howarth R. W. Sharpley A. N., and Smith V. H. 1998. Nonpoint Pollution of Surface Waters with Phosphorus and Nitrogen. *Ecological Applications.* 8(3): 559-568.

Cedfeldt P. T., Watzin M. C., Richardson B. D. 2000. Using GIS to Identify Functionally Significant Wetlands in the Northeastern United States. *Environmental Management.* 26(1): 13-24.

Cheetham, J.L., C.T. Garten, C.L. King & M.H. Smith. 1976. Temperature tolerance and preference of immature channel catfish (Ictalurus punctatus). *Copeia* 1976: 609–612.

Correll D.L. 1998. The Role of Phosphorus in the Eutrophication of Receiving Waters: A Review. *Journal of Environmental Quality.* 27: 261-266.

Courtney L.A. & Clements W.H. 1998. Effects of acidic pH on benthic macroinvertebrate communities in stream microcosms. *Hydrobiologia.* 379(1-3): 135-145.

Crawford J. T., Loken. L. C., Casson N. J., Smith C., Stone A. G., Winslow L. A. 2015. High-Speed Limnology: Using Advanced Sensors to Investigate Spatial Variability in Biogeochemistry and Hydrology. *Environmental Science and Technology.* 49(1): 442-450.

Criss R.E. & Winston W.E. 2008. Discharge predictions of rainfall-driven theoretical hydrograph compared to common models and observed data. *Water Resources Research. DOI:* ***https://doi.org/10.1029/2007WR006415***

Dolan, David, Yui, A., and Geist, R. (1981). Evaluation of River Load Estimation Methods for Total Phosphorus. *Journal of Great Lakes Research.* 7(3): 207-214.

Drake, C.W., Jones, C.S., Schilling, K.E., Amado, A.A. and Weber, L.J., 2018. Estimating nitrate-nitrogen retention in a large constructed wetland using high-frequency, continuous monitoring and hydrologic modeling. *Ecological Engineering*, *117*, pp.69-83.

Duncan, J.M., Welty, C., Kemper, J.T., Groffman, P.M. and Band, L.E., 2017. Dynamics of nitrate concentration-discharge patterns in an urban watershed. *Water Resources Research*, *53*(8), pp.7349-7365.

Edwards P.J., Williard K.W.J., Schoonover J.E. 2015. Fundamentals of Watershed Hydrology. *Water Research & Education*. 154(1): 3-20.

El-Sadek, Alaa, Radwan, M., Abdel-Gawad, S. (2005). Analysis of Load versus Concentration as Water Quality Measures. *International Water Technology Conference.* Sharm El-Sheikh, Egypt.

Fewtrell L. 2004 Drinking-Water Nitrate, Methemoglobinemia, and Global Burden of Disease: A discussion. *Environmental Health Perspectives.* 112(14): 1371-1374.

Heffernan, J.B., Cohen, M.J., Frazer, T.K., Thomas, R.G., Rayfield, T.J., Gulley, J., Martin, J.B., Delfino, J.J. and Graham, W.D., 2010. Hydrologic and biotic influences on nitrate removal in a subtropical spring-fed river. *Limnology and Oceanography*, *55*(1), pp.249-263.

Higashino M. & Stefan H.G. 2019. Variability and change of precipitation and flood discharge in a Japanese river basin. *Journal of Hydrology: Regional Studies.* 21: 68-79.

Hobbie, S. E., J. C. Finlay, B. D. Janke, D. A. Nidzgorski, D. B. Millet, and L. A. Baker. 2017. Contrasting nitrogen and phosphorus budgets in urban watersheds and

implications for managing urban water pollution. *PNAS 2017 April.* 114(16): 4177-4182.

Homer, C.G., Dewitz, J.A., Yang, L., Jin, S., Danielson, P., Xian, G., Coulston, J., Herold, N.D., Wickham, J.D., and Megown, K., 2015, Completion of the 2011 National Land Cover Database for the conterminous United States-Representing a decade of land cover change information. *Photogrammetric Engineering and Remote Sensing*, v. 81, no. 5, p. 345-354.

Howarth RW, Marino R. 2006. Nitrogen as the Limiting Nutrient for Eutrophication in Coastal Marine Ecosystems: Evolving Views Over Three Decades. *Limnology and Oceanography*. 51(1part2):364–76.

Ikenberry, C.D., Soupir, M.L., Schilling, K.E., Jones, C.S. and Seeman, A., 2014. Nitrate-nitrogen export: magnitude and patterns from drainage districts to downstream river basins. *Journal of environmental quality*, *43*(6), pp.2024-2033.

Iowa Department of Natural Resources (DNR). 2005. Total Maximum Daily Load for Turbidity. Storm Lake. Buena Vista County, Iowa. Iowa Department of Natural Resources TMDL & Water Quality Assessment Section. Retrieved From: file:///C:/Users/meulemns/Downloads/stormlake.pdf

Iowa Department of Natural Resources (DNR). 2009. High Resolution Land Cover of Iowa in 2009. Retrieved From: https://geodata.iowa.gov/dataset/high-resolution-land-cover-iowa-2009.

Iowa nutrient reduction strategy. 2017. Iowa State University. Retrieved from: http://www.nutrientstrategy.iastate.edu/.

Jeon H., Ji Y., and Kling C.L. 2016. The Iowa Lakes Valuation Project 2014 Summary and Findings. *Iowa Lakes Valuation Project.* Retrieved From: https://www.card.iastate.edu/lakes/report-to-the-iowa-department-of-natural-resources-2014.pdf.

Jones C.S., Wang B., Schilling K.E., Chan K. 2017. Nitrate transport and supply limitations quantified using high-frequency stream monitoring and turning point analysis. *Journal of Hydrology.* 549: 581-591.

Jones C.S., J.K. Nielsen, K.E. Schilling, L.J. Weber. 2018a. Iowa Stream Nitrate and the Gulf of Mexico. *PLOS ONE, https://doi.org/10.1371/journal.pone.0195930. (OPEN ACCESS).*

Jones C.S., K.E. Schilling, I.M. Simpson, C.F. Wolter. 2018b. Iowa Stream Nitrate, Discharge and Precipitation: 30-Year Perspective. *Environmental Management.*

Jones, C.S., Davis, C.A., Drake, C.W., Schilling, K.E., Debionne, S.H., Gilles, D.W., Demir, I. and Weber, L.J., 2018c. Iowa Statewide Stream Nitrate Load Calculated

Using In Situ Sensor Network. *JAWRA Journal of the American Water Resources Association*, *54*(2), pp.471-486.

Jones, C.S., Kim, S.W., Wilton, T.F., Schilling, K.E. and Davis, C.A., 2018d. Nitrate uptake in an agricultural stream estimated from high-frequency, in-situ sensors. *Environmental monitoring and assessment*, *190*(4), p.226.

Jones, C.S., Schilling, K.E. and Seeman, A., 2019. Relating carbon and nitrogen transport from constructed farm drainage. *Agricultural Water Management*, *213*, pp.12-23.

Krajewski W.F. & Mantilla R. 2010. Why Were the 2008 Floods So Large? In C.F. Mutel (Ed.). *A Watershed Year: Anatomy of the Iowa Floods of 2008.* Iowa City, IA: University of Iowa Press.

Kronvang, G. and Bruhn. 1996. Choice of Sampling Strategy and Estimation Method for Calculating Nitrogen and Phosphorus Transport in Small Lowland Streams. *Hydrological Processes.* 10: 1483- 1501.

Loken L.C., Crawford J.T., Dornblaser M.M., Striegl R.G., Houser J.N., Turner P.A., and Stanley E.H. 2018. Limited nitrate retention capacity in the Upper Mississippi River. *Environmental Research Letters.* 13(7): 074030. https://doi.org/10.1088/1748-9326/aacd51

Lutterschmidt, W.I. & V.H. Hutchison. 1997. The critical thermal maximum: data to support the onset of muscle spasm as the definitive end point. *Can. J. Zool.* 75: 1553–1560.

Maberly S.C. & Spence D.H.N. 1983. Photosynthetic Inorganic Carbon use by Freshwater Plants. *Journal of Ecology.* 71: 705-724.

Mount D.I. 1973. Chronic effect of low pH on fathead minnow survival, growth and reproduction. *Water Research*. 7(7): 987-993.

Neuman R.M., Willis D.W., & Sammons S.M. 1994. Seasonal Growth of Northern Pike (*Esox lucius*) in a South Dakota Glacial Lake. *Journal of Freshwater Ecology.* 9(3): 191-196.

Pellerin, B.A., Bergamaschi, B.A., Gilliom, R.J., Crawford, C.G., Saraceno, J., Frederick, C.P., Downing, B.D. and Murphy, J.C., 2014. Mississippi River nitrate loads from high frequency sensor measurements and regression-based load estimation. *Environmental science & technology*, *48*(21), pp.12612-12619.

Peterson, M.S. 1993. Thermal tolerance of Iowa and Mississippi populations of juvenile walleye, Stizostedion vitreum. *Copeia* 1993: 890–894.

Prior, Jean. 1991. *Landforms of Iowa.* Iowa City, IA: University of Iowa Press. Print

PRISM Climate Group. Oregon State University. http://prism.oregonstate.edu. Created 10 Aug 2018.

Schilling K. E. and Libra R. D. 2000. The Relationship of Nitrate Concentrations in Streams to Row Crop Land Use in Iowa. *Journal of Environmental Quality*. 29:1846-1851.

Schilling K. E. and Lutz D. A. 2004. Relation of Nitrate Concentrations to Baseflow in the Raccoon River, Iowa. *Journal of American Water Resources Association.* 40(4): 889-900.

Schilling, K.E. and Walter, C.F., 2005. Estimation of Streamflow, Base Flow, and Nitrate-Nitrogen Loads in Iowa Using Multiple Linear Regression Models. *Journal of the American Water Resources Association*, *41*(6): 1333-1346.

Schilling K. E. and J. Spooner. 2006. Effects of Watershed-Scale Land Use Change on Stream Nitrate Concentrations. *Journal of Environmental Quality.* 35(6): 2132-2145.

Schilling K.E., Jones C.S., Wolter C.F., Liang X., Zhang. Y.K., Seeman A., Isenhart T., Schnoebelen D. & Skopec M. 2017. Variability of nitrate-nitrogen load estimation results will make quantifying load reduction strategies difficult in Iowa. *Journal of Soil and Water Conservation.* 72(4): 317-325.

Seitzinger S.P. 1991. The effect of pH on the release of phosphorus from Potomac estuary sediments: Implications for blue-green algal blooms. *Esuarine, Coastal and Shelf Science.* 33(4): 409-418.

Smale, M.A. & C.F. Rabeni. 1995. Hypoxia and hyperthermia tolerances of headwater stream fishes. *Trans. Amer. Fish. Soc.* 124: 698–710.

Smith, M.H. & S.L. Scott. 1975. Thermal tolerance and biochemical polymorphism on immature largemouth bass Micropterus salmoides Lacepede. *Georgia Acad. Sci. Bull*. 34: 180–184.

Stenback G.A., Crumpton W.G., and Schilling K.E. 2014. Nitrate loss in Saylorville Lake reservoir in Iowa. *Journal of Hydrology*. 513: 1-6.

Storm Lake Green Infrastructure Plan for Water. 2015. Conservation Design Forum. Retrieved from: https://www.iowaeconomicdevelopment.com/UserDocs/documents/IEDA/StormLakeGreenInfrastructurePlanForWater.pdf

Storm Lake Dredging. Storm Lake, Iowa. Retrieved on 11/14/18. Retrieved From: https://www.stormlake.org/558/Storm-Lake-Dredging

Tanner C. C. and R. H. Kadlec. 2013. Influence of hydrological regime on wetland attenuation of diffuse agricultural nitrate losses. *Ecological Engineering.* 56: 79-88.

Tomer M. D., Meek D. W., Jaynes D. B., Hatfield J. L. 2003. Evaluation of Nitrate Nitrogen Fluxes from a Tile-Drained Watershed in Central Iowa. Publications from USDA-ARS / UNL Faculty. Paper 1360.

Turner RE, Rabalais NN, Justic D. 2006. Predicting Summer Hypoxia in the Northern Gulf of Mexico: Riverine N, P, and Si Loading. *Marine pollution bulletin.* 52(2):139–48.

United States Environmental Protection Agency. National Nutrient Strategy. 2007. https://www.epa.gov/nutrient-policy-data/national-nutrient-strategy.

United States Environmental Protection Agency (USEPA). 2008. Hypoxia in the Northern Gulf of Mexico, An Update by the EPA Science Advisory Board. EPA, Washington, DC.

U. S. Geological Survey. DOTABLES, Dissolved Oxygen Solubility Tables. U. S. Retrieved on 11/26/2018. Retrieved From: https://water.usgs.gov/software/DOTABLES/

U.S. Geological Survey, 2016, National Water Information System data available on the World Wide Web (USGS Water Data for the Nation), accessed September 2018, at URL http://waterdata.usgs.gov/nwis/. http://dx.doi.org/10.5066/F7P55KJN.

Vedachalam, S., Mandelia, A.J. and Heath, E.A. 2019. The impact of source water quality on the cost of nitrate treatment. *AWWA Water Science*, *1*(1), p.e1011.

Walsh C. J., Roy A. H., Feminella J. W. Cottingham P. D. Groffman P. M. and Morgan II R. P. 2005. The urban stream syndrome: current knowledge and the search for a cure. *Journal of the North American Benthological Society.* 24(3): 706-723.

Weber L., Jones C., Davis C. 2015. IIHR 2015 Water Monitoring Report. *University of Iowa: College of Engineering.* Retrieved From: https://iwqis.iowawis.org/assets/monitoring-report-2015.pdf

Weyer P. J., Cerhan J. R., Kross B. C., Hallberg G. R., Kantamneni J., Breuer G., Jones M. P., Zheng W., and Lynch C. F. 2001. Municipal Drinking Water Nitrate Level and Cancer Risk in Older Women: The Iowa Women's Health Study. *Epidemiology.* 12(3): 327-338.

Willems H.P.L., Rotelli M.D., Berry D.F., Smith E.P., Reneau R.B., and Mostaghimi S. 1997. Nitrate removal in riparian wetland soils: Effects of flow rate, temperature, nitrate concentration, and soil depth. *Water Research.* 31(4): 841-849.

Woiwode, J.G. & I.R. Adelman. 1992. Effects of starvation, oscillating temperatures, and photoperiod on the critical thermal maximum of hybrid striped × white bass. *J. Thermal Biol.* 17: 271–275.

Zhao Y, Quigg A. 2014. Nutrient limitation in Northern Gulf of Mexico (NGOM): Phytoplankton Communities and Photosynthesis Respond to Nutrient Pulse. *PLOS one*. 9(2): e88732.

Zimmerman B.A. & Kaleita A.L. 2017. Electrical Conductivity of Agricultural Drainage Water in Iowa. *Iowa State University: Agricultural and Biosystems Engineering Publications*. Retrieved from: https://lib.dr.iastate.edu/cgi/viewcontent.cgi?referer=https://www.google.com/&httpsredir=1&article=2103&context=abe_eng_pubs

APPENDIX

A1: Hydrolab Calibration Log

Table A. 1: The Hydrolab DS5X was calibrated for SPC, pH, and D.O. SPC calibration used standards of 0 and either 2060 or 700 µS cm-1 and checked the linearity using a standard of 445 µS cm-1. We calibrated pH using standards of 7, 4.01, and 10.01. After calibration, we checked pH linearity using a standard of 7.00. D.O. was calibrated using saturated water, measured temperature, and measured barometric pressure.

Date	SPC reading before calibrating to 0 µS cm^{-1}	SPC before calibrating to 2060 µS cm^{-1} standard	**SPC Linearity check (445 µS cm^{-1} standard)**	pH standard of 7.00	pH standard of 4.01	pH standard of 10.01	**pH linearity check with 7.00**	DO % saturation before calibrating to 100%
5/10/2018	1.4	2070	**429**	6.98	3.93	10	**7.01**	101.1
5/28/2018	0	2150	**449**	7.18	3.96	10.06	**7.02**	101.6
6/5/2018	0	2144	**434**	7.01	3.95	9.94	**7.01**	98.7
6/26/2018	0	2140	**437**	7.01	3.97	10.02	**7**	102.4
7/9/2018	0	2130	**439**	7.04	3.98	9.97	**7.04**	102.6
7/15/2018	0	680 (Calibrated to 700)	**450**	6.89	3.86	9.86	**6.98**	98.7
8/6/2018	0	630 (Calibrated to 700)	**451**	7.16	3.95	10.09	**6.95**	99.3

A2: Hydrolab Validation Checks

Table A. 2: Before every day of sampling, we checked the Hydrolab DS5X to ensure no calibration drift occurred. We compared SPC to standards of 700 µS cm-1 and 445 µS cm-1. We compared pH to standards of 7.00 and 10.01. We compared D.O. readings to fully saturated water.

Date	Standard SPC = 700 µS cm^{-1}	Standard SPC = 445 µS cm^{-1}	Standard pH = 7.00	Standard pH = 10.01	DO = 100% saturation
5/14/2018	701	440	6.99	10.02	99.8
5/15/2018	700	438	7.05	9.96	99.7
5/16/2018	700	443	7.06	10.04	98.7
5/17/2018	698	442	6.96	9.98	101.4
5/29/2018	700	444	7.02	10.03	100.7
5/30/2018	689	447	7	9.93	101.1
5/31/2018	702	445	7.03	9.97	100.9
6/7/2018	684	436	7.09	9.99	100.7
6/8/2018	705	450	6.95	9.97	100.9
6/28/2018	698	451	6.95	9.95	98.1
6/29/2018	700	451	7.03	9.97	99.7
8/7/2018	696	443	6.97	10	101.9
8/8/2018	698	444	6.96	10.01	97.5
8/9/2018	697	442	6.95	10.02	98.1